Automated Sewer Inspection Analysis and Condition Assessment

Khalid Kaddoura

A Thesis

In the Department

Of

Building, Civil, and Environmental Engineering

Presented in Partial Fulfillment of the Requirements

For the Degree of

Master of Applied Science in Building Engineering and Construction Management at

Concordia University

Montreal, Quebec, Canada

November 2015

CONCORDIA UNIVERSITY

School of Graduate Studies

This is to certify that the thesis prepared

By: **Khalid Kaddoura**

Titled: **Automated Sewer Inspection Analysis and Condition Assessment**

and submitted in partial fulfillment of the requirements for the degree of

Master of Applied Science (Building Engineering)

complies with the regulations of the University and meets the accepted standards with respect to originality and quality.

Signed by the final examining committee:

______________________________________ Chair
Dr. F. Nasiri

______________________________________ Supervisor
Dr. T. Zayed

______________________________________ Examiner
Dr. M. Z. Kabir External (to program)

______________________________________ Examiner
Dr. A. Bagachi

______________________________________ Examiner
Dr. F. Nasiri

Approved by ______________________________________
Dr. F. Haghighat, GPD
Department of Building, Civil, and Environmental Engineering

Approved by ______________________________________
Dr. Amir Asif, Dean
Faculty of Engineering and Computer Science

Date ______________________________________

ABSTRACT

Automated Sewer Inspection Analysis and Condition Assessment

Khalid Kaddoura

Underground infrastructure serves an essential need for the society. Huge number of facilities is dedicated to facilitate the well-being's needs. Sewer infrastructure, one of the facilities, plays a major role in maintaining healthier environment. Its main duty is to transfer sewage material to treatment plants or any designated disposal area. Therefore, providing well performing sewer systems is essential to avoid any breakdown. Nevertheless, sewer pipelines' condition in North America is deteriorating. In fact, studies have shown that 30% of municipal infrastructure in Canada is in either fair or very poor condition. As a result, there is a significant requirement for inspection and rehabilitation. Many municipalities utilize Closed Circuit Television (CCTV) inspection technique in inspecting sewer pipelines. However, this technique suffers from significant subjective and imprecise conclusions. Hence, studying, analyzing and applying different sewer inspection technologies and designing a condition assessment model are necessary to reduce subjectivity and errors and produce accurate and reliable results.

This research aims to develop an automated tool to quantify: deformation, settled deposits, infiltration and surface damage sewer defects. The automated approach is dependent upon using image processing techniques and several models to analyze output data from 2D laser profiler, sonar and electroscan. Other than using ASTM F1216 formula, the research suggests applying the roundness factor in quantifying the deformation defect.

The research develops a condition assessment model, based on the aforementioned defects, to arrive to an aggregated index suggesting the condition of sewer pipelines. Multi Attribute Utility Theory (MAUT) approach is used for each defect. The research also suggests a methodology to evaluate the surface damage defect of sewer pipelines for reinforced concrete, vitrified clay and ductile iron sewer pipeline materials. An interface, using MATLAB, was developed to implement the designed quantification algorithms and the MAUT model on real case studies.

After implementing and validating the two deformation quantification methods, the Mean Absolute Error (MAE) utilizing the ASTM F1216 was 4.27%, while the MAE using the roundness factor was 4.83%. The maximum difference percentage was found to be 40.06%; however, the minimum difference percentage was 0.59%. The average difference percentage for all the cases was calculated as 16.67%. Later, the MAUT model was validated with actual case studies. Three rounding types (rounding to nearest number, rounding up and down) were tested to change the aggregated index, containing decimals, to a whole number. Mean Absolute Error (MAE) was utilized to compare the rounding types. In all case studies, rounding up type produced the lowest MAE values. When rounding up the computed index in case study 1, the MAE for Concordia Sewer Protocol (CSP), Water Research Centre (WRc) and New Zealand were 0.33, 0.33 and 0.42, respectively.

This research shall encourage subject matters to utilize technologies, other than or beside CCTV, to conclude sound results. The developed automated user interface shall reduce inaccuracy and subjectivity through the application of robust image processing algorithms. After extending this research in including several sewer's components and defects, the condition assessment model shall aid asset managers to allocate their maintenance and rehabilitation budgets.

ACKNOWLEDGEMENTS

First and always, thank God for everything.

Second, I would like to express my sincere appreciation to Professor Tarek Zayed. Professor Zayed provided patience, knowledge and assistance during my studies. His trust and encouragement played as incentives to accomplish the work. His experience in several topics facilitated the work and made it possible.

Also, I would like to thank the Faculty of Engineering and the Department of Building, Civil and Environmental Engineering for the continuous assistance. I am also grateful to my friends, the committees and persons who provided scholarships during my studies.

It is my pleasure to express my gratitude to my beloved parents, my father Mahmoud Kaddoura and my mother Insaf Khalaf. Their continuous encouragement and support was always surrounding me. Although they are thousands of miles away, their care, advice, support, emotions and respect were close to me. Special thanks to my sisters Julia, Manal, Zenat and Aalaa. I am really fortunate as I have loving sisters. I would like to thank them for their support offered prior commencing and during my studies.

I would like to express my sincere appreciation and respect to my wife, Aya Hejjo, for her encouragement and PATIENCE. She always provided working and studying environment. She is a wonderful family to me.

TABLE OF CONTENTS

LIST OF FIGURES

LIST OF TABLES

LIST OF ABBREVIATIONS

2D	Two Dimensional
3D	Three Dimensional
AMSA	Association of Metropolitan Sewerage Agencies
ANN	Artificial Neural Network
ANP	Analytic Network Process
APE	Actual Probability of Existence
ASCE	American Society of Civil Engineers
ASTM	American Society of Testing Materials
AWWA	American Water Works Association
CCTV	Closed Circuit Television
CSP	Concordia Sewer Protocol
EPA	Environmental Protection Agency
GGL	Gamma-Gamma Logging
GFRP	Glass Fiber Reinforced Plastic
GUI	Graphical User Interface

GUIDE	Graphical User Interface Development Environment
HDPE	High Density Polyethylene
KARO	Kanalrobetor
LOG	Laplacian of Gaussian
MAUT	Multi Attribute Theory
NACWA	National Association of Clean Water Agencies
NRC	National Research Council
NZWWWA	New Zealand Water and Waste Water Association
PACP	Pipeline Assessment and Certification Program
PIRAT	Pipe Inspection Real Time Assessment Technique
PPR	Pipe Penetrating Radar
PVC	Plastic Sewer Pipelines
R^2	Coefficient of Determination
ROC	Receiver-Operating Characteristics
ROI	Region of Interest
SAM	Sewer Assessment with Multi-Sensors

SVM	Support Vector Machines
VC	Vitrified Clay
WRc	Water Research Centre

CHAPTER ONE: INTRODUCTION

1.1 Overview

The importance of underground infrastructure cannot be ignored in urban communities. The essential resources needed for any society—including communications, water, sewer systems, and power—are distributed in a huge underground maze (Koo and Ariaratnam 2006). The main use of sewer pipelines is to transfer the sewage from facilities to treatment plants or designated disposal areas. Failure to transport sewage because of structural or operational defects may result in the pipeline's failure. In fact, the condition of sewer pipelines in North America has been deteriorating. The American Society of Civil Engineers (2004) gave the condition of the wastewater system in the United States an overall grade of "D." The Association of Metropolitan Sewerage Agencies (2003), now called the National Association of Clean Water Agencies (NACWA), conducted a survey on sewer inspection frequency. The survey concluded that approximately half of the survey inspects less than 10% of their sewer system annually.

In Canada, researchers and municipalities describe the poor condition of sewer pipelines in the country's cities (Siddiqui and Mirza 1996). Studies show that 30% of Canada's municipal infrastructure is in either fair or very poor condition (Félio et al. 2012). Studies also show that 40.3% of wastewater treatment plants, pumping stations, and storage tanks are in poor condition. Pipelines are designed to operate for a specific number of years; however, their deterioration does not follow a consistent pattern (Najafi and Kulandaivel 2005). Defects may be found at any time in both aging and newly installed pipelines. Municipalities allocate funds to assess and rehabilitate their sewer pipeline systems. Therefore, to budget for the rehabilitation process, an extensive inspection is required for sewer pipelines.

Before the 1960s, inspecting sewer pipelines was a challenging task (Reyna et al. 1994). In most cases, it was difficult for workers to gain access where the inspection was required. In response to this challenge, workers invented methods to avoid the challenging task. This, in turn, led to advanced technologies that enhanced approaches to sewer inspection. Closed Circuit Television (CCTV) camera inspections started in the 1960s (Reyna et al. 1994). Because sewer inspections were important, workers developed nondestructive testing applications to assess sewer pipeline conditions (Sonyok et al. 2008). The selection of the appropriate inspection technique depends on the pipe material, type of utility, and amount of information (Koo and Ariaratnam 2006).

1.2 Closed Circuit Television (CCTV) Inspection

CCTV is a method used to record videos for underground pipelines. It is used to inspect pipelines that can be too small or dangerous for humans to enter. In their early stages, CCTV cameras were winched between two manholes to record the condition of the pipeline. Over time, CCTV cameras were mounted on top of a crawler or a float. Operators were able to control the movement of the robot, as well as that of the camera, from far distances. The camera records the inner-surface condition of the pipeline and supplies information above the flow line. Later, experts use the recorded video to interpret, comment on, and make conclusions about the pipeline's condition. Although some sophisticated technologies have been introduced for sewer inspection, CCTV is still the most commonly utilized technique. A survey by Thomson et al. (2004) showed that 100% of the respondents used CCTV as their primary sewer inspection technique. Figure 1.1 is an example of a CCTV caption of a circumferential crack defect.

Data obtained from CCTV videos are evidence of the following (Feeney et al. 2009):

- Settled deposits

- Deflection
- Offset joints
- Pipe cracks
- Leakage

Figure 1.1 CCTV Caption of a Circumferential Crack Defect

1.3 Problem Statement

Current sewer inspection practices rely on applying CCTV techniques, but researchers have pointed out several CCTV limitations. For example, Tuccillo et al. (2010) mentioned that CCTV can provide information only above the flow line. More importantly, it does not quantify the detected defects such as deformation, settled deposits, infiltration, and surface damage. Therefore, it can be concluded that CCTV helps locate defects but that its inability to quantify certain defects results in subjective conclusions. Consequently, studying and analyzing different sewer inspection technologies is important to overcome the limitations of CCTV. Many sewer condition assessment protocols are used to provide a condition index for sewer pipelines. These protocols rely on CCTV inspection methods. Because CCTV provides evidence that defects exist, several protocols suggest linguistic severity information in grading sewer defects. For example, for a surface damage defect, many protocols provide linguistic severities for concrete or reinforced concrete pipelines only, neglecting other types of materials. Similarly, infiltration defects are assessed using linguistic severities. As a result, an objective assessment model that increases accuracy and provides sound results is required to reach robust conclusions.

1.4 Research Objectives and Deliverables

The objectives of this research are as follows:

a) Study and analyze current practices of sewer pipeline inspection and available technologies
b) Develop a technology-based condition assessment model for sewer pipelines
c) Design an automated user interface tool to quantify and assess sewer pipelines

Table 1.1 lists the research objectives, with the deliverables arranged in a matrix.

Table 1.1 Requirement Traceability Matrix

#	Deliverables	Objectives		
		A	B	C
1	Use outputs of laser profiler, sonar, and electro scan technologies	X		
2	Quantify deformation defects based on the ASTM F1216 ovality formula	X		X
3	Quantify deformation defects using the roundness factor	X		X
4	Modify the Concordia Sewer Protocol (CSP) scale		X	
5	Quantify settled deposits	X		X
6	Quantify surface damage	X		X
7	Produce a condition assessment index		X	X
8	Propose surface damage evaluation methodology		X	
9	Provide an automated tool to quantify deformation, settled deposits, infiltration and surface damage defects			X
10	Save the information of the pipe inspected			X
11	Supply each defect with at least one utility function		X	

1.5 Research Methodology

To accomplish the research objectives, an extensive methodology was planned and executed. A literature review, which includes current practices, automated tools, and condition assessment approaches, was conducted. Figure 1.2 summarizes the methodology steps acquired in the research.

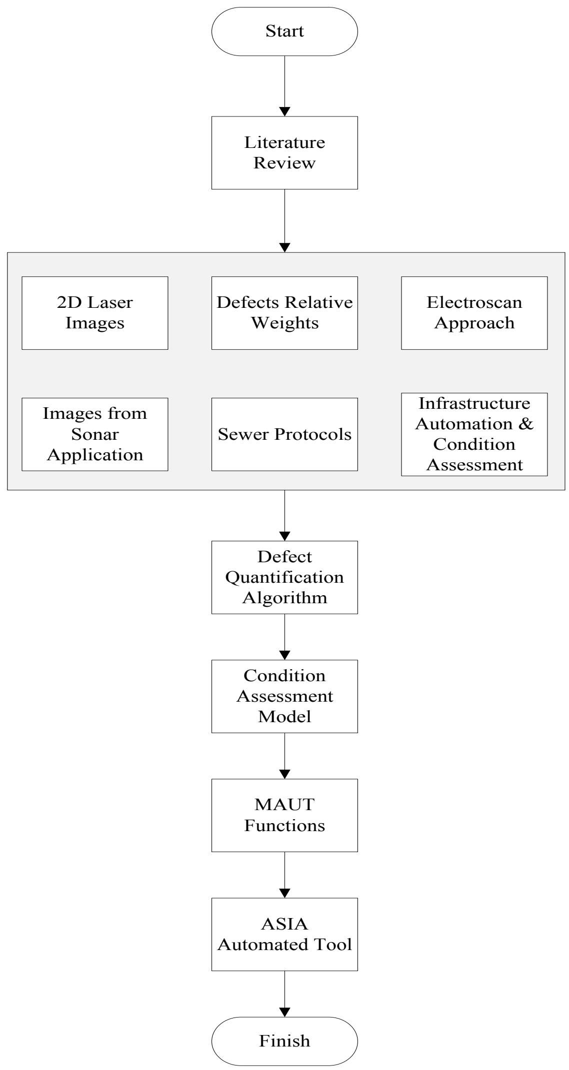

Figure 1.2 Summarized Research Methodology Flowchart

The following steps explain the research methodology:

- Study the work on sewer automation using several tools such as image processing.
- Review image processing tools that can quantify these three defects: deformation, settled deposits, and surface damage.
- Check the approach used with the electro scan that changes the electrical current provided by the machine to infiltration flow (liters/second).
- Collect several laser profiler and sonar inspection reports that include images of defects such as deformation, settled deposits, and surface damage.
- Use MATLAB software to create the image processing codes for each defect.
- Check the decision-making tools to provide a condition assessment tool based on the four defects.
- Use the multi-attribute utility theory (MAUT) approach for each defect to develop a condition assessment model.
- Improve the evaluation of surface damage defects for three types of sewer pipeline materials: reinforced concrete, ductile iron, and vitrified clay.
- Determine the relative importance weights of the four defects and then aggregate the indexes of the defects to create a condition index using the MAUT approach.
- Check the severities of three protocols: WRc, CSP, and New Zealand.
- Utilize the severities of deformation and settled deposits of each protocol to present each defect in a utility function.
- Produce a user interface that can evaluate and quantify defects. Later, the user interface provides the condition of the pipeline using the designed MAUT model.

- Validate the condition assessment model using real case studies from Qatar's and Canada's reports.

1.6 Thesis Organization

This research is divided into six chapters:

Chapter One introduces the research, problem statement, and research objectives and summarizes the methodology of the research.

Chapter Two provides an extensive literature review related to the research. It discusses many of the techniques used for sewer inspection. Additionally, it summarizes the sewer pipeline materials. Later, the chapter discusses previous work done on infrastructure automation and condition assessment techniques. Finally, the chapter states the use of the MAUT method in developing a condition assessment model.

Chapter Three demonstrates the research methodology adopted in the research. It talks about the algorithms to quantify the four defects and states the condition assessment model development procedure with the utility functions generated.

Chapter Four validates the image processing operations with the available case studies and compares the results. It also describes the implementation of the MAUT condition assessment model with real case studies collected and screened for comparison purposes.

Chapter Five demonstrates the developed automated interface tool and discusses the formation of the automated sewer inspection analysis (ASIA).

Chapter Six summarizes the research and presents the results. It also mentions the limitations and recommends some points that may enhance or extend the work.

CHAPTER TWO: LITERATURE REVIEW

2.1 Overview

Figure 2.1 presents an affinity diagram of the literature review, which consists of eight major sections. The techniques that are suggested for quantifying deformation, settled deposits, infiltration, and surface damage defects are explained in 2.2. This section defines each technology and provides information about the defects detected. Other sewer inspection techniques are summarized in the same section.

Several sewer pipeline materials are outlined in 2.3, as some of the materials will be considered in the evaluation of surface damage defects. Some of the current practices that are related to infrastructure automation are listed in 2.4. This section includes the automation techniques utilized as well as the defects detected. Common image processing knowledge and the operations that will be utilized in the research's automated tool are provided in 2.5.

The current models that were developed and utilized in assessing some of the infrastructure facilities are described in 2.6. After studying several decision-making techniques, 2.7 explains the MAUT application. Three sewer protocols are investigated and some of the considered sewer defects are listed in 2.8. Finally, the chapter is summarized and the limitations listed in 2.9.

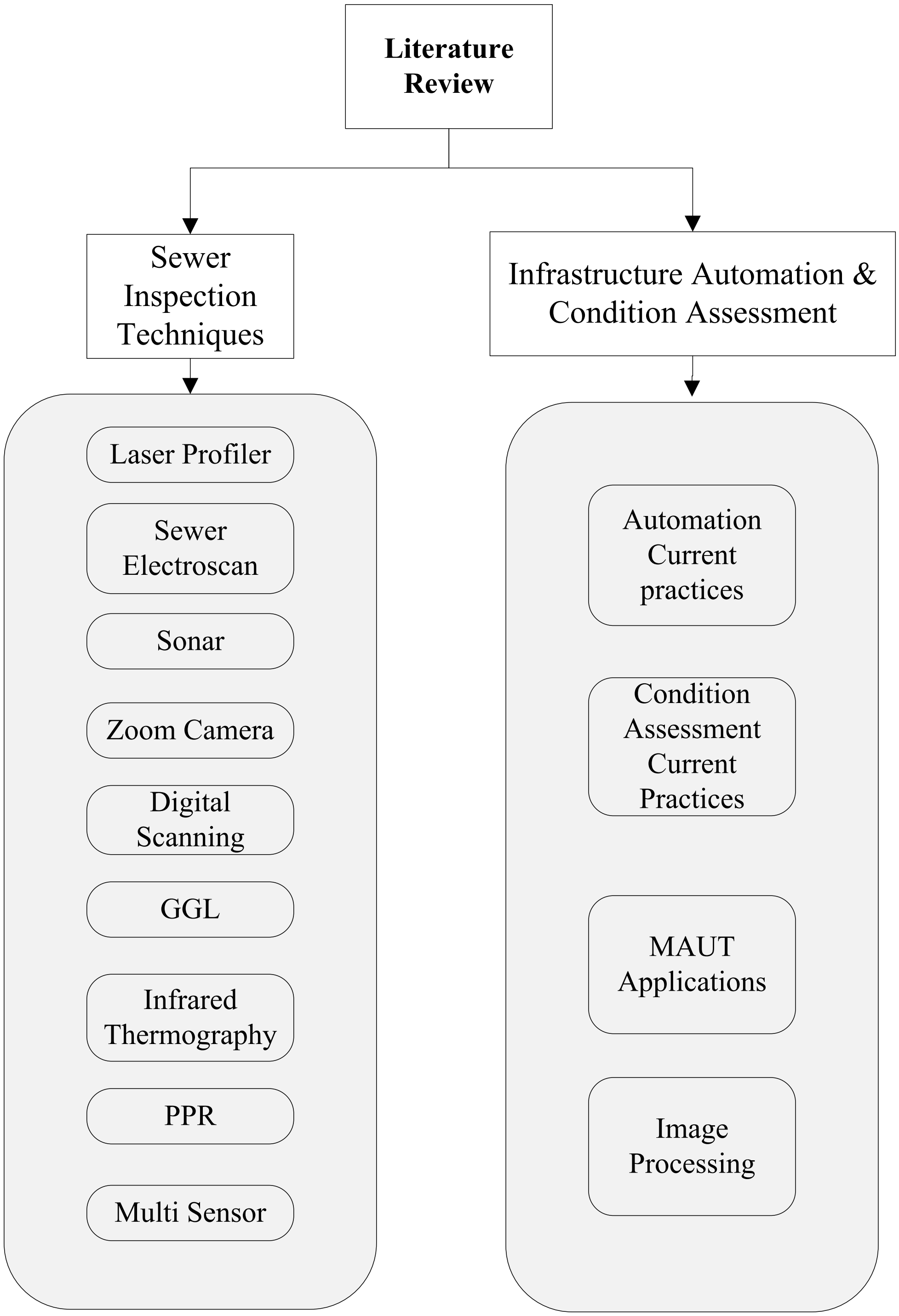

Figure 2.1 Literature Review Affinity Diagram

2.2 Sewer Inspection Techniques

2.2.1 Laser Profiler

An advancement in sewer inspection technology is the laser profiler. The laser profiler is a technology that is able to detect and quantify the changes in the vertical and horizontal shape of pipelines (Tuccillo et al. 2010), known as the deformation of a pipeline. In addition, it can feed the operators with a profile of the interior pipeline wall. CUES company supplies laser profiler sensor for 6” to 80” pipelines with an approximate cost of $76,642.50 US.

Several factors cause deformation of a pipeline. Insufficient design considerations and improper installation of pipelines are the major causes of their deflections (Rinker Materials 2009). Rinker Materials (2009) also claimed that deflection of a pipeline decreases its life expectancy and reduces its overall performance. Hence, evidence of the deformation defect, as provided by CCTV, will not be sufficient to determine the severity of the defect.

There are two types of laser profilers: a two-dimensional (2-D) laser profiler and a three-dimensional (3-D) laser profiler. The 2-D laser profiler technology is based on a ring of light, generated from a laser, around the wall of the pipeline. A camera, usually a CCTV camera, which is attached on the same crawler, detects the ring of light and stores the laser image for further analysis (Tuccillo et al. 2010). Using CCTV alone, the operator may not observe any deflection along the pipeline while analyzing the recorded video. Utilizing a 2-D laser profiler, however, would clearly present the actual condition of the pipeline.

The accuracy of the 2-D image depends on the calibration of the camera and the alignment of the laser with the cross section of the pipeline. Inexact alignment of the laser may contribute to difficulty in analyzing the data, which causes misleading results (Dettmer et al. 2005). The authors mentioned that placing the laser in a position that makes an angle with the longitudinal axis would result in an oval image. Making the exact alignment may be possible along the centerline of the pipeline in case it runs in a straight direction. However, pipelines usually diverge from the central pipeline's axis (Thayer et al. 2009) to fit the city's infrastructure plan. Where pipelines diverge, alignment distortion may occur. As a result, the output image may suggest that the pipeline is deformed, as clearly explained in Figure 2.4 (Thayer et al. 2009). The authors concluded that the bigger the pipe, the more complex the situation because of existing defects like debris and structural defects.

Nevertheless, the 3-D laser profiler can eliminate the aforementioned drawback. It uses laser point beams, which have a receiver and a two-way transmitter (Tuccillo et al. 2010). The output of the inspection is a 3-D plot of X, Y, and Z coordinates of the pipeline (point cloud). The point cloud data captures the full pipeline segment and the true cross section of the pipeline (O'Neill 1997), unlike the 2-D laser profiler, which utilizes single-data acquisition (Hartley and Zisserman 2000). The extracted 3-D representation of the pipe shows its real cross section regardless of the divergence angle from the centerline of the pipeline (Thayer et al. 2009).

Laser profilers are used mostly with a CCTV camera (Tuccillo et al. 2010). Using the two technologies would provide the complete condition of a pipeline, as suggested by Redzone (2008). For instance, laser is able to capture any small changes in the geometry of the pipeline, which are difficult to detect with a CCTV camera. On the other hand, CCTV cameras can detect cracks and fractures. Using both technologies provides cost savings and better rehabilitation plans. Moreover, in some case studies, using CCTV alone resulted in misleading conclusions. Figure 2.2 is a picture from a CCTV recorded video where slight or no deflection can be detected. For the same location of the pipeline, Figure 2.3 is the 2-D laser image, showing a deformation of 12% to 13%.

Figure 2.2 CCTV Caption of a Sewer Pipeline, Acquired from CUES

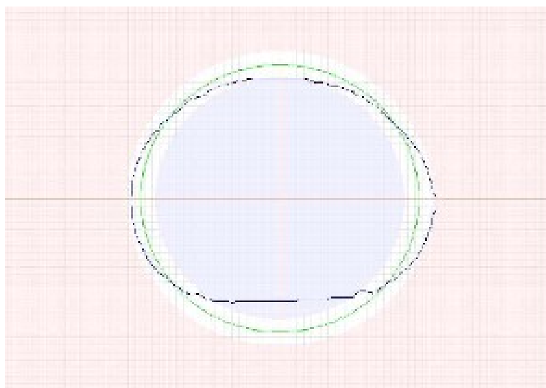

Figure 2.3 Laser Profiler Output of the Same CCTV Caption at Figure 2.2 Location, Acquired from CUES

In another case study, the CCTV camera analysis provided several structural defects, including multiple fractures and a hole in a pipeline (Redzone 2008). However, when the laser profiler was used, it did not detect any of the defects reported by CCTV. It was concluded that the hole presented in the CCTV camera video was a shadow and light reflection was detected as wall fractures in the CCTV video interpretation. Such a conclusion saved thousands of dollars of rehabilitation work.

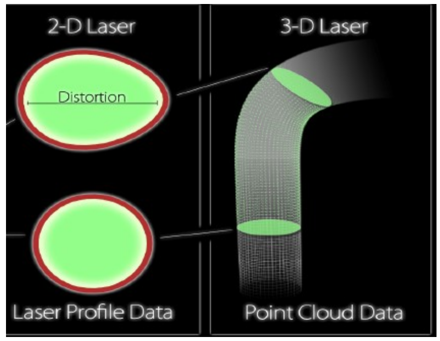

Figure 2.4 A Comparison between 2-D and 3-D Laser Images (Thayer et al. 2009)

2.2.2 Sewer Electro Scan

Among the major pipeline defects, infiltration accounts for 16% of sewer defects that lead to poor pipeline conditions (Moselhi and Shehab-Eldeen 1999a). Infiltration can severely increase operating costs. The effects include varying energy consumption and effluent amounts that are greater than the designed capacity of the treatment plants or wastewater collection systems (Nelson et al. 2010). Consequently, treatment plant costs will increase by 10% (deMonsabert and Thornton 1997). In some cases, overflow scenarios may occur. In addition, infiltration can remove soil that surrounds the pipeline, causing the pipe to collapse (Joannis et al. 2002).

The current practice to detect leakage in sewer pipelines is to use a CCTV camera. For instance, it can record water flow because of root intrusion from a joint (Harris and Tasello 2004). This happens after a heavy rainfall. By that time, CCTV cameras cannot be used because the pipe will be full. In addition, CCTV requires active infiltration to identify sources of defects (Electro Scan 2013). Also, it relies on visual observations to record defects (Electro Scan 2013). Therefore, a major advancement has been made to lessen the drawbacks of CCTV in detecting infiltration.

Electro Scan, Inc. developed sewer inspection equipment that can detect and quantify infiltration defects in pipelines. Approximately, the machine and its accompanying items cost in total $200,000

US excluding shipping and other fees. The innovation is based on measuring the resistance of the pipe wall to evaluate the infiltration defects of the pipeline. This method can be implemented on nonconductive pipeline materials, which are resistant to electric current, such as plastic, concrete, reinforced concrete, clay, and brick. The equipment detects leakage defects up to +/–40%, assuming 304.8 mm head of groundwater and 1% of slope. As its name suggests, the equipment uses an electrical approach.

As Figure 2.5 shows, the voltage is applied between the Sonde, the electrode in the pipe, and the surface electrode. The pipe should be full of water at the Sonde location. Between the two electrodes, the electrical resistance is very low; however, the pipe wall's electrical resistance is high. As a result, the high electrical resistivity will prevent any leakage of the current. Any crack or hole will indicate a current's leakage (Harris and Dobson 2006). Cracks or fractures that do not leak provide low threshold anomalies.

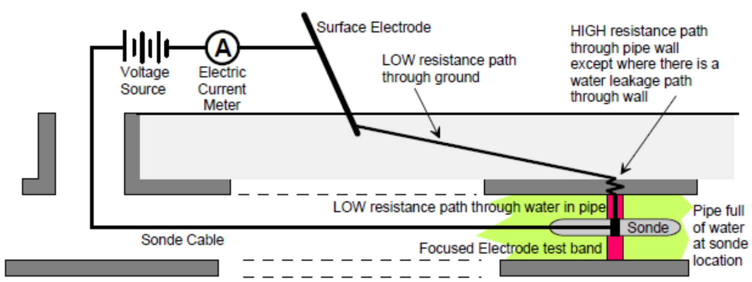

Figure 2.5 Mechanism of Electro Scan Machine (Harris and Tasello 2004)

Figure 2.6 shows a sample result of an electro scan inspection of a pipeline. It shows the electrical current values along the distance traveled. With an accuracy of +/–40%, electro scan overcomes the drawbacks of CCTV.

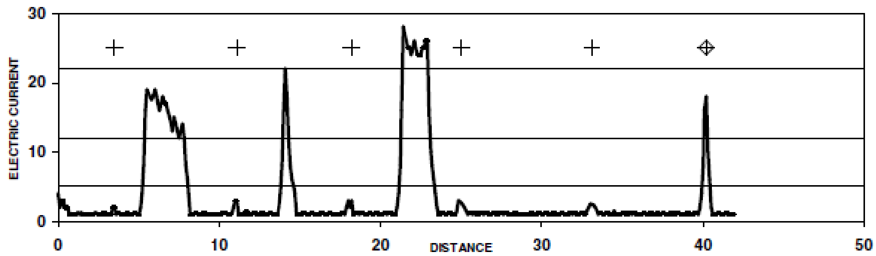

Figure 2.6 An Example of Electro Scan Current Output (Harris and Dobson 2006)

In comparing the CCTV and electro scan equipment, the CCTV camera fails to do the following (Electro Scan 2013):

- Automatically find potential sources of infiltration
- Automatically find leaks inside joints
- Find leaks in service connections
- Locate sources of infiltration at cracks
- Find leak locations
- Quantify leaks in liters per minute
- Find defects that leak from bad couplings
- Find leaks if settled deposits are on the bottom of the pipe
- Conduct inspection if pipe is full of water
- Determine size of leak if root is available

The same report also stated that the productivity rate of a CCTV is 3 feet per minute, whereas that of the electro scan equipment is 50 feet per minute (Electro Scan 2013). This means that the production rate of the electro scan is 16 times greater than that of a CCTV. In some cases, CCTV fails to detect any infiltration. For example, CCTV and electro scan inspections were accomplished in a 500 mm fiberglass pipeline in Switzerland (Electro Scan 2014). The figures below demonstrate situations whereby the CCTV inspection failed to identify infiltration defects. In Figure 2.7, the CCTV caption showed no infiltration; however, the electro scan equipment showed an infiltration of 0.16 liter per second. In another situation from the same pipeline, shown in Figure 2.8, the CCTV showed no infiltration, whereas the electro scan detected a 0.21 liter per second infiltration. Therefore, the electro scan inspection was able to overcome some of the CCTV camera limitations.

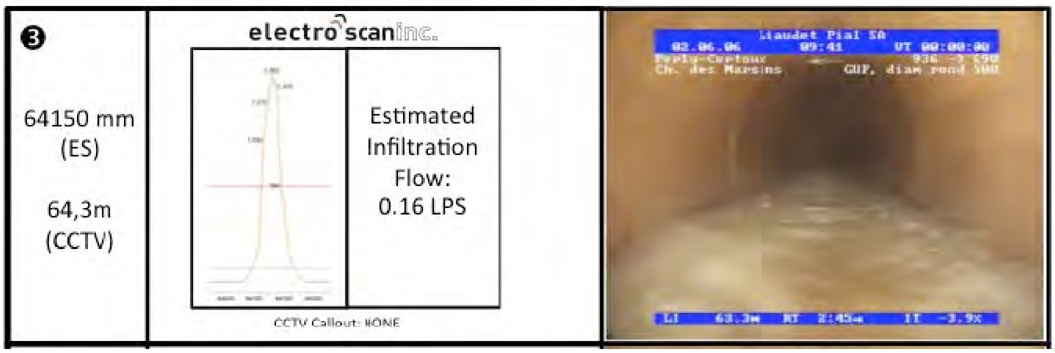

Figure 2.7 CCTV vs. Electro Scan Results, Acquired from Electro Scan Reports

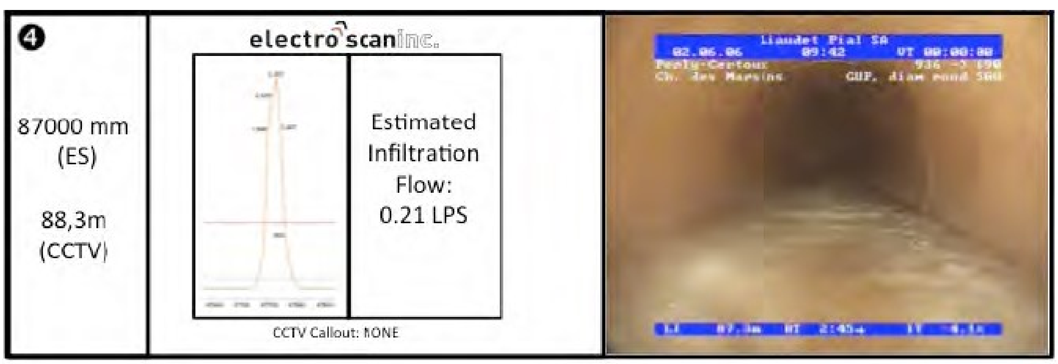

Figure 2.8 CCTV vs. Electro Scan Results, Acquired from Electro Scan Reports

Another case study was conducted in New Zealand to compare electro scan and CCTV camera inspections (O'Keefe 2013). The inspections were run on a total of 15 pipe sections, length of 690 m, on distinct pipeline materials and sizes. The electro scan readings identified 284 pipe defects, whereas the CCTV camera detected only 40 pipe defects. The results showed that the electro scan was able to detect an average of 7.1 times more defects that those detected by the CCTV camera.

Electro scan was able to quantify the total infiltration of the 15 pipe sections to be 301.3 liters per minute.

2.2.3 Sonar

Accumulation of settled deposits in sewer pipelines has received little attention (Mattsson et al. 2014). Accumulation can severely affect the operational performance of the sewer system; in some cases, it may cause sanitary sewer overflows (Mattsson et al. 2014). A number of researchers have pointed out the causes of sewer pipeline blockages. DeSilva et al. (2011) stated that sewer blockage is due to sediments, solids, fat, oil, and grease. Littlewood and Butler (2003) claimed that blockage is due to deposition of solids. Tang et al. (2012) pointed out that sewer blockage is due to fat, oil, and grease.

The most widely used sewer inspection practice is CCTV. CCTV can provide evidence of settled deposits (Martel et al. 2010). However, the current practice depends on flow-line level. Sometimes pipes cannot be cleaned, and the flow line remains in the pipe (U.S. Army Corps of Engineers 2013). CCTV can provide information only above the flow line, which misses information regarding settled deposits (Martel et al. 2010).

Sonar is an application of acoustical technologies. It is based on the implementation of sound energy where the magnitude of the frequency is higher than humans can hear (Birks and Green 1991). Sound beams travel through the inspected material. The waves reflect whenever there is a change in the density of material. Some of the reflected waves pass through the new medium, whereas others return to the surface. The image produced by the sonar sensor is affected by the selection of the acoustic frequency (Andrews 1998). When the acoustic frequency increases, the penetrating power decreases.

Also, travel speed can affect the image quality (Andrews 1998). A speed of 100 mm per second of the device could detect critical defects but might not detect small defects.

Many industries, including medical, aerospace, and oil and gas, have adopted sonar technology (Makar 1999). The sewer inspection industry can apply sonar in any type of pipeline material (Tuccillo et al. 2010), and it is used most often to quantify settled deposits such as grease and debris. A sonar sensor supplied by CUES can reach up to $75,000. However, it is commonly used with a CCTV camera. In sophisticated robots, sonar is used with laser profilers and CCTV cameras.

The sonar sensor is mainly utilized below the flow line to measure the volume of settled deposits. Sonar can provide experts with the total volume of settled deposits and the percentage of blockage in pipes. When using the sonar sensor with laser profilers and CCTV cameras, a 3-D model can be generated to show the existing condition of the pipeline.

Several sonar images will provide the actual condition of the pipeline below the flow line, whereas laser profilers and CCTV cameras will provide information above the flow line. The integration of the laser profiler and sonar provide information about the geometrical shape of the pipeline, demonstrating any deformation, wall loss due to corrosion, and settled deposits on the bottom of the pipeline.

2.2.4 Zoom Camera

Zoom cameras provide still imagery and/or recorded video. Unlike the conventional CCTV camera, a zoom camera remains stationary and records the data where it is installed. The camera is lowered to the manhole while it is mounted on a pole, crane, truck, or tripod. Then it can record the data by zooming in the camera. New cameras can pan and tilt up to 360 degrees.

The production rate of this inspection method may reach up to 1 mile of inspection per day, depending on conditions (Tuccillo et al. 2010). Therefore, many crews adopt this inspection method in order to move quickly. In addition, the method decreases inspection costs and prioritizes pipes for further detailed inspection. Nevertheless, zoom cameras have some drawbacks. Similar to CCTV, the conclusions about the pipe's condition are subjective. Additionally, the recorded video does not give any information about the pipeline's condition below the flow line (Tuccillo et al. 2010). Also, limited resolution and lighting capabilities may result in misleading condition assessment.

2.2.5 Digital Scanning

Digital scanning utilizes cameras. The cameras are installed on a crawler, which moves along the pipeline. Digital scanning uses two types of high-resolution cameras. These two cameras provide information about the sides of the pipeline as well as a circular view of the pipeline, similar to what a CCTV camera does. The inspection rate for this method can reach up to two or three times more than that of the CCTV inspection (Tuccillo et al. 2010). In addition, the operator is free from panning and tilting all the way along the pipeline because digital scanning offers this information automatically. However, it does not provide information below the flow line, and the recorded data's conclusions are subjective.

2.2.6 Gamma-Gamma Logging (GGL)

In GGL, gamma rays are emitted from a source and then reflected when obstructed by a material. The backscattered rays are detected in proportion to the density of the surrounding material. The GGL equipment consists of a probe with a radioactive material, which is used as the gamma source (Tuccillo et al. 2010). In addition, the equipment consists of a scintillation receiver to detect the gamma rays. When it receives the radiation, a crystal inside the scintillation receiver sends out light pulses. Those pulses are then changed to electrical signals. This equipment is installed on a crawler and used to detect any cavities in soil surrounding the pipe (Eiswirth et al. 2001).

2.2.7 Infrared Thermography

Infrared radiation flows from warm to cool places. This principle applies to any material. However, each material retains heat differently, as each has distinct insulating properties. This concept has been applied to sewer inspection. Infrared thermography utilizes a camera to measure the infrared radiation of the pipeline's surface. The system contains an infrared sensor, an optics head, a microprocessor, a monitor, data acquisition, analysis equipment, image recording, and retrieving devices (Tuccillo et al. 2010).

2.2.8 Pipe Penetrating Radar (PPR)

This method applies the theory of a radar system, where an antenna produces high-frequency radio waves (Feeney et al. 2009). PPR is applied in-pipe, so the signal will penetrate the pipe's wall to the surrounding soil (Sterling et al. 2009). The system can operate using two or three antennas that are able to detect several frequencies to evaluate the surroundings and the structure of the pipe itself. The SewerVUE robot, which applies the concept of PPR, can provide information about the wall's thickness, rebar's alignment, cover, and the condition of the pipe's liners for nonferrous pipe materials. The robot is also equipped with CCTV and LIDAR technologies (SewerVUE 2014).

2.2.9 Multisensor Technology

Many researchers have proposed inspecting sewer pipelines using several sewer condition inspection technologies to detect several defects in a single inspection (Eiswirth et al. 2001, Kuntze and Haffner

1998). Other than CCTV, multisensor robots may include several sophisticated sensors like sonar, a laser profiler, infrared, and radioactive. Some of the multisensor robots follow:

- KARO
- PIRAT
- KURT
- KANTARO

KARO is a German robot that contains multisensors for sewer inspection. The robot includes CCTV and 3-D optical, ultrasonic, and microwave sensors. The microwave is adopted to evaluate the condition beyond the pipe's wall. The 3-D optical is used to measure the deformation defect by applying triangulation techniques. KARO utilizes a sensor fusion based on fuzzy logic for defect detection (Morrison and Thomson 2003). PIRAT is a system developed by Melbourne Water and CSIRO. The system can collect in-pipe data and interpret the information through an analysis system. A laser produces a beam of light to measure the pipe's radius. Additionally, the system includes a sonar scanner to measure the dimensions below the flow line. The interpretation system applies artificial intelligence techniques to detect and classify the pipeline's defects (Morrison and Thomson 2003). Sewer assessment with multisensors (SAM) is another German development for sewer inspection and assessment. The platform includes sensors such as acoustical and geoelectrical, gamma-gamma, radiometric probe, hydrochemical, microwave, and 3-D optical. The collected data can be interpreted by a neuro-fuzzy based on multisensor fusion (Morrison and Thomson 2003).

2.3 Sewer Pipeline Materials

Many types of pipeline materials are used in the sewer network industry, and each has its own characteristics. Popular pipeline materials include cast iron, ductile iron, steel, asbestos cement, plain cement concrete, reinforced concrete, brick, plastic (PVC), high-density polyethylene (HDPE), vitrified clay, and glass fiber reinforced plastic (GFRP).

In the past, bricks were used for sewer networks; however, today's infrastructure utilizes different pipe materials, depending on the municipality. Selecting a specific material depends on several factors (ACPA 1980, EPA 2000, NPTEL n.d.): cost, availability, hydraulic characteristics, resistance to corrosion and abrasion, strength and durability, weight, and imperviousness.

Nevertheless, the key characteristics in the selection of the material are the interior and exterior corrosion resistance, the scouring factor, leak tightness, and hydraulic characteristics (EPA 2000). Pipe manufacturers use specific standards set by the American Society of Testing Materials (ASTM) and the American Water Works Association (AWWA) in manufacturing pipelines. These standards are essential, as they cover the manufacturing process and specify the size and dimensions such as the inside and outside diameters and wall thickness (EPA 2000).

2.4 Automation in Infrastructure

Automation is applied to get fast, accurate, and reliable results. Many researchers have adopted this method in the infrastructure field. It has been used in assessing the condition of highways, bridges, water networks, sewer networks, and tunnels. There are many automation techniques that can be used for this purpose. This section provides some of the previous research in the automation of assessing the condition of infrastructure, mainly in sewer systems.

Many techniques were utilized to detect multiple defects. For example, Yang and Su (2009) developed a methodology to detect broken pipes, cracks, and open joint defects. They used CCTV data to segment pipe defects from CCTV images. On a gray-scale (intensity) image, they applied an erosion operation, followed by dilation with certain structuring elements. They compared rectangular and disk structuring elements to produce the optimum smoothing effect. They concluded that a disk structuring element of radius 4 should be used. As they stated, these operations were adopted to segment the pipe's defects. Later on, they implemented Otsu's technique to find the appropriate threshold value for the gray-scale image, to transform it to a binary image. The segmented defects of the original images were then reviewed for morphological features: area, major axis length, minor axis length, eccentricity, and the major to minor axis length ratio.

In addition, an automated tool detected pipeline cracks, deflections, and discontinuity defects (Duran et al. 2002). The authors developed a multisensor data processing algorithm. They proposed that a laser profiler and a CCD camera could measure the drained pipeline geometry while a sonar scanner measures the flooded part. According to the researchers, the assembly of a laser profiler and a CCTV camera had many advantages over the traditional CCTV inspection method. Because the differential information was adopted, there was no need for any reference level of intensity. The entire pipeline segment could be inspected simultaneously. The output image of the assembly was an elliptical shape of the existing interior pipeline geometry. Hough transform was used to fit the elliptical shape into a cone equation. However, some image processing tools were used before the Hough transformation. They increased the contrast of the images so that the elliptical shape was easier to distinguish. Later, the researchers used the Canny edge detection method to segment the elliptical shape from the original image. With the multiple frames of the inspections, the authors were able to find cracks from the intensity variations.

Expanding the number of the aforementioned defects, Duran et al. (2007) were able to use the raw data of the camera/laser-based profiler to analyze the data using a neural classifier tool. They followed the same segmentation process in detecting the elliptical shape of the camera/laser-based images. After that, they extracted the features by intensity and surface computations. Later, they were able to obtain the intensity map, intensity surface map, and surface maps. Surface maps were cut into the cylindrical polar pipe surface and unwrapped on the x-axis (displacement), y-axis (intensity map), and z-axis (surface map). Their research provided a general method based on an artificial neural network to classify the defective and nondefective areas. They studied and classified holes, longitudinal cracks, radial cracks, joints, and obstacles. Also, cracks and deformation defects were automated to assess the structural condition of sewers (Xu et al. 1998). The authors extracted the joint structures in the images by applying image processing techniques: edge detection and binary image thresholding. They also used Fourier transforms and distortion computations to fill the curves of the joint-bottom area.

An image processing tool detected corrosion, pipe connections, roots, and holes (Mashford et al. 2007, 2009, 2010b). The authors suggested the pixel-based approach of unfolded color images. They also utilized the support-vector machines to distinguish region of interest (ROI) into several divisions. The authors also employed some morphological operations to identify the flow-line regions and pipe joints.

Likewise, Chae and Abraham (2000) used SSET images to detect multiple defects such as joints, cracks, laterals, and corrosion and implemented image processing tools and the ANN application. The authors applied filtering and gray-scale transformation isolation of regions. After the image processing approach, the ANN was used to identify the defects mentioned above. Each defect has its own network. The output of the ANN of each defect included the parametric characteristics of the defect. For more accurate results, they used fuzzy logic.

Halfawy and Hengmeechai (2014) proposed a methodology for crack detection using image processing. Their methodology was based on CCTV output images. The images were subjected to a preprocessing step by detecting a group of cracks from the original images. They used the Sobel edge detection method to segregate the cracks as a binarized image. Next, they used the Hough transform to remove unwanted image labels. The Hough transform enabled the authors to eliminate the rectangular labels found in CCTV images. After that, the isolated cracks were filled by a closing operation with a disk structural element of a radius of 5. They also filled the gaps between the detected edges to form a connected crack. Unwanted pixels that did not correspond to cracks were filtered. The authors were able to use morphological erosion with 10-pixel long and several angles to split the horizontal cracks from the vertical cracks in an image.

Sinha and Fieguth (2006) proposed an algorithm for crack detection features in concrete pipelines. They began by transforming the original images to gray-scale images. Their steps involved using statistical characteristics, first crack detector, and second crack detector to obtain crack features from the segmented images. They used a linking procedure to connect missing pixels from the actual crack detected. The authors identified minor, major, multiple, mushroom, transverse, and longitudinal cracks using their approach.

In another operation, infiltration defects were detected using a combination of ANN and an image processing approach (Moselhi and Shehab-Eldeen 1999b, 2000). The authors employed image processing techniques for segmentation image analysis and feature extraction and ANN for the automation detection and classification of infiltration defects in sewer pipelines (Shehab-Eldeen and Moselhi 2005). In addition, flow lines in an image were detected by Kirstein et al. (2012). The authors suggested an algorithm to detect the flow lines on digital scanning unfolded images. In their research, they used image processing tools such as the Canny edge detection method, the Hough transform, and Dijkstra’s shortest path algorithm.

The change detection technique can be used to compare a reference image with other images to detect defects. Guo et al. (2009) proposed a methodology for automated defect detection and classification for sewer pipelines. In fact, there was no detailed approach concluded. However, change detection was considered in the automated defect detection. They conducted preprocessing methods before moving to image classification. Images were passed for image histogram matching and equalization to reduce the illumination effect. Later, noise was removed from the images. The authors used a reference CCTV image with no defects and other images containing defects for image subtraction. An automated change detection between the images was established.

Other than using automation in sewer pipelines, image processing techniques were also utilized in other assets. For example, Cheng and Miyogim (1998) employed image processing in the evaluation of pavement distress. They utilized image enhancement, image thresholding, analysis, classification, and severity. Also, Abdel-Qader et al. (2003) utilized an image processing technique for bridge evaluation. The authors applied four types of edge detection techniques to detect cracks in the images and compared their performance: Canny, Sobel, fast Fourier transform, and fast Haar transform. They concluded that the fast Fourier transform was the most reliable edge detection method in identifying bridge cracks.

Likewise, Maode et al. (2007) employed image processing methodology to detect cracks in pavement. The researchers used images that contained pavement cracks and used four structural elements in the process of separating cracks from the images. The spaces between cracks were filled using morphological operations. In another related work, Marchewka (2010) adopted an image processing procedure to detect cracks in pavement images. The first-level approach was identifying the lowest and highest intensity values in the horizontal and vertical directions of the image. These points were predicted as points that fall on the crack section. Later, the author showed that the lines connecting each pair of those points were claimed as cracks.

In a study related to concrete, Fujita et al. (2006) adopted an image processing tool to detect cracks in concrete surfaces. The image used had noise levels that were a result of illumination. The authors adopted a preprocessing tool to eliminate the noise level before applying a linear filtering and thresholding technique to isolate cracks from the background.

2.5 Image Processing

Humans' vision is based on a 3-D domain. They recognize multiple surroundings by what their eyes receive from information. Information is then translated by the database available in their brains. Similarly, computer image processing methods are applied to imitate the use of the human brain in translating digital images. Unlike common human vision, computer image processing is mostly based on 2-D images. It uses several algorithms in applying multiple operations on digital images (Kumar and Nanda 2008). It is the most popular topic in the field of information technology (Chan et al. 2010).

Huge efforts are made to implement image processing in construction automation (Hastak and Skibniewski 1993). Experts agree that automation in pipeline inspection can save significant time and money. It also increases accuracy and consistency (Gutierrez 2005). The computer vision tool utilizes the methods of mathematics, artificial intelligence, and pattern recognition (Besel et al. 1985). After applying some form of algorithm, the output can be an image, a set of characteristics, or parameters that are related to the original image. Simply, it allows the computer to understand the content of the image by defining certain parameters.

This research employed image processing techniques to analyze images and quantify defects. Common image processing operations were used, as explained in the next section.

2.5.1 Common Image Processing Procedures

Image processing has many applications. However, a common process is summarized in Figure 2.9. The first step of image processing is image acquisition, which can be acquired from a camera or other technology. An image is considered a discrete representation of data holding its spatial and color characteristics (Solomon and Breckon 2011). The image is exposed to several image processing operations.

The contrast of an image can be adjusted using image intensity adjustment tools. Additionally, structuring elements are utilized to define a matrix with certain shapes and specific parameters that can be used to isolate the regions of interest. Dilation can thicken narrow objects, while erosion removes small isolated pixels or breaking part joints. Some of the images processed may acquire a significant degree of noise, which can be reduced by noise removal operations. Noise in an image is defined as a sequence of irrelevant disturbances that arise during image recording (Solomon and Breckon 2011).

One major part of image processing is image segmentation. The main goal of image segmentation is to separate objects from the original image. Thus, the output image includes the segmented objects (Solomon and Breckon 2011). Intensity thresholding and edge detection are two examples of image segmentation. The idea of intensity thresholding is to choose a certain threshold value. Any pixel that is greater than the threshold value is assigned a 1 region (on). However, values that are below the threshold value are assigned as a 0 pixel (off). The outcome is a binary image from the gray-scale image. In contrast, edge detection represents a large number of techniques (Law et al. 1996) and is considered the easiest option to find edges in the images. Edges can be distinguished in the image as areas of intensity transitions between objects. There are several edge detection methods: Sobel, Prewitt, Roberts, Canny, and Laplacian of Gaussian (LoG). Some problems accompany the approach, as edges may not be identified by the edge detection methods. Those problems occur because of image noise if the real edge does not make any border in the image or if a nonreal edge is identified. However, Solomon and Breckon (2011) claimed that the Canny method is the best edge detection technique.

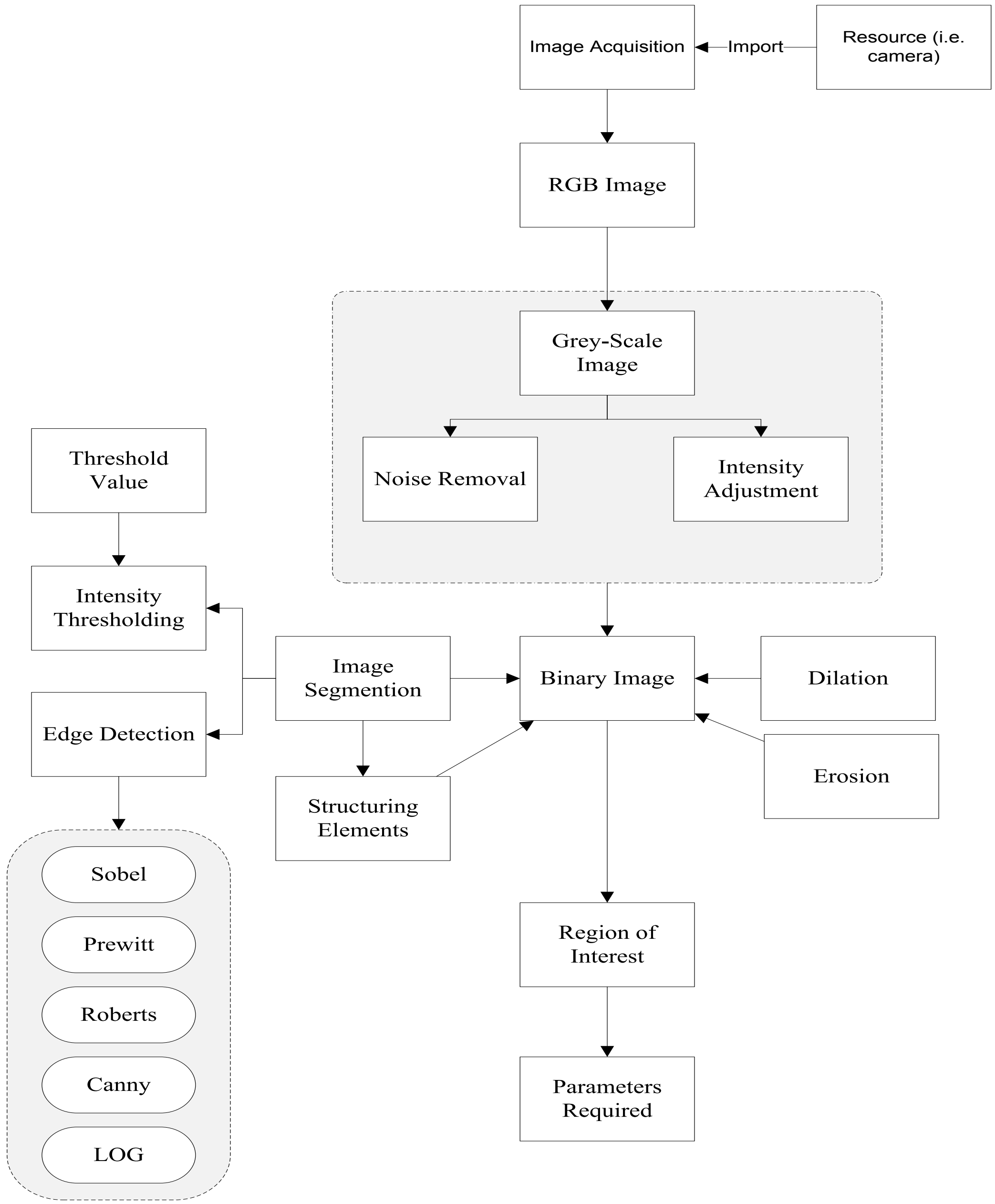

Figure 2.9 Common Image Processing Procedure

2.6 Condition Assessment Models

Condition assessment is a vital tool for infrastructure asset management. This section explains the current practices utilized in assessing the condition of an asset, mainly in sewer systems. Several condition assessments of sewer studies were conducted. The techniques developed were inspired by the assessment and deterioration models for bridges and pavements (Abraham et al. 1998).

Fuzzy logic was used to develop condition assessment models. For example, Yan and Vairavamoorthy (2003) developed a fuzzy approach in their sewer condition assessment. Several linguistic criteria were translated into numerals, using the fuzzy approach theory, to assess the condition of sewers. The numerals translated information was used to propose a model that ranked the pipes according to their conditions. The major linguistic variables considered in the model were the environmental conditions surrounding the pipe and the traffic density.

Another condition assessment model was designed using the ANN (artificial neural network) approach. For instance, Kulandaivel (2004) proposed a model based on a trained ANN, which was able to predict the condition of sewer pipelines depending on the historic condition assessment information. Later, the model was tested and validated. Likewise, Najafi and Kulandaivel (2005) proposed an ANN model using historical data in assessing sewers.

Support vector machines (SVMs) were used to assess the condition of sewer pipelines as well (Mashford et al. 2010a). The authors developed four SVM models. The first model used the intrinsic characteristics of the asset such as its age, diameter, and material. The second model used soil characteristics in addition to the first model inputs. The third model used the inputs of the first model and added grade and angle information. The fourth model considered all sewer characteristics, sewer configurations, and the surrounding environment.

Condition assessment models were developed utilizing ANN and other accompanying techniques. As an example, Chae and Abraham (2001) combined the use of ANN and fuzzy logic to accurately analyze and interpret the data for sewer pipeline condition assessment. However, Sousa et al. (2014)

used ANN and SVM methods to predict the structural condition of sewer pipelines. They collected complete data about the pipelines, including material type, diameter, size, length, age, depth, and slope. They also computed the design flow velocity and entered it as a variable in their model. The authors grouped the condition of pipes into two categories. The first category, conditions 1, 2, and 3, included "sewers that do not require immediate intervention." The second category, conditions 4 and 5, included sewers that "require immediate intervention." Sousa et al. then quantified the uncertainties associated with ANN and SVMs.

Sewers were also assessed utilizing simulation models. Ruwanpura et al. (2004) developed a rule-based simulation model to predict the condition of sewers. The simulation model included CCTV data analysis. Later, the authors developed the actual probability of existence (APE) from the data collected. The model considered the characteristics of the pipe, such as the age, material, length, and APE value. Also, Stein and Partner (2005) used a Monte Carlo simulation to analyze the environmental impacts defects caused in sewer systems. The results obtained from the simulation proposed a link between the local ancillary condition and the unique sewer defect attribute. Additionally, Denys et al. (2004) proposed a model that simulated the factors that affected the sewer system. The model was able to indicate the level of performance of the system by "moduli." In addition, from the data collected, the authors used statistical analysis to evaluate risks.

Others, however, adopted logistical models to assess the condition of an asset. Ariaratnam et al. (2001) used historical data in developing logistical models to evaluate the condition of sewers. The models proposed helped decision makers manage and plan for future inspections. The model probability was developed by using pipe characteristics such as age, diameter, and type of waste. Additionally, the authors adopted a sensitivity analysis to validate their model. They concluded that the quality of the results highly depended on the quality of the data collected.

Chughtai and Zayed (2008) recommended a methodology for predicting the structural and operational condition of sewers using regression models. Historical data was used to develop models for each sewer pipeline material: concrete, asbestos cement, and PVC. Baur and Herz (2002) also used historical data to construct transition curves to predict the condition of sewers. Fenner et al. (2000) suggested a model to predict the likelihood of sewer failure in a grid square. The model was built by analyzing the pipe information in grid squares defined by GIS software. Based on global and local matrices, each grid had a consequence factor. Later, a 2-D risk plot built after combining the likelihood and consequence values facilitated identifying the "critical grid squares." In an effort to enhance the application of the CUES total pipe score formula, Islam et al. (2009) developed a condition grading system, which described the status of the pipe from A (no obvious defects) to D (failure or failure obvious).

Harvey and McBean (2014) used the random forests algorithm to predict an individual sewer pipe's structural condition. They were able to distinguish the uninspected pipeline, which was likely structurally defective, for future inspection. The authors established a classification task in a binary format (good or bad pipes); later, they used the receiver operating characteristic (ROC) curves to "establish alternative cutoffs for predicted class probability." The authors claimed that the results illustrated a successful option for predicting the condition of individual sewer pipes.

2.7 Multi-Attribute Utility Theory (MAUT)

MAUT is an evaluation scheme that evaluates objects, products, and services. It is one of the popular decision-making techniques used in several industries. It is designed to handle the trade-offs among multiple objectives. MAUT is based on the expected utility theory (Savage 1954). The expected utility theory states that if a utility is assigned to a possible consequence and the predicted utility of each alternative is found, the best alternative will be that with the highest score (Ananda and Herath

2005). With different criteria considered, the utility functions are used to convert numerical attribute scales to utility unit scales. Hence, it allows direct comparison of different measures.

The MAUT method provides the decision maker with an overall condition of an object or a product. An object is evaluated by several value dimensions, which can be a criteria of the same object being evaluated. To clarify the point, the selection of *n* number of cars can depend on the value of the dimensions of each car's horsepower, maximum speed, and year of production.

Schäfer (2001) provided an explanation for the MAUT application as follows:

The overall evaluation is described by the following overall value function

$$v\,(\mathrm{x}) = \sum_{\mathrm{i}=1}^{\mathrm{n}} w_i\, v_i\,(x)\ [2.1]$$

Where $v_i\ (x)$ is the evaluation of the object on the i-th value dimension, and w_i is the weight determining the impact of the i-th value of the dimension of the overall evaluation; in other words, it is the relative importance (Schäfer 2001). Variable n is the number of different value dimensions. The summation of w_i shall equal 1.

$$\sum_{i=1}^{n} w_i\ = 1\ \ [2.2]$$

For each value dimension d_i, the evaluation $v_i(x)$ is defined as the evaluation of the relevant attributes.

$$\sum_{ae\ Ai}^{n} w_{ai}\, v_{ai}\,(l(a))\ \ [2.3]$$

Where A_i is the set of all attributes relevant for d_i, and $v_{ai}(l(a))$ is the evaluation of the actual level $l(a)$ of attribute and d_i. The weight determining the impact of the evaluation of attribute a on value dimension d_i is w_{ai} (Schäfer 2001).

2.8 Sewer Protocols

As discussed earlier, sewer infrastructure is an important asset for every city. Therefore, sewer coding and condition assessment is of great significance in acquiring critical information about the network (Thornhill and Wildbore 2005). Many protocols and codes clearly explain sewer network defects. Thornhill and Wildbore (2005) demonstrated the history of sewer condition assessment protocols, as shown in Figure 2.10.

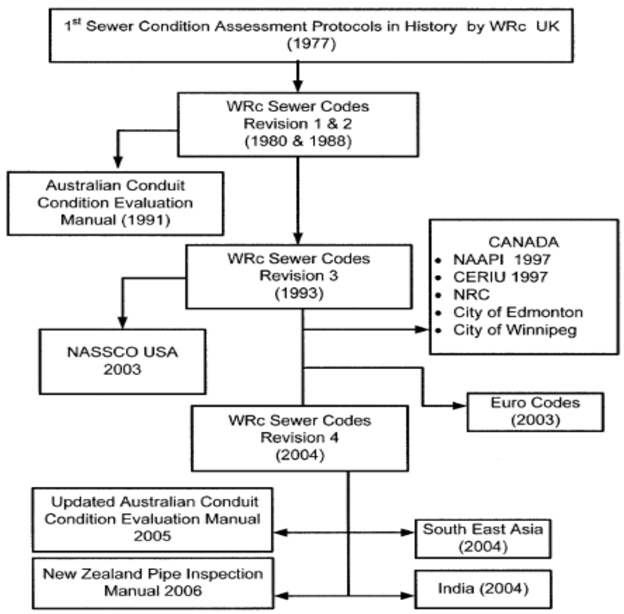

Figure 2.10 History of Sewer Condition Protocols (Thornhill and Wildbore 2005)

2.8.1 Water Research Centre (WRc) Protocol

In 1977, the Water Research Centre (WRc) in the United Kingdom developed the first sewer condition assessment protocol and in 1980, published the first sewer condition classification. Figure 2.10 shows that different countries follow distinct protocols to assess sewer network conditions. However, the WRc sewer assessment condition is accepted worldwide (Chughtai 2007) and adopted by many municipalities. Some countries, like Canada, have designed their own sewer coding systems. The National Research Council (NRC) based its coding concepts on the WRc theory. The structural and service condition ratings of the pipeline are based on the correspondent number of defects. A pipeline assessed by the WRc coding system receives a number from 1 to 5 (WRc 2004); the number reflects the condition of the pipeline inspected. The severity of WRc condition grades and the rehabilitation priorities are explained in Table 2.1 (WRc 2004). After grading the pipeline, its condition can be judged using the description in the table. Additionally, the rehabilitation priority can be signaled, accordingly.

Table 2.1 WRc Grade Description and Rehabilitation Priority

Grade	Description	Rehabilitation Priority
1	Acceptable condition	Not Required
2	Minimal collapse but potential for further deterioration	Low
3	Collapse unlikely but further deterioration likely	Medium
4	Collapse likely in near future	High
5	Collapse imminent or collapsed	Immediate

The condition grades (1–5) are found by calculating the score based on each defect detected in each pipeline. The operator assigns the value for each defect and determines the consequence a defect may cause for the pipeline. The total score describes the addition of all deduct values; however, the peak score (equation 2.4) reflects the maximum deduct value. Thus, it explains the magnitude of the most severe defect in a segment. The mean score (equation 2.5) represents the overall condition of a pipeline and can be found by the average scores per unit length (WRc 2004).

$$Peak\ Score = Maximum\ Deduct\ Value \quad [2.4]$$

$$Mean\ Score = \left(\frac{\Sigma Deduct\ Value}{Length\ of\ Pipe}\right) \quad [2.5]$$

According to the WRc protocol (2004), sewer pipeline defects are divided into two major categories: structural and operational.

2.8.1.1 Structural Defects

Structural defects of a sewer pipeline reflect its physical condition. The scores of each defect depend on the severity of the defect and the pipeline material. Table 2.2 lists some of the structural defects considered by WRc (2004), including defect details, defect scores, and unit of measure. According to the table, many of the defects have multiple details depending on their severity. The more is the defect score, the more severe is the case.

Table 2.2 WRc Structural Defect

Defect Type	Defect Detail	Defect Score	Unit
Crack	Circumferential	1	Per crack
	Longitudinal	2	Per crack
	Multiple	5	Each
Fracture	Circumferential	8	Per fracture
	Longitudinal	15	Per fracture
	Multiple	40	Each
Deformation	<5%	20	Each
	6%–10%	80	Each
	>10%	165	Each
Hole	Radial extent <1/4	80	Each
	Radial extent >1/4	165	Each
Broken Pipe	Broken Sewer	80	Each
Collapsed Pipe	Collapsed Sewer	165	Each
Joint Opening	Slight	0.1	Per joint
	Medium	0.5	Per joint
	Large	2	Per joint
Joint Displacement	Slight	0.1	Per joint
	Medium	0.2	Per joint
	Large	5	Per joint
Surface Damage	Increased Roughness/Surface Wear Slight	5	
	Increased Roughness/Surface Wear Medium	20	
	Increased Roughness/Surface Wear Large	120	
	Spalling Slight	5	

Table 2.2 WRc Structural Defect (continued)

Defect Type	Defect Detail	Defect Score	Unit
Surface Damage	Spalling Medium	20	
	Spalling Large	120	
	Aggregate Visible	5	
	Aggregate Projecting from Surface/Surface Wear Medium	20	
	Reinforcement Visible	120	

The overall structural condition grade of a pipe segment can be calculated from the peak structural scores found in the same segment. Table 2.3 describes the peak scores and their corresponding overall structural grades. The lowest grade is 1 when the peak score is less than 10; the highest grade is 5 when the peak score is 165 or more.

Table 2.3 Structural Peak Score

Overall Structural Condition Grade of a Pipe Segment	Peak Structural Scores Found in the Same Segment
1	<10
2	10–39
3	40–79
4	80–164
5	165 or more

2.8.1.2 Operational Defects

These defects define the operating capability of a sewer pipe to serve its main task in transporting the sewer medium as designed. Operational condition rules and guidelines are similar to the guidelines of the structural conditions described earlier. Condition grades for the structural condition and operational condition can be calculated. Nevertheless, WRc is unable to represent the condition of the pipe with one index for the combined action of the structural and operational conditions. Some of the operational defects are presented in Table 2.4, where the defect details and defect scores are tabulated. The lowest defect score observed is 1; the highest is 10.

Table 2.4 WRc Operational Defects

Defect Type	Defect Detail	Defect Score
Encrustation	Light	1
	Medium	2
	Heavy	5
Debris	Blockage <5%	1
	5%–20%	2
	20%–50%	5
	50%–75%	8
	>75%	10
Obstruction		10
Infiltration	Seeping	Seeping
	Dripping	Dripping
	Gushing	Gushing
Roots	Fine	1
	Tap	5
	Root <5%	2
	5%–20%	4
	20% or more	10

After calculating the mean operational score of each pipeline and the peak value, the overall operational condition of each segment is found according to Table 2.5 (WRc 2004). When the mean defect score and the peak operational score are less than 0.5 and 1, respectively, the overall operational grade is 1. When the mean defect score and the peak operational score are equal to or greater than 5 and 10, respectively, the overall operational grade is 5.

Table 2.5 WRc Operational Peak Score

Overall Operational Condition Grade of a Pipe Segment	Peak Operational Scores Found in the Same Segment	Mean Defect Score of Each Pipeline
1	<1	<0.5

Table 2.5 WRc Operational Peak Score (continued)

Overall Operational Condition Grade of a Pipe Segment	Peak Operational Scores Found in the Same Segment	Mean Defect Score of Each Pipeline
2	1–1.9	0.5–0.9
3	2–4.9	1–2.4
4	5–9.9	2.5–4.9
5	>10	>5

2.8.2 New Zealand Protocol

The New Zealand pipeline inspection manual is another sewer condition assessment protocol used in the industry. It provides technical specifications and practice methodologies to carry out CCTV inspection (NZWWWA 2006). Scoring analysis depends on CCTV inspection and the evaluator's judgment. The process involves assigning weighted scores, provided by the manual, to the defects observed in the recorded video. The weighted scores depend on the influence of the structural condition and the serviceability of the pipeline. Once the weighted scores are assigned, mean and peak scores are calculated. The calculated values are compared with the thresholds to determine the state of the pipeline. The condition rating is generated from the frequency and the severity of the defects. The severity codes and scores (Table 2.6) considered in the protocol are S, M, and L. Code S is small, code M is medium, and code L is large. Defects not expected to cause problems in the near future are coded S. However, defects with potential failure in the long term are coded M, and defects that require immediate attention are coded L.

Table 2.6 New Zealand Severity Codes

Severity Code	Severity Score
S	Defects that should not cause a problem in the near future and/or could have the potential to deteriorate in the long term. In general, the score is less than 10 points.
M	Defects with little short-term failure risk, yet potential failure in the long term. Attention is required but is not urgent. In general, the score is between 10 and 25 points.
L	Defects for which there is an immediate risk of failure or severe service interruption. In general, the score is 30 points or more.

The New Zealand sewer protocol uses peak score and mean score values in grading the sewer pipelines. Peak score represents the magnitude of the worst defect in each pipeline. It is the maximum defect score for any length of the pipe. The mean score reflects the overall condition of the pipeline. It is the average of the defect scores per meter of the pipeline.

2.8.2.1 Structural Defects

The structural defects of a sewer pipeline reflect its physical condition. There are several criteria considered in evaluating the structural condition of the pipeline, such as the defects that reduce the service life of the pipeline and lead to failure. Some of the structural defects provided by the New Zealand protocol with their condition ratings are listed in Table 2.7. The table provides the condition rating score as small, medium, and large. The description of the defect is included in the column labeled Defect Detail. According to the table, the most critical defect is when the pipeline collapses, as its corresponding score is 100.

Table 2.7 New Zealand Structural Defects

Description	Condition Rating Score	Defect Detail	Score
Crack Circumferential	S	Crack visible but not open	2
	M	Crack open but no evidence that the crack extends to the outside wall	15
	L	Crack open and evidence that it extends through to the outside wall	30
Crack Longitudinal	S	Crack visible but not open	3
	M	Crack open but no evidence that the crack extends to the outside wall	15
	L	Crack open and evidence that it extends through to the outside wall	30
Crack Multiple	S	Crack visible but not open	10
	M	Crack open but no evidence that the crack extends to the outside wall	20

Table 2.7 New Zealand Structural Defects (continued)

Description	Condition Rating Score	Defect Detail	Score
Crack Multiple	L	Crack open and evidence that it extends through to the outside wall	40
Deformation	S	Not used	
	M	Deformation 10% or less	15
	L	Deformation greater than 10%	65
Hole	S	The hole has been repaired	5
	M	The hole is up to 20% of the pipe circumference and has not been repaired	25
	L	The hole is greater than 20% of the pipe circumference and has not been repaired	40
Broken Pipe	S	Damage extends up to 10% of the circumference; parts of the pipe are displaced by less than half the pipe wall thickness	15
	M	Damage extends between 10% and 25% of the circumference, and parts of the pipe are displaced by less than half the pipe wall thickness or parts of the pipe are displaced between half the pipe wall thickness and the full pipe wall thickness	30
	L	Damage extends over 25% of the circumference, and parts of the pipe are displaced by less than half the pipe wall thickness or parts of the pipe are displaced by more than the pipe wall thickness or pieces of the pipe have totally dislodged. Alternatively, the pipe is close to collapse, in which case alert the engineer immediately	75
Collapsed Pipe	S	N/A	
	M		
	L	Pipe no longer functions	100
Joint Opening	S	Displacement is less than 20 mm	0
	M	Displacement is 20 mm to 40 mm	5
	L	Displacement is greater than 40 mm	25
Surface Damage	S	Superficial only. Cement lining spalled from steel pipe	3

Table 2.7 New Zealand Structural Defects (continued)

Description	Condition Rating Score	Defect Detail	Score
Surface Damage	M	Aggregate exposed or pipe wall otherwise significantly affected. Cement lining spalled from steel pipe and evidence of corrosion in the steel	20
	L	Reinforcing exposed or no longer present due to corrosion, severe corrosion, or deep voids in pipe wall	60
Infiltration	S	Infiltration seeping or dripping	2
	M	Running flow	15
	L	Gushing	30

2.8.2.2 Service Defects

Service defects are similar to operational defects. These defects cause interruption to the pipe's operational task. Table 2.8 lists the type of defects, the three linguistic condition rating scores, defect details, and the corresponding scores. The three linguistic rating scores explain the severity of each defect. The more severe is the case, the larger is the score.

Table 2.8 New Zealand Sewer Protocol Service Defects

Description	Condition Rating Score	Defect Detail	Score
Encrustation	S	The clear diameter is reduced by less than 10%	0
	M	The clear diameter is reduced by 10% to 25%	5
	L	The clear diameter is reduced by more than 25%	20
Silty Debris	S	The clear diameter is reduced by less than 10%	8
	M	The clear diameter is reduced by 10%–25%	20
	L	The clear diameter is reduced by more than 25%	40
Greasy Debris	S	The clear diameter is reduced by less than 10%	8

Table 2.8 New Zealand Sewer Protocol Service Defects (continued)

Description	Condition Rating Score	Defect Detail	Score
Greasy Debris	M	The clear diameter is reduced by 10% to 25%	20
	L	The clear diameter is reduced by more than 25%	40
Obstruction Permanent	S	The clear diameter is reduced by less than 10%	10
	M	The clear diameter is reduced by up 10% to 25%	20
	L	The clear diameter is reduced by more than 25%	35
Obstruction Temporary	S	The clear diameter is reduced by up to 10%	8
	M	The clear diameter is reduced by 10% to 25%.	20
	L	The clear diameter is reduced by more than 25%	40
Roots	S	Roots restrict flow by 10% or less of full flow	5
	M	Roots restrict flow by 10% to 25% of full flow	25
	L	Roots restrict flow by more than 25% of full flow	70

2.8.3 Concordia Sewer Protocol (CSP)

Similar to the previous protocols, CSP, developed by Daher (2015), evaluates the sewer system. It was built using fuzzy synthetic evaluation. The defects were divided into three groups: structural, operational, and installation. The analytical network process (ANP) was applied to obtain the priorities of components, defect groups, defects, and defect types. Later, fuzzy membership functions were developed for each defect to fuzzify the severity of the defects. The overall scale used in the protocol was 0 to 10; it was changed to 1 to 5 to represent the overall condition of the sewer system (Table 2.9). The sewer systems are graded as excellent, good, fair, poor, and critical; they are interpreted as number ranges. The worst is the case, the closest the grade is to 10.

Table 2.9 CSP Condition Grading Scale

Linguistic	Grade
Excellent	0–1

Table 2.9 CSP Condition Grading Scale (continued)

Linguistic	Grade
Good	1–3
Fair	3–6
Poor	6–8
Critical	8–10

2.8.3.1 Structural Defects

The protocol considered several structural defects, which explained the physical condition of the pipeline. Table 2.10 lists the structural defects of the CSP. Based on the table, the description and its corresponding grade are described. Some defects include the five linguistic grades, whereas others have only the critical linguistic grade.

Table 2.10 CSP Structural Defects

Defect	Grade	Description
Longitudinal Crack	Excellent	0–1 crack per unit length; no leakage
	Good	1–2 cracks per unit length; no leakage
	Fair	2–3 cracks per unit length; leakage
	Poor	>3 cracks per unit length; leakage
	Critical	N/A
Circumferential Crack	Excellent	0–1 crack per unit length; no leakage
	Good	1–2 cracks per unit length; no leakage
	Fair	2–3 cracks per unit length; leakage
	Poor	>3 cracks per unit length; leakage
	Critical	N/A
Spiral Crack	Excellent	0–1 crack per unit length; no leakage
	Good	1–2 cracks per unit length; no leakage
	Fair	2–3 cracks per unit length; leakage
	Poor	>3 cracks per unit length; leakage
	Critical	N/A
Multiple/Radiating Crack	Excellent	N/A
	Good	N/A
	Fair	N/A
	Poor	N/A
	Critical	Always

Table 2.10 CSP Structural Defects (continued)

Defect	Grade	Description
Longitudinal Fracture	Excellent	0–1 fracture per unit length or single fracture with 5 mm width with visible opening
	Good	1–2 fractures per unit length or 5–10 mm wide single fracture
	Fair	2–4 fractures per unit length or 10–20 mm wide single fracture
	Poor	4–5 fractures per unit length or 20–25 mm wide single fracture
	Critical	4–5 fractures per unit length or >25 mm wide single fracture with no transverse displacement
Circumferential Fracture	Excellent	0–1 fracture per unit length or single fracture with 5 mm width with visible opening incomplete circular round
	Good	1–2 fractures per unit length or 5–10 mm wide single fracture
	Fair	2–4 fractures per unit length or 10–20 mm wide single fracture/complete circular round
	Poor	4–5 fractures per unit length or 20–25 mm wide single fracture
	Critical	4–5 fractures per unit length/or >25 mm wide
Spiral Fracture	Excellent	0–1 fracture per unit length or single fracture with 5 mm width with visible opening
	Good	1–2 fractures per unit length or 5–10 mm wide single fracture
	Fair	2–4 fractures per unit length or 10–20 mm wide single fracture
	Poor	4–5 fractures per unit length or 20–25 mm wide single fracture
	Critical	4–5 factures per unit length or >25 mm wide single fracture with no transverse displacement
Hole	Excellent	0
	Good	N/A
	Fair	1 clock position
	Poor	2 clock positions
	Critical	>3 clock positions or if soil visible-void visible
Sag	Excellent	0
	Good	0–50 mm change of flow level

Table 2.10 CSP Structural Defects (continued)

Defect	Grade	Description
Sag	Fair	50–100 mm change of flow level
	Poor	>100 mm change of flow level
	Critical	N/A
Deformation	Excellent	0% diameter change
	Good	0%–5% diameter change
	Fair	5%–10% diameter change and leakage
	Poor	10%–25% diameter change and leakage
	Critical	>25% diameter change
Broken	Excellent	N/A
	Good	N/A
	Fair	N/A
	Poor	N/A
	Critical	Always
Collapse: >50% of cross section is lost	Excellent	N/A
	Good	N/A
	Fair	N/A
	Poor	N/A
	Critical	Always
Surface Damage	Excellent	0/increased roughness
	Good	<5 mm wall thickness missing, slight spalling
	Fair	5–10 mm of wall thickness missing, aggregate visible
	Poor	10–15 mm of wall thickness missing, aggregate projecting, reinforcement visible, reinforcement projecting
	Critical	>15 mm of wall thickness missing, aggregate missing, reinforcement missing/corroded (100% critical)

2.8.3.2 Operational Defects

The protocol also considers operational defects in the evaluation of sewer pipelines. Table 2.11 lists the operational defects that CSP considers. Based on the table, many of the defects are divided according to the five linguistic grades. Unlike the New Zealand sewer protocol, which considered infiltration a structural defect, the CSP protocol considers it an operational defect.

Table 2.11 CSP Operational Defects

Defect	Grade	Description	Unit
Roots	Excellent	0%–5% reduction in diameter	Each
	Good	5%–10% reduction in diameter	
	Fair	10%–25% reduction in diameter	Each
	Poor	25%–50% reduction in diameter	
	Critical	>50% reduction in diameter	
Debris	Excellent	0%–5% reduction in diameter	Meter
	Good	5%–10% reduction in diameter	
	Fair	10%–25% reduction in diameter	
	Poor	25%–50% reduction in diameter	
	Critical	>50% reduction in diameter	
Encrustation	Excellent	0%–5% reduction in diameter	Meter
	Good	5%–10% reduction in diameter	
	Fair	10%–25% reduction in diameter	
	Poor	25%–50% reduction in diameter	Meter
	Critical	>50% reduction in diameter	
Foul	Excellent	0%–5% reduction in diameter	Meter
	Good	5%–10% reduction in diameter	
	Fair	10%–25% reduction in diameter	
	Poor	25%–50% reduction in diameter	
	Critical	>50% reduction in diameter	
Protruding Services	Excellent	0%–5% reduction in diameter	Each
	Good	5%–10% reduction in diameter	
	Fair	10%–25% reduction in diameter	
	Poor	25%–50% reduction in diameter	
	Critical	>50% reduction in diameter	
Soil Intrusion	Excellent	0%–5% reduction in diameter	Meter
	Good	5%–10% reduction in diameter	
	Fair	10%–25% reduction in diameter	
	Poor	25%–50% reduction in diameter	
	Critical	>50% reduction in diameter	
Infiltration	Excellent	NA	NA
	Good	seeping	
	Fair	dripping	
	Poor	running	
	Critical	gushing	

2.9 Summary and Limitations of Previous Research

This chapter discussed the literature related to sewer systems. It outlined the conventional method used in inspecting sewer pipelines. In addition, it listed and explained other technologies that overcome CCTV limitations. The literature discussed the work pertinent to infrastructure automation and methods used to assess sewer pipes. Later, image processing knowledge was shared. A number of sewer condition assessment tools were summarized. Additionally, the literature examined three sewer protocols, WRc, CSP, and New Zealand, and listed the major defects of each. Based on the literature review, several limitations emerged.

- Many researchers depended solely on CCTV images to detect sewer pipeline defects. CCTV presented evidence for some defects, including cracks, fractures, and holes. The research suggests the need for laser profilers, sonar, and electro scan to quantify deformation, settled deposits, infiltration, and surface damage defects, which are not extensively studied. As a result, the research utilizes the data extracted from the application of those technologies to quantify the aforementioned defects. An automated tool will be designed to facilitate the analysis of the four defects.
- Many sewer protocols evaluate surface damage defects linguistically, and some protocols collect numerical information. However, this information seemed to be limited to certain diameter sizes and materials. Consequently, a new evaluation of surface damage defects is adopted for three different sewer pipeline materials.
- No implementation of MAUT exists in sewer condition assessment. The research adopts MAUT in calculating an aggregated index that gives an overview of the sewer pipeline condition based on four defects: deformation, settled deposits, infiltration, and surface damage. This method is appropriate, as the research considers the lower and upper limits for

each defect. The model shall rely on the effect of the overall quantified defect values as an input. Thus, it reduces the subjectivity of many protocols.

CHAPTER THREE: RESEARCH METHODOLOGY

3.1 Overview

This chapter discusses the methodology and the research model implemented in the research. This chapter includes several major sections; Figure 3.1 provides the process chart of this chapter. After summarizing the literature reviewed in 3.2, 3.3 presents the defects algorithms. It provides information about the data obtained to complete the image processing operations. The same section presents the quantification algorithms with step-by-step examples. The condition assessment model adopted is described in 3.4. Utility functions are developed for each defect: deformation, settled deposits, infiltration, and surface damage. Additionally, in 3.5 relative importance weights are used from previous research to aggregate the indexes of the four defects to arrive at an aggregated condition assessment index. Finally, 3.6 adopts the CSP scale and performs major and minor modifications to enhance the utilization of the scale.

3.2 Literature Review

The research included a comprehensive literature review, which is summarized herein. The inspection techniques the research considers is explained in 2.2, wherein the application of the laser profiler, electro scan, and sonar are described. Additionally, 2.3 summarizes other sewer inspection techniques, such as the zoom camera, digital scanning, GGL, and infrared thermography.

Several sewer pipeline materials that are utilized in sewer systems are reviewed in 2.4. Next, 2.5 shares some of the infrastructure's automation, which includes the techniques utilized and the defects detected. Common image processing knowledge and procedures implemented in the research's automated tool are provided in 2.6. The current models that assess some of the infrastructure's facilities are described in 2.7. The knowledge of applying the MAUT model in providing an aggregated condition assessment index is explained in 2.8. Finally, 2.9 investigates three sewer protocols: WRc, CSP, and New Zealand.

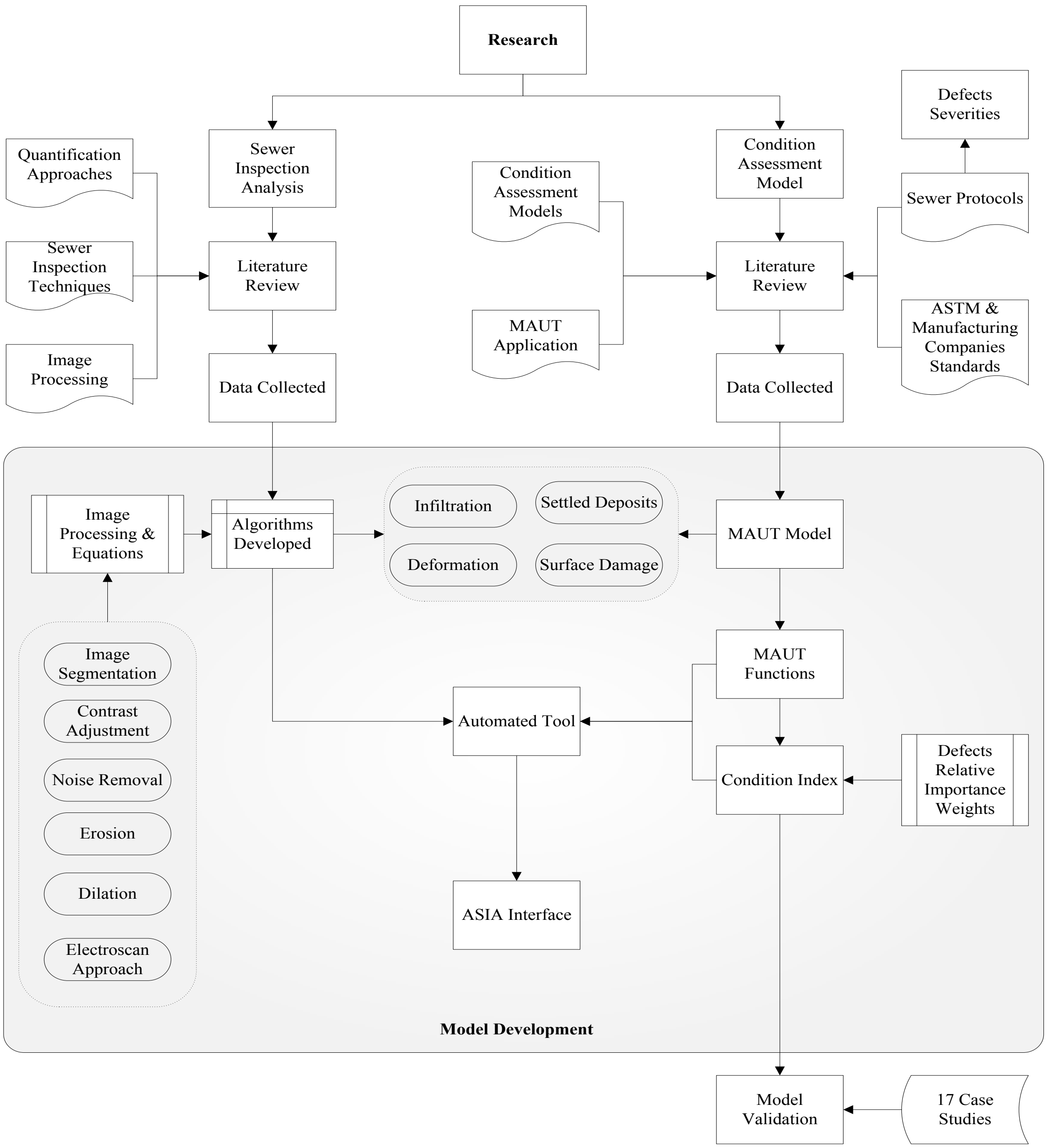

Figure 3.1 Research Methodology Flow Chart

3.3 Defects Algorithms

Before the automated tool was developed, the images collected were treated as an exam question to be solved by hand. Therefore, several steps were listed to reach the information needed to quantify each image. Hence, simple mathematical equations reinforced the matter. Several image processing techniques were utilized in the quantification process, which are represented in Figure 3.2: image segmentation, contrast adjustment, noise removal, dilation, and erosion. The end product shall be a binary image that allows the application of the basic mathematical equations for the purpose of quantifying the defects. Therefore, deformation, settled deposits, and surface damage defect approaches were accomplished. However, the infiltration defect algorithm was adopted from an already used electrical approach.

3.3.1 Data Collection

To implement image processing techniques, numerous images were required. Several companies that supply laser profilers and sonar were contacted. Unfortunately, only two companies responded and provided sample reports, namely Redzone Robotics and CUES. The reports were further analyzed and few images were found. The data considered contained four images of deformation defects, four images of settled deposits defects, and two images of surface damage defects. These images were essential to design the automated tool for quantification purposes.

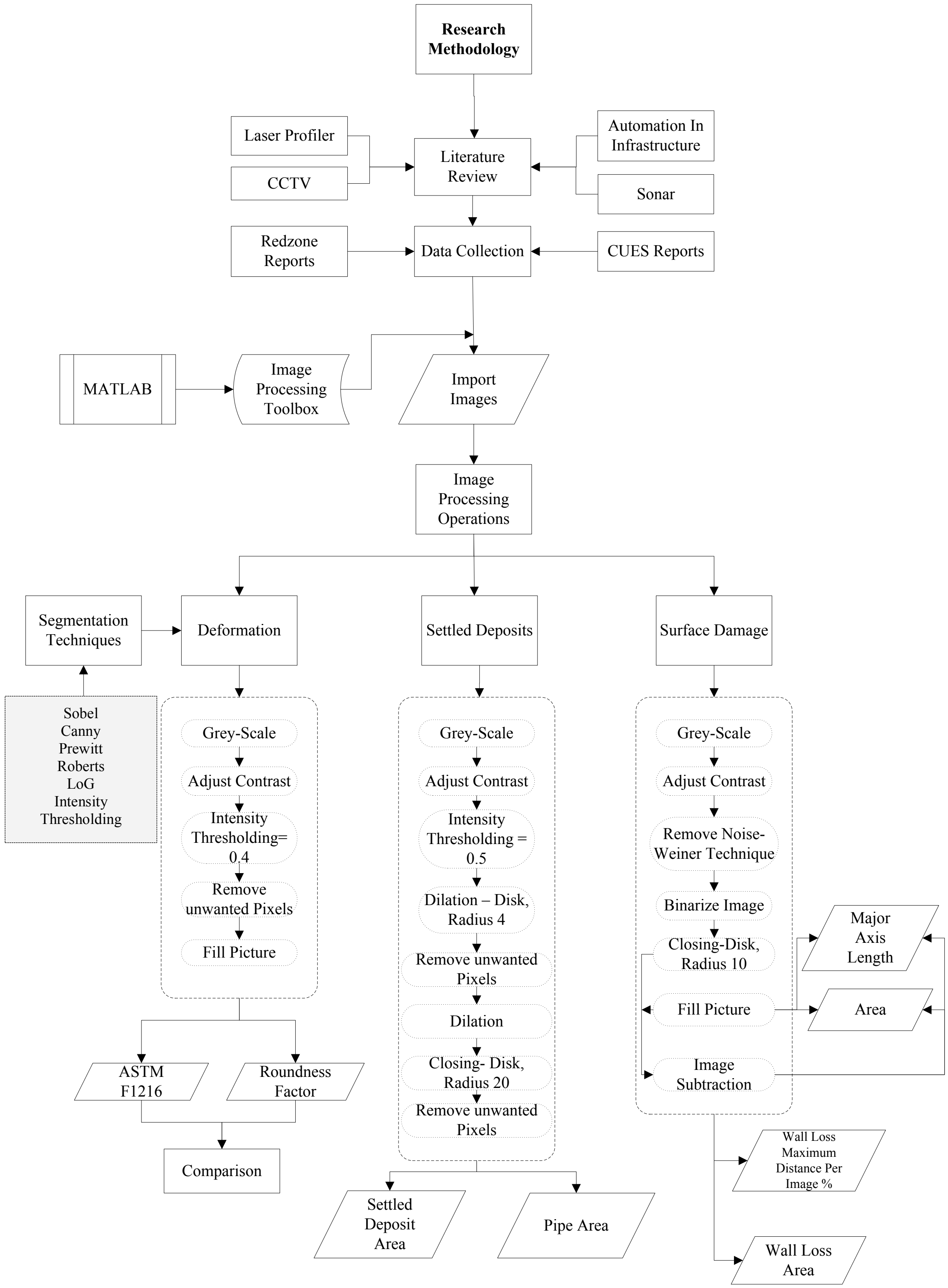

Figure 3.2 Defects Image Processing Algorithms

3.3.2 Deformation (Ovality)

Images for deformed pipes are used to quantify the deformation defect. The quantification algorithm is based on the ASTM F1216 ovality formula and the application of the roundness factor formula. The ASTM formula is used for unfilled and half-filled pipes, as described in the following sections.

3.3.2.1 ASTM F1216 Ovality Formula (Unfilled Pipe)

Several companies utilize equation 3.4 to measure the deformation of the pipes from the laser profiler images. This section shall explain the development of equation 3.4. Figure 3.3 is a representation of an unfilled sewer pipeline. The figure illustrates a deformed pipeline that describes the minimum and maximum inside diameters. The minimum inside diameter is located at the vertical axis, while the maximum inside diameter is located at the horizontal axis.

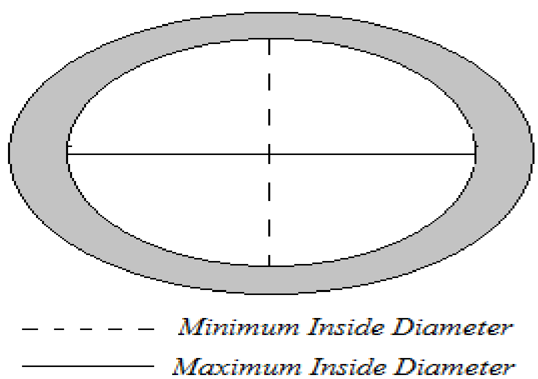

Figure 3.3 Drawing Representing an Unfilled, Deformed Sewer Pipe

The deformation (ovality) formula is computed using either of the following formulas:

$$\left(\frac{Mean\ Inside\ Diameter - Minimum\ Inside\ Diameter}{Mean\ Inside\ Diameter} * 100\right) \quad [3.1]$$

Or

$$\left(\frac{Maximum\ Inside\ Diameter - Mean\ Inside\ Diameter}{Mean\ Inside\ Diameter} * 100\right) \quad [3.2]$$

By definition, the mean inside diameter is found by calculating the actual diameters over 90 directions at each section (Motahari and Abolmaali 2010). For an unfilled pipe, Redzone Robotics (2011) assumed that the maximum and minimum diameters are orthogonal to each other and applied this concept in its inspection work. Considering the following, the mean inside diameter will be equal to

$$\left(\frac{Maximum\ Inside\ Diameter + Minimum\ Inside\ Diameter}{2} * 100\right) \quad [3.3]$$

Therefore, ASTM F1216 is equal to

$$\left(\frac{Maximum\ Inside\ Diameter - \ Minimum\ Inside\ Diameter}{Maximum\ Inside\ Diameter + Minimum\ Inside\ Diameter} * 100\right) \quad [3.4]$$

3.3.2.2 ASTM F1216 Ovality Formula (Half-Filled Pipe)

This section describes the development of the half-filled pipe deformation quantification equation. Similar deformation equations were applied, as in the previous section; in fact, the analysis of the image changed. The maximum inside diameter remained complete as presented in Figure 3.4. However, the minimum inside diameter will be half of the actual, as one of the halves is covered with the flow line.

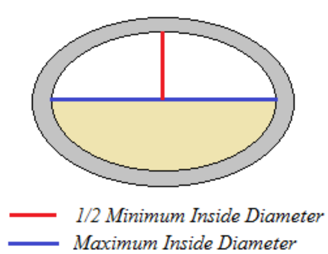

Figure 3.4 Drawing Representing a Half-Filled Sewer Pipe

Assuming the minimum inside diameter and the maximum inside diameter are orthogonal (Redzone Robotics 2011), ASTM F1216 for half-filled pipes is as equation 3.5.

$$\left(\frac{Maximum\ Inside\ Diameter - \ 2xMinimum\ Inside\ Diameter}{Maximum\ Inside\ Diameter + 2xMinimum\ Inside\ Diameter} * \ 100\right) \text{[3.5]}$$

3.3.2.3 Roundness Factor

The roundness factor, a dimensionless factor, is one of the shape factors image analysts use to identify the circular objects in the images. This factor is a function of the existing area and perimeter. Pharmaceutical and biopharmaceutical studies use the roundness factor to measure the circularity of a pellet (Law and Deasy 1998). It is also used in sea research to measure oocyte sizes (Thorsen and Kjesbu 2001). In human pathology, researchers use the roundness factor to find the circularity of the nuclear factor in detecting prostate cancer (Montironi et al. 2005). Therefore, it can be concluded that many major and critical fields adopt the roundness factor. For the purpose of studying the circularity of an object, the roundness factor has been adopted in the research and presented in equation 3.6.

$$Roundness\ Factor\ Formula \ = \left(\frac{4 \ * \ \pi * \ A}{P^2} \ * \ 100\right) \text{[3.6]}$$

Figure 3.5 explains the parameters *A* and *P*. According to the figure, *A* represents the existing area of the deformed pipeline, and *P* represents the existing perimeter of the deformed pipeline. Based on the roundness factor formula, the ratio of an exact circular object that is not deformed is 1. Therefore, it has no ovality, and in this context, deformation of the shape will be 0. Applying the same concept, if a shape has a factor less than 1, the difference between 1 and the roundness factor represents the deformation. As a result, the deformation based on the roundness factor is presented in equation 3.7.

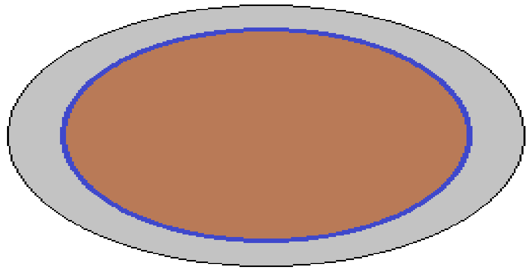

Figure 3.5 Drawing Representing a Deformed Sewer Pipe

$$Deformation\,\% = (100 * (1 - Roundness\ Factor)) \quad [3.7]$$

The next subsections list the image processing steps implemented to find the deformation percentages using the ASTM formula and the roundness factor concepts.

3.3.2.4 Image Segmentation

To isolate the laser light from the background, a number of techniques have been done on the original 2-D laser profiler image. The results are demonstrated in Figures 3.6 to 3.11, as each had different edge detection representation. The original image was imported to MATLAB. Later, the image was changed to gray scale, where the contrast was adjusted so that the laser light can clearly be distinguished. Several edge detection methods were utilized to identify the laser light from the background. Sobel and Prewitt edge detection methods provided similar outputs. However, some missing pixels were observed in the perimeter. Similarly, the Roberts edge detection method also had missing pixels.

LoG and Canny methods detected the whole laser light; however, the latter's binary image had more noise than the LoG binary image. When the contrast of the image was adjusted, the laser light became easier to identify. Some edge detection methods failed to accomplish the tasks, while others detected the laser light completely. Another segmentation technique, intensity thresholding, found that a threshold of 0.4 provided the best binary image output in terms of less noise and joined laser light. Based on the study, the intensity segmentation provided the required output. Therefore, the intensity segmentation technique of 0.4 threshold was adopted in the deformation quantification algorithm. The next subsection will demonstrate the image processing steps.

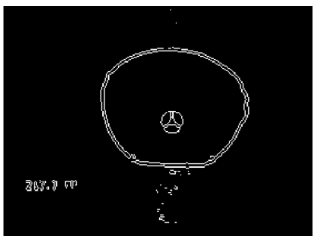

Figure 3.6 Sobel Method

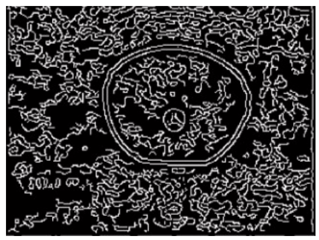

Figure 3.7 Canny Method

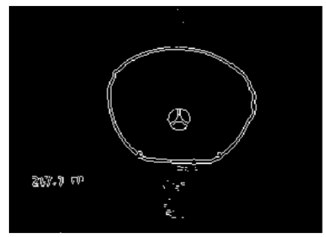

Figure 3.8 Prewitt Method

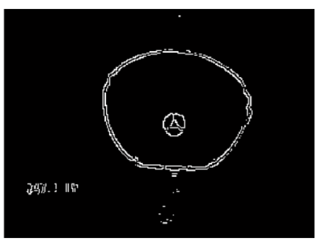

Figure 3.9 Roberts Method

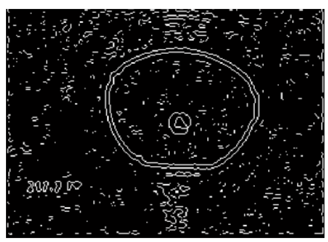

Figure 3.10 LoG Method

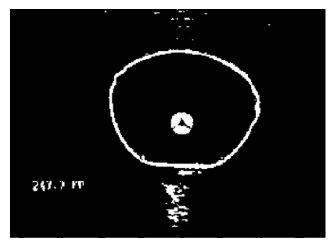

Figure 3.11 Intensity Thresholding of 0.4

3.3.2.5 Image Processing Procedure

Several image processing operations were implemented. This section lists step-by-step results as follows:

A) The first step was importing the image to MATLAB, which represented the original image.

B) The second step was changing the original image to gray scale.

C) To distinguish the laser light, the contrast of the image was increased.

D) The thresholding technique was used to transform the image into a binary image. The threshold used was 0.4. The binarized image represented the laser light of the existing pipeline's shape, pixels from the flow line, some labels in the image, and other unwanted pixels.

E) Unwanted pixels were removed so that the value of 1 represented the laser light.

F) The images were filled to obtain certain parameters that facilitated the quantification of the deformation.

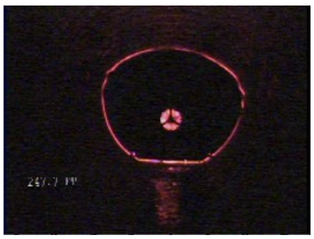

Figure 3.12 Deformation Step A

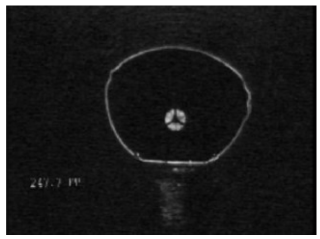

Figure 3.13 Deformation Step B

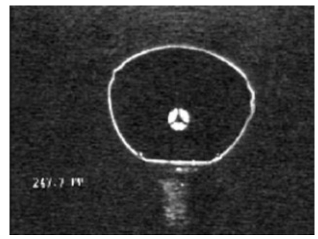

Figure 3.14 Deformation Step C

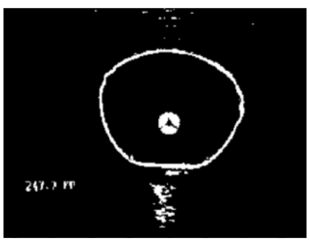

Figure 3.15 Deformation Step D

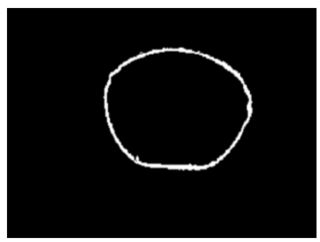

Figure 3.16 Deformation Step E

Figure 3.17 Deformation Step F

After Step F, several parameters were found: major axis length, minor axis length, area, and perimeter. Based on the parameters, the following results were obtained:

- Applying equation 3.4, the ASTM formula:
  - Deformation is 18.54%
- Applying the deformation roundness factor, equations 3.6 and 3.7:
  - Deformation is 18.65%

3.3.3 Settled Deposits

This subsection demonstrates the algorithm developed in quantifying the settled deposits area and volume from the images. A number of mathematical equations are used to achieve the methodology.

3.3.3.1 Proposed Algorithm

An image processing algorithm was utilized to quantify the settled deposits volume along a segment of a pipe. Images from Redzone's sonar application were used for this purpose. The images were imported to MATLAB, where several operations were done. Basic mathematical formulas were used to determine the settled deposits percentage from the pipe's diameter. Figures 3.18 and 3.19 simulate a sewer pipe of length *L* and radius *r*.

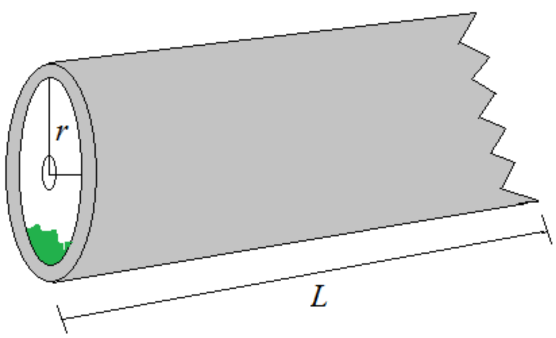

Figure 3.18 Sewer Pipeline 3-D View Representation

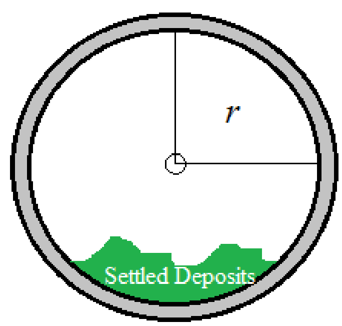

Figure 3.19 Cross-Sectional View of Figure 3.18

The proposed image processing methodology is dependent on reaching a binary image that isolates the settled deposits from each original image, similar to Figure 3.19. Equations 3.8, 3.9, and 3.10 are used in this regard.

$$Pipe\ Area\ = (\pi r^2\ )\ [3.8]$$

$$Blockage\ Rate\ per\ Image\ = \frac{Settled\ Deposit\ Area}{Pixel\ Pipe\ Area} * 100\ [3.9]$$

$$Actual\ Settled\ Deposit\ Area\ = Blockage\ Rate\ per\ Image\ *\ Pipe\ Area\ [3.10]$$

Blockage rate per image is found from the mathematical operations in MATLAB. For each image, the process is applied to isolate the settled deposits area, if any, from the pipeline's section. Doing so, the settled deposit area can be found by using MATLAB's mathematical parameters. The actual settled deposit area is calculated once the user inputs the original pipe's radius.

These operations are done automatically for each image after feeding it to MATLAB. The actual settled deposits area will be used in the calculation of the total settled deposits volume. Because it is assumed that the images are taken every 0.3 m, the total segment's length will depend on the number of images fed to MATLAB.

$$Total\ Segment\ Length = \sum_{i=1}^{n} 0.3(n-1)\quad [3.11]$$

Where n refers to the number of images imported. For instance, the first image (n = 1) will be at location 0 m. The second image (n = 2) will be at location 0.3 m. Once the actual settled deposits area has been found at each 0.3 m, it yields the calculation of the settled deposits volume. The actual deposit areas will be scattered in a 2-D plot at each respective position. The points in the graph will be joined with a straight line, assuming that the change in the settled deposits area is linear, as demonstrated below.

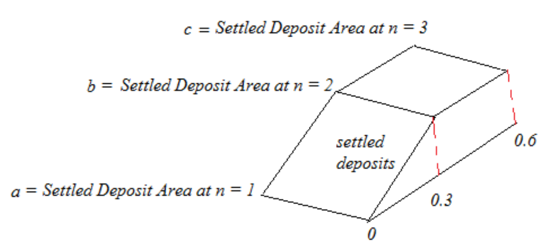

Figure 3.20 3-D View of Settled Deposits Volume Assumption

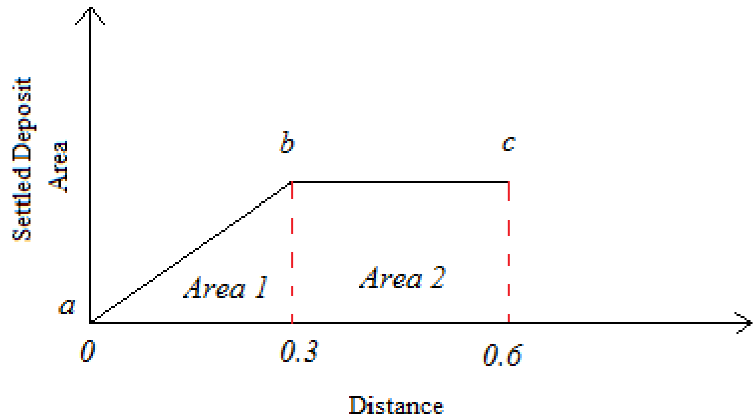

Figure 3.21 2-D View of Figure 3.20

Therefore, the area under the curve will represent the total volume of the actual settled deposits on the bottom of the inside surface of the pipeline. For example, in Figure 3.21, the volume will equal the summation of Area 1 and Area 2 as follows:

$$Area\ 1 = The\ Area\ of\ a\ Triangle = ½ * 0.3 * b \ [3.12]$$

$$Area\ 2 = The\ Area\ of\ a\ Rectangle = 0.3 * c \ [3.13]$$

$$Volume\ of\ Settled\ Deposits\ (m^3) = Area\ 1 + Area\ 2 \ [3.14]$$

Similarly, in the case of *n* points, the volume of settled deposits (m^3) is found as per equation 3.15.

$$Volume\ of\ Settled\ Deposits\ (m^3) = Area\ 1 + Area\ 2 + \cdots + A(n-1) \ [3.15]$$

Once the settled deposits volume is found, the segment total blockage rate is calculated according to equation 3.16.

$$Segment\ Total\ Blockage\ Rate = \frac{Volume\ of\ Settled\ Deposits}{Pipe\ Area * Total\ Segment\ Length} * 100 \ [3.16]$$

3.3.3.2 Image Processing Procedure

The explained procedure was applied in an automated tool. Images containing settled deposits material were fed to the tool. Hence, image processing operations commenced as follows:

A) The first step was importing the original image to MATLAB.

B) Next, the original image, in Step A, was changed to a gray-scale image.

C) To identify the inside perimeter of the pipeline, the contrast should be adjusted. From the image, the inside perimeter of the pipeline was darker than the outer perimeter.

D) To binarize the image, the intensity segmentation approach was utilized with a threshold value of 0.5. Interestingly, the inside diameter of the pipeline as well as the settled deposits area remained in the binary image. However, some unwanted pixels surrounding the circle were noticed. These pixels were removed in a separate operation.

E) Dilation was applied to fill the gap between the settled deposits areas and to join the broken lines for any missing pixels around the inside perimeter of the pipeline. The process used a disk structural element of radius 4.

F) Pixels surrounding the connected circle represented the remaining pixels of the outer diameter of the pipeline. They were removed accordingly.

G) The next step was to isolate the settled deposits area so that the required parameters were calculated. Any holes in the image were given a value of 1. The existing values of 1 were changed to 0 and vice versa.

H) Later, the image was dilated to isolate the settled deposits area from the image.

I) The values of 1 were changed to 0 and vice versa.

J) The closing operation was implemented using a disk structural element of radius 20 to fill the settled deposits area.

K) Unwanted pixels were removed to find the parameters.

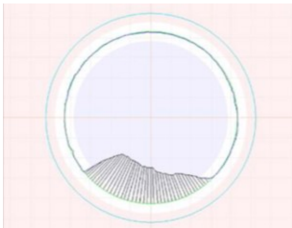

Figure 3.22 Settled Deposits Step A

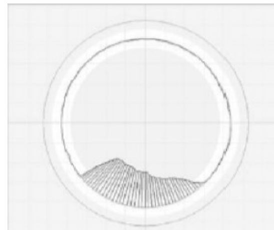

Figure 3.23 Settled Deposits Step B

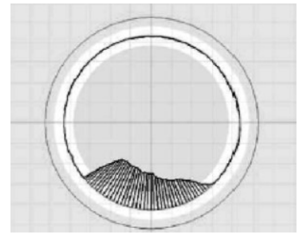

Figure 3.24 Settled Deposits Step C

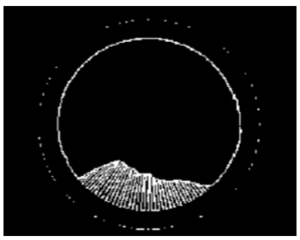

Figure 3.25 Settled Deposits Step D

Figure 3.26 Settled Deposits Step E

Figure 3.27 Settled Deposits Step F

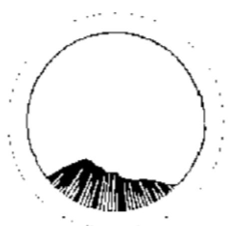

Figure 3.28 Settled Deposits Step G

Figure 3.29 Settled Deposits Step H

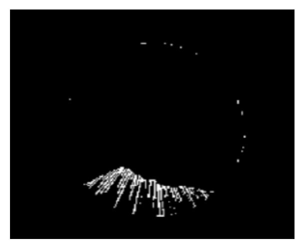

Figure 3.30 Settled Deposits Step I

Figure 3.31 Settled Deposits Step J

Figure 3.32 Settled Deposits Step K

The previous listed operations isolated the settled deposits area from the pipe section. Therefore, the settled deposits area and the pipe's area were found in pixels to calculate the blockage rate per image and the actual settled deposits area.

The results are as follows:

- Settled deposits area = 2,022 pixel units
- Pipe pixel area = 16,417 pixel units

Hence, the blockage rate per image for Figure 3.22 is equal to 12.32%.

3.3.3.3 Settled Deposits Volume Calculation

It is important to find the volume of settled deposits present in a sewer segment. It is also important to investigate the blockage percentage along the segment. Figure 3.33 plots the settled deposits area versus the distance of an actual pipeline in Qatar's case study 1. The inspected length was 9 m. The report provided the blockage percentages at different locations. Later, the settled deposits area was calculated, scattered, and joined to calculate the area under the curve. The volume of the settled deposits was calculated as per equation 3.15. The volume was found to be 0.0186 m^3. Equation 3.16 was utilized to find the segment total blockage rate, which was 11.33%.

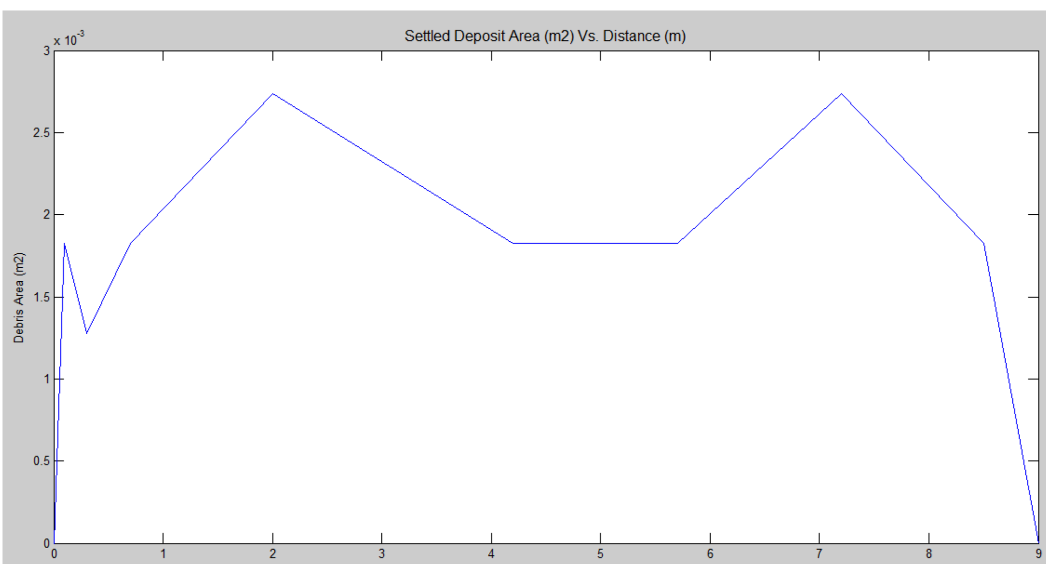

Figure 3.33 Qatar's Case Study 1: Settled Deposits Area vs. Distance

3.3.4 Infiltration

Electro scan's outputs of current values quantify the infiltration defect. The approach was adopted from Moy et al. (2012) in transferring the current values to flows that measure the infiltration amount. The authors stated that the flow of water through a pipe defect depends on the following:

A) The size of the defect

B) The shape of the defect

C) The water head above the defect, which is the pressure that moves the water inside the pipe

The major defect that allows infiltration is a crack. Considering the smallest crack having a width of 0.635 mm, a length ranging from 17 mm to 72 mm, and a water head of 304.8 mm, the flow of water per slot area was calculated as 0.0012 +/– 0.0002 liter/sec/mm^2. Assuming the conductivity of the medium is 110 micro-Siemens/mm and the voltage of the electro scan machine is 10 volts, the authors determined that the flow in liter/second is as per equation 3.17.

$$Flow\ (liter/second) = 0.000109 * I * T \quad [3.17]$$

T is the pipe's thickness in millimeters and I is the increase in the defect current in 10^{-4} amps. Therefore, the electro scan machine will record the currents and provide them as an output. The current values are fed into the program, which automatically finds the flow at each witnessed location and the total flow in the pipeline's segment. The average total infiltration is calculated as per equation 3.18.

$$Average\ Total\ Infiltration\ Flow\ \left(\frac{liter}{second}\right) per\ length = \left(\frac{Total\ Flow\ in\ Pipeline}{Total\ Pipeline\ Length}\right) \quad [3.18]$$

3.3.5 Surface Damage

By definition, surface damage is one type of a sewer's structural defects in which the inside wall of the pipe deteriorates by abrasion, erosion, or chemical corrosion (NZWWWA 2006). Figure 3.34 lists the subdefects of the surface damage defect from the least severe to the most severe. The next subsection explains the algorithm proposed to quantify the surface damage defect.

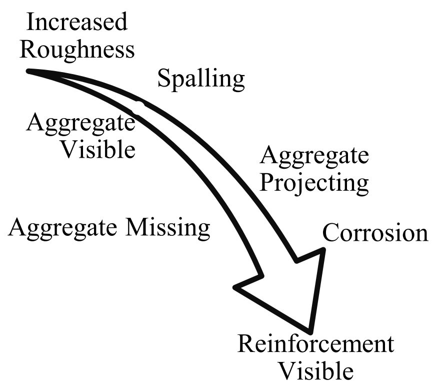

Figure 3.34 Surface Damage Subdefects

3.3.5.1 Proposed Algorithm

The quantification of the surface damage was found by applying mathematical equations. The algorithm developed in MATLAB was able to find the wall loss area percentage compared to the inside pipe area. In addition, it provided the maximum wall loss percentage compared to the pipe's diameter. Thus, the volume of the wall loss along the inspected segment was calculated as explained in the settled deposits volume calculation. Figure 3.35 represents a sewer pipeline having a surface damage with a certain pattern. Figure 3.36 magnifies the clouded part, which corresponds to the maximum wall loss in the pattern. In Figure 3.36, a refers to the maximum distance of loss in the section, and in Figure 3.35, b is equal to the inside diameter + a. Several basic mathematical equations are considered in the development of the methodology.

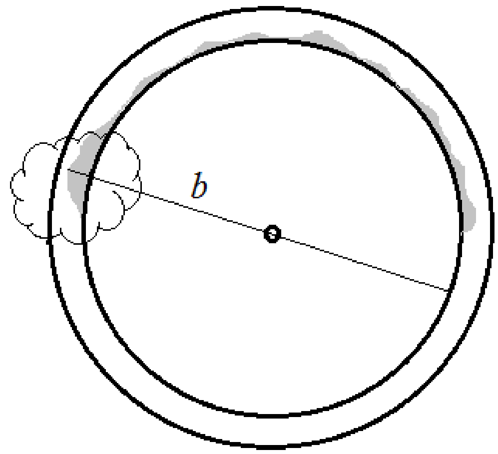

Figure 3.35 Representation of a Sewer Pipeline with Wall Loss

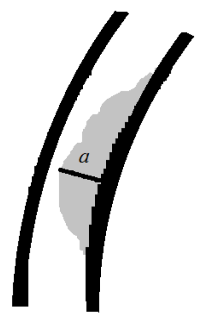

Figure 3.36 Magnified Part of the Clouded Area in Figure 3.35

$$Inside\ Pipe\ Area\ = \pi r^2\ [3.19]$$

$$Wall\ Loss\ \%\ = \frac{Wall\ Loss\ Area}{Inside\ Pipe\ Area} *\ 100\ [3.20]$$

$$Wall\ Loss\ Maximum\ Distance\ \%\ per\ Image\ = \frac{a}{b-a} *\ 100\ [3.21]$$

$$Actual\ Wall\ Loss\ Area\ per\ Image = Wall\ Loss\ \% *\ Inside\ Pipe\ Area\ [3.22]$$

$$Segment\ Wall\ Loss\ Maximum\ Distance\ \%$$

$$= \frac{\sum_{\mathrm{i=1}}^{\mathrm{n}}\ \text{Equation [3.21]}}{Total\ Segment\ Length};\ where\ n\ is\ the\ number\ of\ images\ [3.23]$$

3.3.5.2 Image Processing Procedure

Images that contained surface damage defects were extracted from the Redzone reports to run several image processing operations that quantified the wall loss of the pipeline.

A) The first step was reading the image that contained the surface damage defect.
B) The original image imported was converted to a gray-scale image for further image processing applications.
C) To detect the surface damage pixels as well as the pipe's shape, the image intensity was adjusted.
D) If Step C were changed to a binary image, the grid lines would be present. Therefore, they were considered noise. Hence, the noise resulting from the background was reduced using the Weiner technique with a neighborhood of $m = 5$ and $n = 5$.
E) The reduced noise image was converted to a binary image. Clearly, the background was not detected in the conversion to a binary image. The white pixels represented the surface damage terrain as well as the pipe's shape.
F) To fill the surface damage area, the closing operation was accomplished using a disk structural element of radius 10.
G) The area of the pipe's shape was filled so that in later processes, the pipe's area could be found.

After reaching Step G, several parameters were computed, which were essential in applying the mathematical equations mentioned. Hence, the major axis and the area of the resulting filled shape were found as follows:

- Major axis length = 180.74 pixel units

- Pixel area = 25,274 pixel units

The computations found would be used in the calculations of the wall loss % (equation 3.20) and the wall loss maximum distance % per image (equation 3.21).

H) To find the filled pipe's area, the two previous images were subtracted.

Similarly, the filled pipe's area's major axis length and area were found from Step H:

- Major axis length = 171.86 pixel units
- Pixel area = 23,195 pixel units

Therefore, the wall loss maximum distance % per image was computed as well as the wall loss area %:

- Wall loss maximum distance % per image = 5.17%
- Wall loss area % = 8.96%

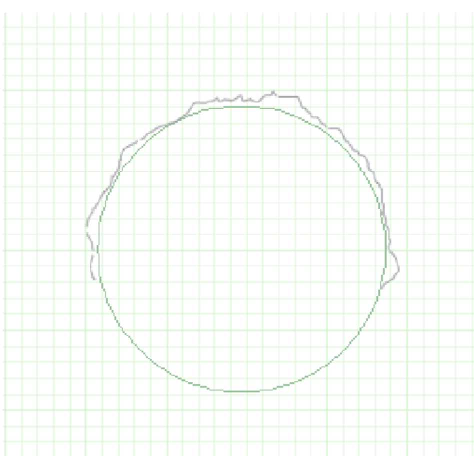

Figure 3.37 Surface Damage Step A

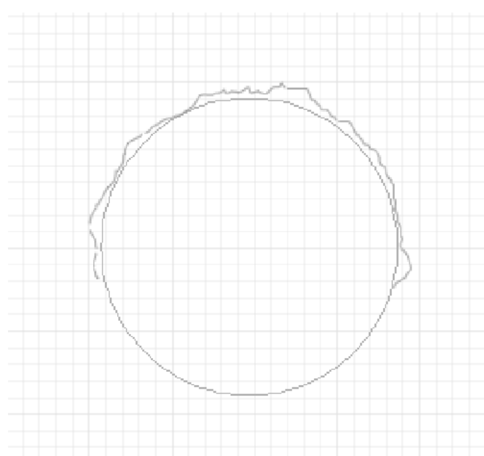

Figure 3.38 Surface Damage Step B

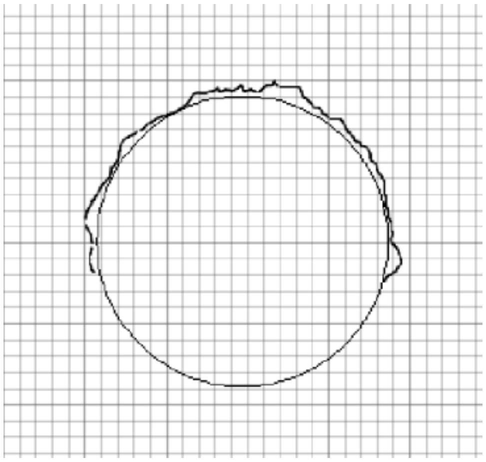

Figure 3.39 Surface Damage Step C

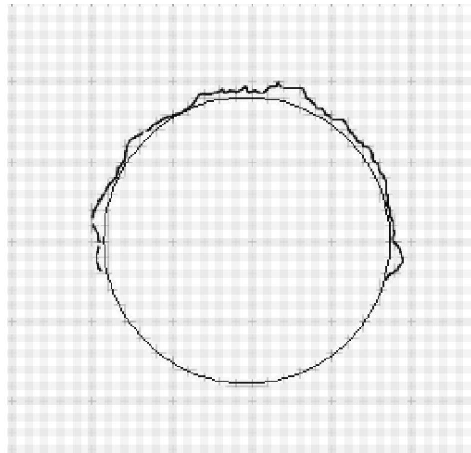

Figure 3.40 Surface Damage Step D

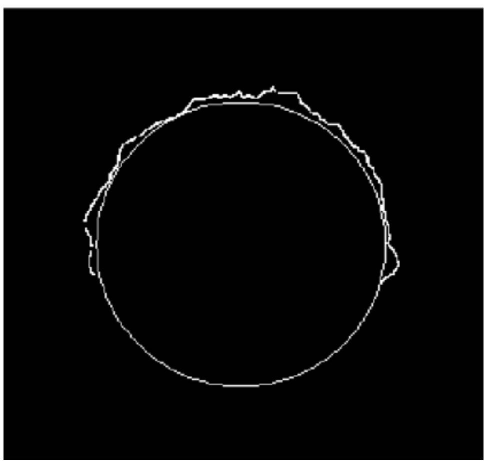

Figure 3.41 Surface Damage Step E

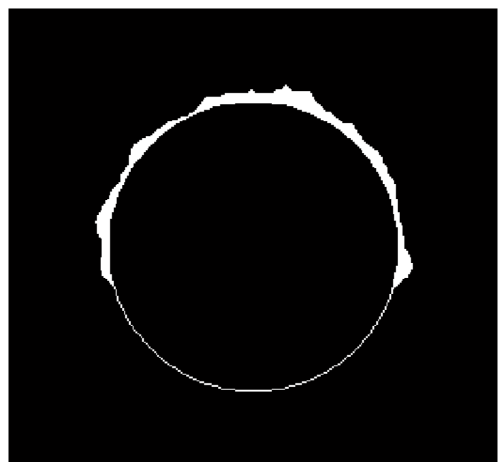

Figure 3.42 Surface Damage Step F

Figure 3.43 Surface Damage Step G

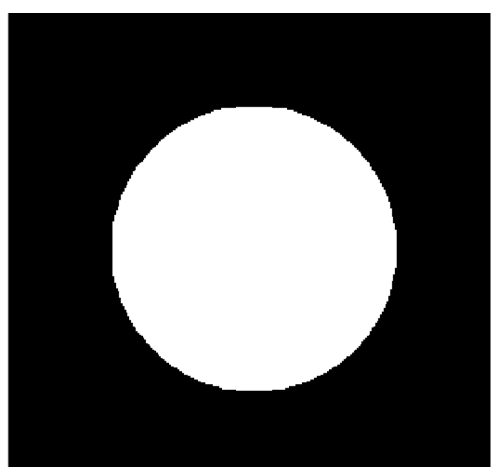

Figure 3.44 Surface Damage Step H

3.3.5.3 Surface Damage Volume Calculation

The volume of settled deposits computation is similarly applied to that of the wall loss volume computation in a segment. Equation 3.20 provides the percentage of the wall loss area compared to the inside pipeline area. Hence, providing the actual inside radius in equation 3.19 will allow the computation of the actual wall loss per image, as in equation 3.22. Scattering the computed values at every 0.3 m, from equation 3.22, and connecting them will present a graph of the wall loss area versus distance. From the graph, the area under the curve will denote the volume of the wall loss, as previously achieved in the settled deposits defect.

3.4 Condition Assessment Model

This subsection is concerned with developing utility functions for each of the four defects. The functions are generated by utilizing lower and upper limits that are adopted from WRc, CSP, and New Zealand sewer protocols, electro scan, and ASTM standards. After generating the functions, each function of each defect will supply an index that defines the severity of the defect. Later, the computed indexes of the four defects will be aggregated using relative importance weights. A scale that is already available in CSP will be modified to reduce some of its subjective evaluations.

3.4.1 MAUT Development Procedure

To develop a utility function for each defect, perform the following functions:

A) Specify the lower and upper limit ranges for each defect's severity.

B) Specify the scale to be adopted. For example, in this research, a scale from 0 to 10 is considered, where 0 is excellent and 10 is critical.

C) Develop a utility function by any trend (regression type) that provides the highest R^2 (coefficient of determination).

Each defect will have a unique utility function; for the surface damage defect, each pipe size will have a separate utility function. According to WRc (2004), for instance, sewer defects can be categorized based on their structural and operational behaviors. Nevertheless, this model's overall condition index depends on four defects. Those pertinent to structural defects are deformation and surface damage, and the operational defects considered are settled deposits and infiltration. The pipeline condition assessment index depends mainly on these four defects, as shown in Figure 3.56.

The severities of two defects—deformation and settled deposits—were extracted from three protocols. WRc, New Zealand and CSP do not have any numerical severities for infiltration. Therefore, infiltration severity was taken from Electro Scan's infiltration evaluation. WRc and New Zealand protocols provide linguistic severity evaluation of the surface damage defect. However, CSP provides linguistic and numerical severities. Nevertheless, the numerical information specifies neither the diameters inspected nor the material in concern.

In this research, the surface damage defect model was developed for three materials: reinforced concrete, vitrified clay, and ductile iron. The model relied on their structural behavior. The unit scale considered for developing the utility functions is 0 to 10, where 0 is excellent and 10 is critical. Later, the aggregated index will be computed, using equation 2.1, and will range from 1 to 5, where 1 is excellent and 5 is critical. To change the protocol indexes to the MAUT unit scale, equations 3.24, 3.25, and 3.26 are used.

$$Protocol\ Range = Maximum\ Protocol\ Value\ - Minimum\ Protocol\ Value \quad [3.24]$$

$$MAUT\ Range = Maximum\ MAUT\ Value\ (10) - Minimum\ MAUT\ Value (0) \quad [3.25]$$

$$New\ Scale = \frac{(Protocol\ Value\ - Minimum\ Protocol\ Value) * MAUT\ Range}{Protocol\ Range} + Minimum\ MAUT\ Value \quad [3.26]$$

3.4.1.1 Utility Function Inputs

The four defects were evaluated and the process to quantify them was automated in 3.3. Multiple results were concluded from each algorithm. However, this model considers the following outputs of each defect's algorithm, as per Table 3.1.

Table 3.1 Outputs Considered in MAUT Model

Defect	Output Considered
Deformation	ASTM F1216
Settled Deposits	Segment Total Blockage Rate
Infiltration	Total Infiltration
Surface Damage	Segment Wall Loss Maximum Distance %

3.4.1.2 Deformation Utility Functions

Pictures of deformed sewer pipelines are imported to the program. The program automatically evaluates the deformed pictures and provides the percentages using the two approaches, the ASTM formula and the roundness factor. Because the ASTM formula provided the least mean absolute error (MAE) percentage, as per 4.2, it was considered in the MAUT model. To calculate the MAUT grade using a 0 to 10 scale for a pipeline segment, an average of all ASTM percentages is considered, as per equation 3.27.

$$\left(\frac{\Sigma\ \text{ASTM Percentages}}{Total\ Number\ of\ Percentages} * 100\right) \quad [3.27]$$

3.4.1.2.1 WRc Utility Deformation Function

Table 3.2 presents the severities provided by WRc. From the table, the defect detail explains the percentage of deformation that is present in each section of a pipeline. The protocol considered three grades for the deformation defect ranging from 20 to 165.

Table 3.2 WRc Deformation Severity

Code	Defect Detail	Grade	Unit
WRc	0–5	20	Each
	6–10	80	Each
	>10	165	Each

- After using equations 3.24, 3.25, and 3.26, the MAUT unit scales were calculated. Table 3.3 lists the defect detail considered for each MAUT unit scale. 10 MAUT unit scale was considered for any deformation percentage equal to 10 or greater.

Table 3.3 WRc Deformation MAUT Scale

Code	Defect Detail Considered (x-value)	MAUT Unit Scale (y-value)
WRc	0	0
	6	4.14
	10 or greater	10

- Next, the x-value and y-value from Table 3.3 are plotted. As per Figure 3.45, the curve produced is a polynomial of degree 2. Based on the figure, the regression type perfectly plots the data considered, as its R^2 equals 1.

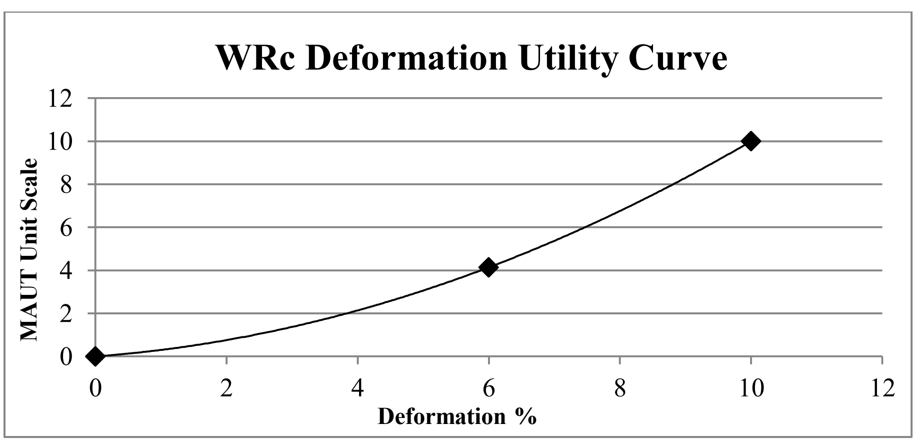

Figure 3.45 WRc Deformation Utility Curve

- Hence, the function that represents the curve follows:

$$WRc\ Utility\ Deformation\ Function = 0.0775(Deformation\ \%\ )^2 + 0.225(Deformation\ \%)\ [3.28]$$

3.4.1.2.2 CSP Utility Deformation Function

CSP considers five grades, 1 to 5, for the deformation defects that are tabulated in Table 3.4. The most critical case is when the deformation percentage reaches 25% or more.

Table 3.4 CSP Deformation Severity

Code	Definition	Grade	Deformation Percentage
CSP	Excellent	1	0
	Good	2	0%–5%
	Fair	3	5%–10%
	Poor	4	10%–25%
	Critical	5	>25%

- Table 3.5 lists the MAUT unit scales computed using equations 3.24, 3.25, and 3.26. The highest percentage of each range was used. However, to produce five coordinates, the average value of the "poor" grade was considered.

Table 3.5 CSP Deformation MAUT Scale

Code	Deformation Percentage Considered (x-value)	MAUT Unit Scale (y-value)
CSP	0	0
	5	3
	10	5
	18.5	7
	25 or greater	10

- Next, the x-value and y-value from Table 3.5 are plotted. As per Figure 3.46, the curve produced is a polynomial of degree 3. Based on the figure, the regression type perfectly plots the data considered, as its R^2 equals 0.9995.

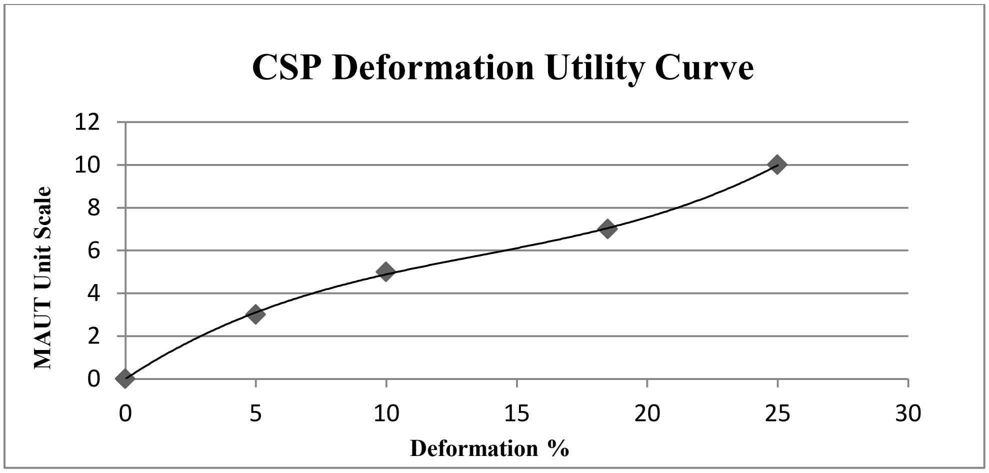

Figure 3.46 CSP Deformation Utility Curve

- Hence, the function that represents the curve follows:

$$CSP\ Utility\ Deformation\ Function$$
$$= 0.0001(Deformation\ \%)^3 - 0.042(Deformation\ \%)^2$$
$$+ 0.8056(Deformation\ \%)\ [3.29]$$

3.4.1.2.3 New Zealand Utility Deformation Function

New Zealand sewer protocol severities are adopted as well to find the deformation utility function. The protocol's severities are shown in Table 3.6. Based on the protocol, two grades were taken into account in evaluating the deformation defect.

Table 3.6 New Zealand Deformation Severity

Code	Grade	Deformation Percentage
New Zealand	Medium, score = 15	Deformation ≤10%
	Large = 65	Deformation >10%

- The deformation percentage considered with the MAUT unit scales are shown in Table 3.7. According to the table, two points were generated due to the two grades the protocol provided.

Table 3.7 New Zealand Deformation MAUT Scale

Code	Deformation Percentage Considered (x-value)	MAUT Unit Scale (y-value)
New Zealand	0	0
	10 or greater	10

- Because only two points are used, the expected plot shall produce a linear equation, as per Figure 3.47.

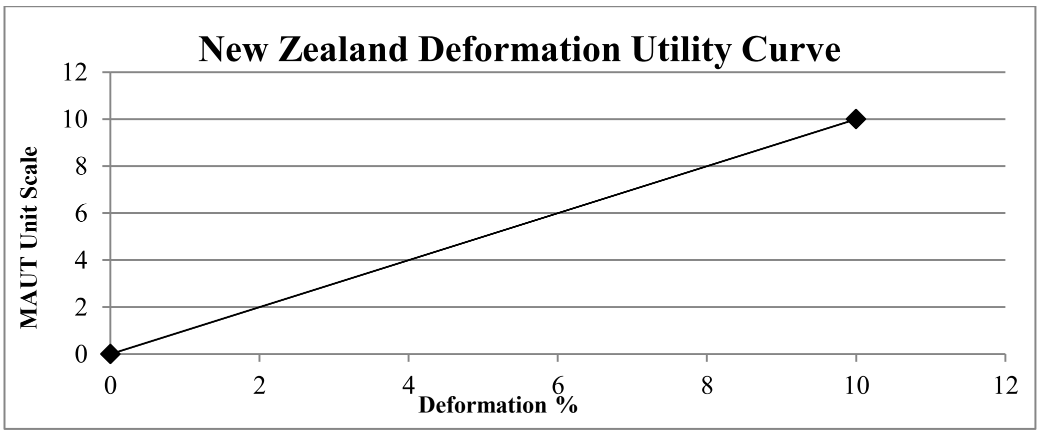

Figure 3.47 New Zealand Deformation Utility Curve

- The function that represents the straight line follows:

$$New\ Zealand\ Utility\ Deformation\ Function = Deformation\ \% \quad [3.30]$$

3.4.1.3 Settled Deposits Utility Functions

Image processing automation will analyze the images that contain settled deposits. Several computations will result from the automated tool. Segment total blockage rate is considered in the utility functions. Similar to the deformation utility functions scheme, severities of the three protocols are extracted. Graphs are plotted and utility functions are presented.

3.4.1.3.1 WRc Settled Deposits Utility Function

WRc severities for settled deposits are shown in Table 3.8. The table lists five grades that evaluate the settled deposits defect. The highest grade considered was 10 and the lowest was 1.

Table 3.8 WRc Settled Deposits Severity

Code	Grade	Deposits Percentage
WRc	1	5%
	2	5%–20%
	5	20%–50%
	8	50%–75%
	10	>75%

- Table 3.9 lists the MAUT unit scales computed using equations 3.24, 3.25, and 3.26. Although WRc does not account for settled deposits less than 5%, 0% settled deposits is considered and set at a 0 MAUT unit scale. Then the highest percentage of each range is considered and the scales are computed accordingly.

Table 3.9 WRc Settled Deposits MAUT Scale

Code	Deposits % Considered (x-value)	MAUT Unit Scale (y-value)
WRc	0	0
	5	1.11
	20	4.44
	50	7.78
	75 or greater	10

- The x and y values from Table 3.9 are used to plot the curve. The best regression line is drawn. Based on Figure 3.48, the regression type perfectly plots the data considered, as its R^2 is 0.9993.
- Therefore, the function that represents the regression curve is a polynomial of degree 3.

$$WRc\ Utility\ Settled\ Deposit\ Function$$
$$= 2x10^{-5}(Settled\ Deposit\ \%)^3 - 0.0035(Settled\ Deposit\ \%)^2 + 0.2789(Settled\ Deposit\ \%)\ [3.31]$$

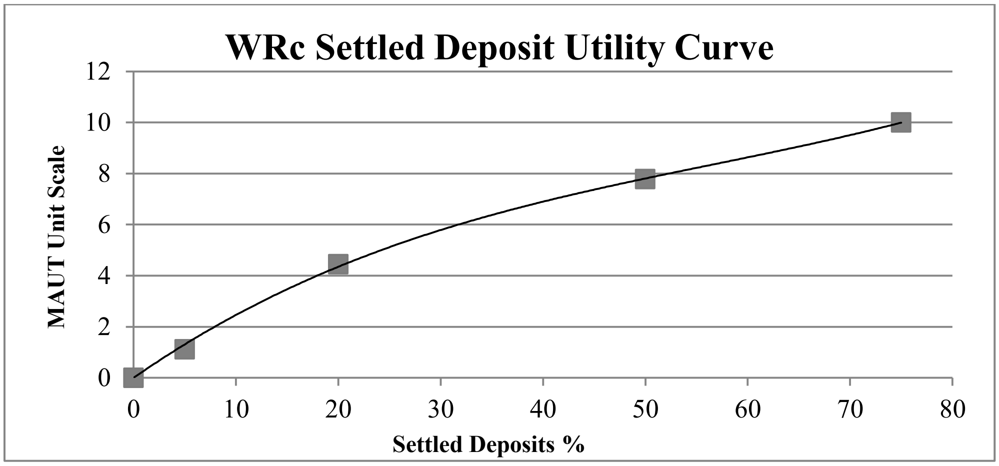

Figure 3.48 WRc Settled Deposits Utility Curve

3.4.1.3.2 CSP Settled Deposits Utility Function

The severities of the CSP are listed in Table 3.10. Based on the table, five grades explain the criticality levels of the settled deposits defect. The most critical case is when the deposits reach 50% or above.

Table 3.10 CSP Settled Deposits Severity

Code	Grade	Debris Percentage
CSP	1	0%–5%
	2	5%–10%
	3	10%–25%
	4	25%–50%
	5	>50%

- The grades are changed to the MAUT unit scale using equations 3.24, 3.25, and 3.26. The lowest percentage of each range is considered. Hence, the values considered are listed in Table 3.11.

Table 3.11 CSP Settled Deposits MAUT Scale

Code	Deposits % Considered (x-value)	MAUT Unit Scale (y-value)
CSP	0	0
	5	3
	10	5
	25	7
	50 or greater	10

- According to the x-values and y-values listed in Table 3.11, the points are plotted and the best regression type is considered. The optimum regression curve is a polynomial of degree 3. Based on Figure 3.49, the regression type perfectly plots the data considered, as its R^2 is 1.
- The function that represents the plotted curve follows:

$$CSP\ Utility\ Settled\ Deposits\ Function$$
$$= 0.0003(Settled\ Deposits\ \%)^3 - 0.0246(Settled\ Deposits\ \%)^2 + 0.7173(Settled\ Deposits\ \%) \quad [3.32]$$

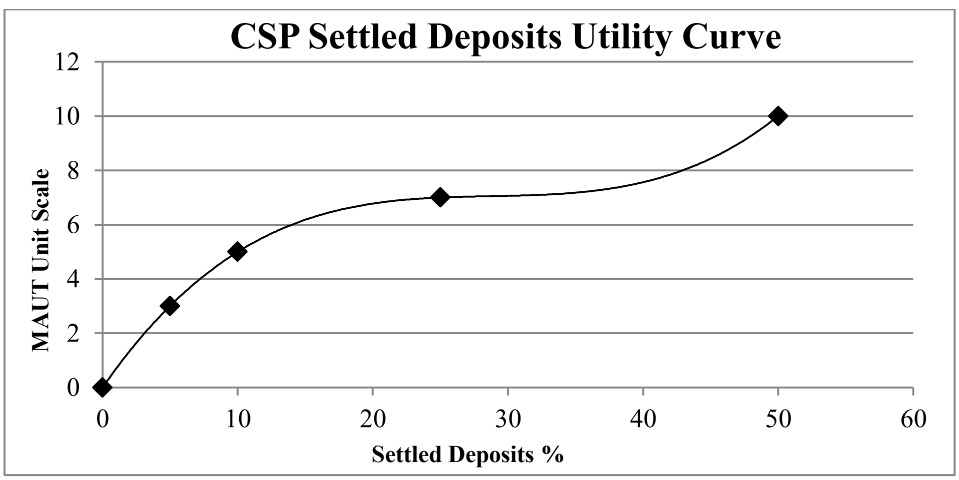

Figure 3.49 CSP Settled Deposits Utility Curve

3.4.1.3.3 New Zealand Utility Settled Deposits Function

New Zealand protocol's severities for settled deposits defect are reviewed and tabulated in Table 3.12. Three grades are considered in evaluating the settled deposits defect, ranging from 8 to 40.

Table 3.12 New Zealand Settled Deposits Severity

Code	Grade	Debris Percentage
New Zealand	Small, score = 8	<10%
	Medium, score = 20	10%–25%
	Large, score = 40	>25%

- Equations 3.24, 3.25, and 3.26 are used to change the grades to a 0 to 10 MAUT unit scale, as per Table 3.13. Three x- and y-values are computed, which will be scattered in a graph.

Table 3.13 New Zealand Settled Deposits MAUT Scale

Code	Deposits % Considered (x-value)	MAUT Unit Scale (y-value)
New Zealand	0	0
	10	3.75
	25 or greater	10

- Using the aforementioned points, the optimum regression curve is plotted and shown in Figure 3.50. The function that represents the curve is a polynomial of degree 2. Based on the figure, the regression type perfectly plots the data considered, as its R^2 is 1.
- The function that represents the curve follows:

$$New\ Zealand\ Utility\ Settled\ Deposits\ Function =$$

$$0.0017(Settled\ Deposits\ \%)^2 + 0.3583(Settled\ Deposits\ \%)\ [3.33]$$

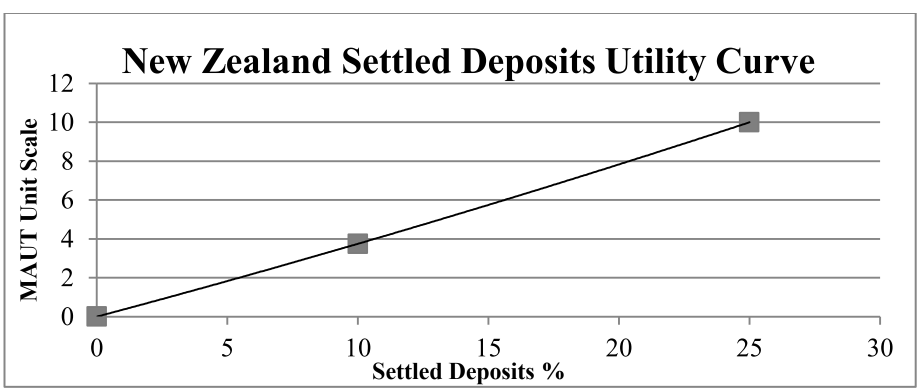

Figure 3.50 New Zealand Settled Deposits Utility Curve

3.4.1.4 Infiltration Utility Function

The three studied protocols recommended linguistic evaluation of infiltration defects (e.g., seeping and gushing). Consequently, no utility functions are prepared from these protocols. However, electro scan's infiltration evaluations are used. Electro scan considers the following flow ranges at each infiltration location of the pipeline section. Table 3.14 explains the linguistic grades considered by the electro scan. Any flow that is less than 4 liters/minute is small; however, any flow that is greater than 15 liters/minute is large.

Table 3.14 Electro Scan Infiltration Severity

Standard	Grade	Infiltration Flow
Electro Scan	Small	Less than 4 l/min
	Medium	From 4 l/min to 15 l/min
	Large	Greater than 15 l/min

- As Table 3.14 shows, numerical information about the infiltration flow is given in liters/minute. Hence, they will be changed to liters/second.
- The grades are linguistic. They should be changed to numerical ones, per Table 3.15. Therefore, they are divided equally, 0 representing small, 5 representing medium, and 10 representing large.

Table 3.15 Electro Scan Infiltration MAUT Scale

Standard	Flow Considered (x-value)	MAUT Unit Scale (y-value)
Electro Scan	0	0
	0.068	5
	0.25	10

- These points are plotted and the best regression type, which is a polynomial of degree 2, is considered, per Figure 3.51. Based on the figure, the regression type perfectly plots the data considered, as its R^2 is 1.

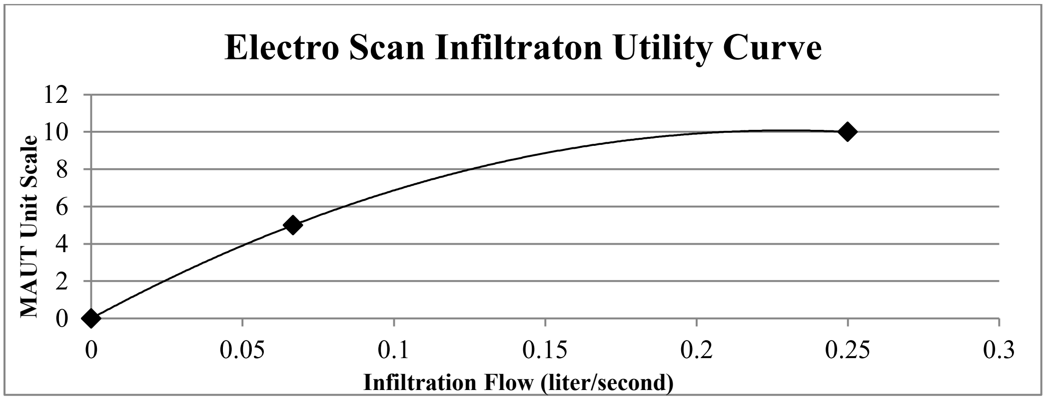

Figure 3.51 Electro Scan Infiltration Utility Curve

- The function that represents the regression curve follows:

$$Electro\ Scan\ Utility\ Infiltration\ Function$$
$$= -190.91(Infiltration\ Flow)^2 + 87.727\ (Infiltration\ Flow)\ [3.34]$$

3.4.1.5 Surface Damage Utility Functions

In reality, several sewer pipeline materials are utilized in sewer systems: cast iron, ductile iron, steel pipes, asbestos cement, plain cement concrete, reinforced cement concrete, brick sewers, plastic sewer pipes, high-density polyethylene, vitrified clay, and glass fiber reinforced. Many of these pipelines are manufactured and later laid down in sewer systems. Nonetheless, many of the sewer protocols are limited to certain pipeline materials when evaluating the surface damage defect.

For example, the New Zealand sewer pipeline protocol evaluates the surface damage defects according to three severities: small, medium, and large (NZWWWA 2006):

- Small: superficial only. Cement lining spalled from steel pipe.
- Medium: aggregate exposed or pipe wall otherwise significantly affected. Cement lining spalled from steel pipe and evidence of corrosion in the steel.
- Large: reinforcing exposed or no longer present due to corrosion, severe corrosion, or deep voids in the wall.

WRc, for instance, evaluates the surface damage defect according to different subdefects: increased roughness, surface wear, spalling, internal blister or bulge, aggregate visible, aggregate projecting from surface, reinforcement visible, reinforcement projecting from surface, reinforcement corroded, and corrosion products (WRc 2004). However, CSP extracts similar descriptions but fewer subdefects from WRc. Although CSP suggests numerical values in its considered subdefects, the information provided is general and not specified for material, condition, and pipeline size. Hence, more detailed examination of surface damage defects shall be considered. This research studies three sewer pipeline materials: reinforced concrete, ductile iron, and vitrified clay pipelines. The methodology depends on the structural point of view. Some of ASTM's and manufacturing companies' specifications are adopted in proposing the approach.

3.4.1.5.1 Reinforced Concrete (RC) Pipelines

A) The approach starts by grasping one of the most severe subdefects under the surface damage, which is reinforcement visible as described by WRc (2004), NZWWWA (2006), and Daher (2015). Obviously, reinforced concrete pipelines contain steel reinforcements to maintain their ductile behavior and added structural strength. These reinforcements are arranged to produce a steel cage with the shape of the pipeline. The steel cage consists of circumferential and longitudinal reinforcements. Circumferential reinforcements are lines of circumferential rebars, while the latter completes the steel cage as it maintains the reinforcements in shape and in position (ASTM 2011). Any negative effects on the steel rebars, such as corrosion, will reduce its strength. Corrosion occurs when steel rebars are exposed to sewer medium. Therefore, the critical case is considered when the reinforcement is visible.

B) According to ASTM (2011), when one line of circular reinforcement is used, it shall be placed from 35% to 50% of the wall thickness of the pipeline. Several assumptions are taken into account pertinent to the pipeline's cross section:

- One layer of circular reinforcement is used
- No extra concrete cover in the pipeline cross section
- Circular rebars will be placed at 50% of the wall thickness
- Minimum standard wall thickness is considered

C) Figure 3.52 is a cross-sectional view of the reinforced concrete pipeline wall thickness. According to the figure, the first layer of reinforcement, starting from the inside face, is the circumferential reinforcement. Therefore, for any RC pipeline size, the most severe case occurs when losing 50% or more of the wall thickness. For clarification, if the wall thickness loss reaches 50% or more, circular reinforcements will be visible. Hence, more corrosion will take place. As a result, structural strength drops and the pipeline becomes susceptible to failure.

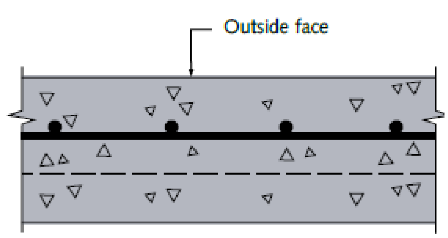

Figure 3.52 Wall Thickness Cross-Section of a Concrete Pipeline (Humes 2009)

D) Table 3.16 lists the standard RC pipeline sizes and the standard minimum wall thickness of each size (Humes 2009). The third column is the distance of the reinforcement circular rebars from the inside pipeline face.

E) The wall loss maximum distance % per image is the ratio between the maximum wall loss distance to the inside pipe diameter. For a segment wall loss calculation, the segment wall loss maximum distance % is used. The latter parameter will be utilized in the utility functions.

F) Therefore, the concrete permissible wall loss percentage shall be based on the ratio of the 50% of the thickness of each size to the inside pipe diameter of the same size (equation 3.35). The calculated percentages are presented in Table 3.16.

$$Concrete\ Permissible\ Wall\ Loss\ Percentage\ = \left(\frac{50\%\ of\ Thickness}{Inside\ Pipe\ Diameter} * 100\right) \text{[3.35]}$$

G) After finding the concrete permissible wall loss percentage, utility functions are computed. Because each pipeline size retains a unique permissible wall loss percentage, each will have a different utility function. A MAUT unit scale from 0 to 10 is used, where 0 is set at 0 percentage and 10 is set at the concrete permissible wall loss percentage. Any value that exceeds the concrete permissible wall loss percentage will be considered as a 10 MAUT unit scale. The utility functions generated are straight-line functions, as per equation 3.36.

$$Straight - Line\ Utility\ Function$$
$$= Factor\ *\ Segment\ Wall\ Loss\ Maximum\ Distance\ \%\ \text{[3.36]}$$

As an example, for an inside diameter of 15-inch pipeline, the permissible percentage is calculated as 7.50%. Hence, Figure 3.53 is plotted and the straight-line equation is taken as the utility function for the respective pipeline size. Based on the figure, the utility equation is presented in equation 3.37.

$$15\ in.\ Inside\ Diameter\ Concrete\ Pipeline\ Utility\ Function$$

$$= 1.333 * Segment\ Wall\ Loss\ Maximum\ Distance\ \%\ [3.37]$$

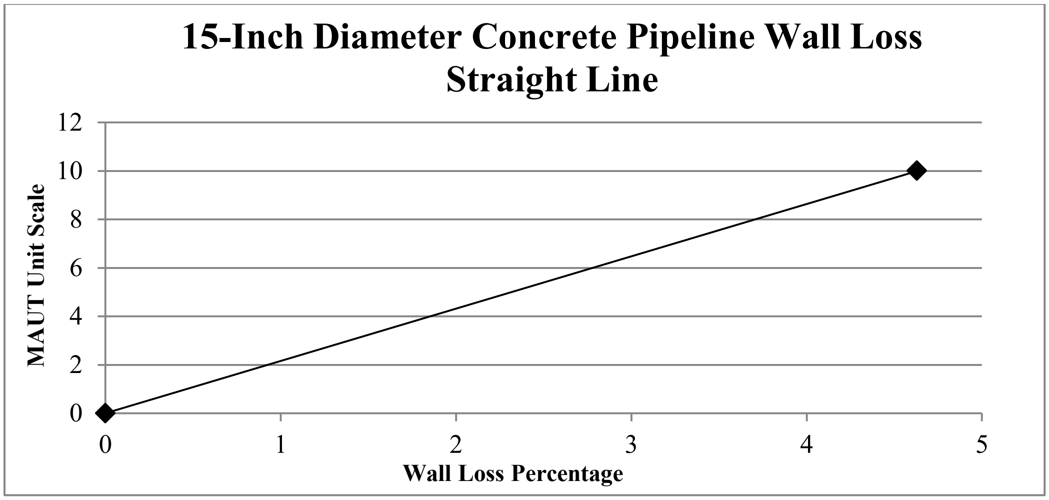

Figure 3.53 15-Inch Diameter Concrete Wall Loss Straight Line

Table 3.16 Concrete Pipeline Standard Sizes, Permissible Wall Loss % and Utility Functions

Inside Diameter (inch)	Minimum Wall Thickness (inch)	Circumferential Reinforcement Location from Inside Face (inch)	Permissible Thickness Wall Loss Percentage	Factor
12	2	1	8.33%	1.20
15	2.25	1.125	7.50%	1.33
18	2.5	1.25	6.94%	1.44
21	2.75	1.375	6.55%	1.53
24	3	1.5	6.25%	1.60
27	3.25	1.625	6.02%	1.66
30	3.5	1.75	5.83%	1.72
33	3.75	1.875	5.68%	1.76

Table 3.16 Concrete Pipeline Standard Sizes, Permissible Wall Loss % and Utility Functions (continued)

Inside Diameter (inch)	Minimum Wall Thickness (inch)	Circumferential Reinforcement Location from Inside Face (inch)	Permissible Thickness Wall Loss Percentage	Factor
36	4	2	5.56%	1.80
42	4.5	2.25	5.36%	1.87
48	5	2.5	5.21%	1.92
54	5.5	2.75	5.09%	1.96
60	6	3	5.00%	2.00
66	6.5	3.25	4.92%	2.03
72	7	3.5	4.86%	2.06
78	7.5	3.75	4.81%	2.08
84	8	4	4.76%	2.10
90	8.5	4.25	4.72%	2.12
96	9	4.5	4.69%	2.13
102	9.5	4.75	4.66%	2.15
108	10	5	4.63%	2.16

3.4.1.5.2 Ductile Iron Pipelines

A) Similar to RC sewer pipelines, the methodology of analyzing the surface damage defect is commenced by studying the structural design of ductile iron pipelines. ASTM specifications provide extensive information regarding the design of ductile iron pipelines. The *American Pipe Manual* (n.d.) provided many bedding types that are used when laying ductile iron:

- Type 1: flat bottom trench, loose backfill

- Type 2: flat bottom trench, backfill lightly consolidated to centerline of pipe
- Type 3: pipe bedded in 4-inch minimum loose soil, backfill lightly consolidated to top of pipe
- Type 4: pipe bedded in sand, gravel, or crushed stone to depth of 1/8 pipe diameter, 4-inch minimum, backfill compacted to top of pipe
- Type 5: pipe bedded to its centerline in compacted granular material, 4-inch minimum under pipe, compacted granular or selected material to top of pipe

B) Several assumptions are considered:

- Type 4 condition is chosen.
- The maximum pressure class is considered for each pipeline size.
- Pipeline depth is 16 feet.
- The required thickness is similar to the thickness at failure.

C) Tables of calculated internal, external, and standard pressure thicknesses are used (*American Pipe Manual*). Moreover, the largest thickness is considered the designed thickness of the pipeline.

D) The required thicknesses are assumed to act as the maximum loss a pipeline can reach. The actual manufactured thickness is calculated, as per equation 3.38.

$$Actual\ Manufactured\ Thickness = \frac{Outside\ Diameter - Inside\ Diameter}{2} \quad [3.38]$$

E) Thus, to get the ductile iron permissible wall loss percentage, the same wall loss maximum distance % per image parameters, inside diameter and maximum wall loss, shall be applied. Hence, the ductile iron permissible wall loss percentage is shown in equation 3.39.

$Ductile\ Iron\ Permissible\ Wall\ Loss\ Percentage$

$$= \left(\frac{Actual\ Manufactured\ Thickness - Required\ Thickness}{Inside\ Diameter} * 100\right) [3.39]$$

F) The utility function is found for each pipeline size. The closest is the percentage to the permissible percentage; the worst is the condition related to the surface damage defect. A MAUT unit scale of 10 is considered for any percentage that is equal to or greater than the permissible percentage, which is the percentage of the maximum thickness wall loss compared to the inside pipeline material allowed; 0 unit scale is considered for 0 wall loss percentage in the pipeline section. Because only two points are used, a straight-line Utility function is generated and equation 3.36 is used. The concept is employed on each pipeline's diameter, and the utility function factors are displayed in Table 3.17.

As an example of the utility function development, 32-inch pipe is considered. From the table, the permissible percentage is 0.46%, which is set at a 10 MAUT unit scale. Figure 3.54 plots the straight line.

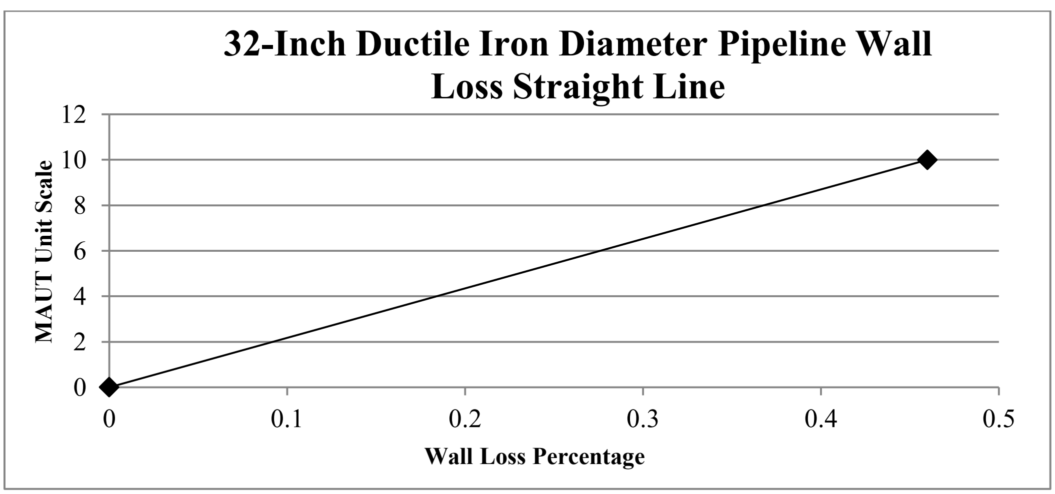

Figure 3.54 32-Inch Diameter Ductile Iron Pipeline Wall Loss Straight Line

The utility equation that refers to the example is as per equation 3.40.

$$32\ in.\ Diameter\ Ductile\ Iron\ Wall\ Loss\ Utility\ Function$$

$$= 21.74 * Segment\ Wall\ Loss\ Maximum\ Distance\ \% \quad [3.40]$$

Table 3.17 Ductile Iron Pipeline Standard Sizes, Permissible Wall Loss % and Utility Functions

Outside Diameter (inch)	Inside Diameter (inch)	Manufactured Thickness (inch)	Designed Thickness (inch)	Permissible Wall Loss Percentage	Factor
4.8	3.98	0.41	0.25	4.02%	2.49
6.9	6.04	0.43	0.25	2.98%	3.36
9.05	8.15	0.45	0.25	2.45%	4.08
11.1	10.16	0.47	0.26	2.07%	4.83
13.2	12.22	0.49	0.28	1.72%	5.81
15.3	14.28	0.51	0.31	1.40%	7.14
17.4	16.36	0.52	0.34	1.10%	9.09
19.5	18.44	0.53	0.36	0.92%	10.87
21.6	20.52	0.54	0.38	0.78%	12.82
25.8	24.68	0.56	0.43	0.53%	18.87
32	30.74	0.63	0.49	0.46%	21.74
38.3	36.84	0.73	0.56	0.46%	21.74

3.4.1.5.3 Vitrified Clay Pipelines

The last pipeline material examined for the surface damage defect is vitrified clay, another material common to sewer infrastructure.

A) Two formulas were employed to find the designed thicknesses required. These two equations were proposed by Hobrecht (1902).

- For diameters ≤400 mm:

$$Thickness\ (mm) = \left(\frac{Diameter(mm)}{20} + 9\ mm\right) [3.41]$$

- For diameters >400 mm:

$$Thickness\ (mm) = \left(\frac{Diameter(mm)}{18} + 9\ mm\right) [3.42]$$

B) The calculated thicknesses from the equations are assumed to be the designed ones. However, the standard thicknesses are listed in Table 3.18.

C) The vitrified clay permissible wall loss percentage is calculated based on equation 3.43.

$$Vitrified\ Clay\ Permissible\ Wall\ Loss\ Percentage = \left(\frac{Standard\ Thickness - Calculated\ Thickness}{Inside\ Diameter} * 100\right) [3.43]$$

D) Afterward, utility functions shall be established for each pipeline size. The permissible percentage is set at a 10 MAUT unit scale, and 0 MAUT unit scale is set at 0 percentage. Any percentage that exceeds the permissible percentage is taken as 10. Consequently, each pipeline diameter will possess one utility function supplied from a straight line, as per equation 3.36. Table 3.18 tabulates the information used to determine the utility functions.

As an example, for the inside diameter size of 36 inches, the permissible wall loss percentage is 3.2%. Thus, a straight line is plotted in Figure 3.55, and the utility function is found accordingly. From the plot, the example's utility function is as per equation 3.44.

$$36\ in.\ Diameter\ Vitrified\ Clay\ Wall\ Loss\ Utility\ Function = 3.13 * Segment\ Wall\ Loss\ Maximum\ Distance\ \%\ [3.44]$$

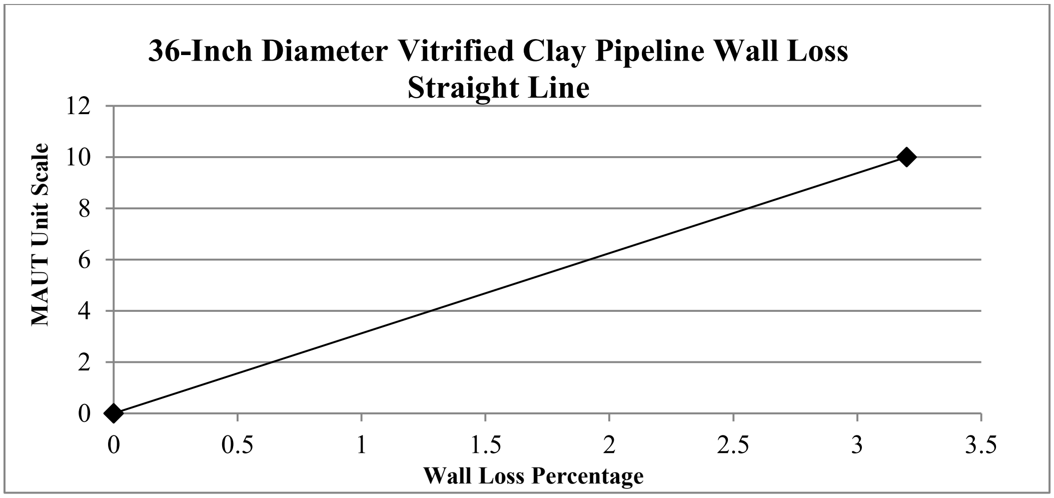

Figure 3.55 36-Inch Diameter Vitrified Clay Pipeline Wall Loss Straight Line

Table 3.18 Vitrified Clay Pipeline Standard Sizes, Permissible Wall Loss% and Utility Functions

Inside Diameter (inch)	Standard Thickness (inch)	Calculated Thickness (inch)	Permissible Wall Loss Percentage	Factor
6	0.935	0.65	4.68%	2.14
8	1.01	0.75	3.20%	3.13
10	1.235	0.85	3.81%	2.62
12	1.26	0.95	2.55%	3.93
15	1.65	1.19	3.08%	3.24
18	1.935	1.35	3.23%	3.10
21	2.39	1.52	4.14%	2.42
24	2.425	1.69	3.07%	3.26
27	2.885	1.85	3.82%	2.62
30	3.03	2.02	3.36%	2.75
33	3.26	2.19	3.25%	3.08
36	3.505	2.35	3.20%	3.13
39	3.71	2.52	3.05%	3.28
42	4.085	2.69	3.33%	3.00

3.5 Aggregated Index

To assess the condition of the pipeline, the indexes generated from the defects' utility functions are aggregated.

A) Each defect shall retain a unique weight that describes its importance to the other defects. Daher (2015) conducted a survey to find the importance weights among many of the pipeline defects. Because this research evaluates only four defects, their relative weights were found in the responses to his questionnaire. Figure 3.56 presents the relative weights calculated for each defect group and its subdefects.

B) When building the utility functions, a 0 to 10 scale was considered, where 0 represented no severity of pipeline segment and 10 was critical. Therefore, from the utility functions, each defect will provide a specific value, between 0 and 10, pertinent to the condition of the pipeline concerning the same defect.

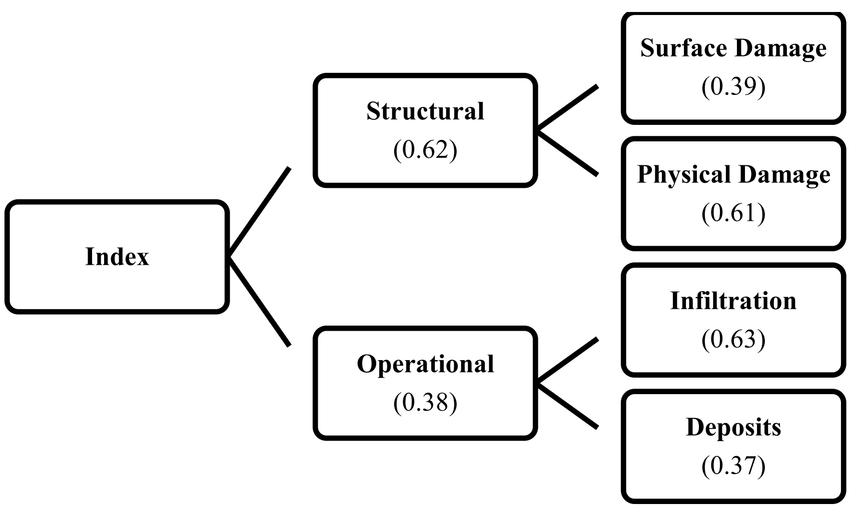

Figure 3.56 Weights of Defect and Subdefects Groups

C) Later, the defect of the same group's MAUT scale values and its corresponding relative importance weights are used to aggregate the defects of the same defect group using equation 2.1. For example, assume the MAUT scale values of infiltration and settled deposits are 3 and 5, respectively. Using equation 2.1, the calculated aggregated operational subdefects (S_OP) are 0.63*3 + 0.37*5 = 3.74. A similar approach is used to calculate the structural defects (S_ST).

D) The relative importance of the defect group to the pipeline index is calculated by multiplying the relative importance percentage of the defect group by the value resulting from Step C. Therefore, the pipeline index = 0.38* S_OP + 0.62* S_ST.

E) The index resulting from Step D is then changed to a scale from 1 to 5.

3.6 CSP Scale Modification

The importance of the grade index is to inform decision makers of the condition of the sewer pipeline. The definition of the index and grade computed is based on a protocol scale that defines its severity and the action plan required. Hence, the CSP scale suggested by Daher (2015) is revisited and modified as per Table 3.19. Some modifications were minor; others were major, as mentioned in the note in the table.

Table 3.19 CSP Modified Scale

#	MAUT Scale	Linguistic Scale	Description	Defect Example	Action Plan
1	0–1	Excellent	No defect	- *Deformation % = 0* - *Segment Wall Loss Maximum Distance = 0* - *Segment Blockage Rate = 0* - *No Infiltration*	Not required; inspect and monitor certain areas/ intervention not needed
2	1–3	Good	Minor defects of low to medium severity where defects started to evolve	- Deformation <5% - *Segment Wall Loss Maximum Distance >0%–25% of Permissible Wall Loss Percentage* - *Segment Blockage Rate ≤5%*	Remove operational defects and put in place measures to identify defect causes
3	3–6	Fair	Moderate defects of medium severity—deterioration in progress	- *Segment Wall Loss Maximum Distance ≤25%–50% of the Permissible Wall Loss Percentage* - Deformation ≥5%–10% - *Segment Blockage Rate ≥5%–25%* - *Total Segment Infiltration <0.067 liter/second*	Remove operational defects and put in place measures to identify defect causes. Increase inspection frequency. Consider medium- to long-term rehabilitation options to repair fractures/leaking joints (e.g., patch repair/resin injection, etc.)
4	6–8	Poor	Severe defects	- *Segment Wall Loss Maximum Distance ≥50%–75% of Permissible Wall Loss Percentage* - *Segment Blockage Rate ≥25%–50%* - *Deformation ≥10%–25%* - *Total Segment Infiltration ≥0.067 l/s–0.25 l/s*	Remove operational defects in the immediate term and put in place measures to identify cause/source. Evaluate the criticality of the sewer and, subject to the findings, implement remedial measures (replace/rehabilitate) in the immediate to medium term
5	8–10	Critical	Very severe defects/total loss of structural integrity	- *Segment Wall Loss Maximum Distance ≥75% of Permissible Wall Loss Percentage* - *Deformation % ≥25%* - Segment Blockage Rate ≥50% - *Total Segment Infiltration ≥0.25 l/s*	Sewer replacement is needed due to complete disruption of service (failure). Immediate action to remedy operational deficiencies and investigate the cause to prevent its recurrence

Note: Underlined sentences are minor changes to the CSP scale. *Italic* sentences are added or majorly modified sentences.

3.7 Summary

This chapter concentrated on the acquired methodology of the research. The research methodology started with analyzing the four defects: deformation, settled deposits, infiltration, and surface damage. The analysis was based on image processing tools and an electrical approach.

Later, the research developed utility functions for each defect. Deformation and settled deposits functions were based on three protocols. Hence, each acquired three different functions. The infiltration utility function was based on the electro scan's suggested severity. Nevertheless, the surface damage defect utility function was based on using the structural behavior for three sewer materials: reinforced concrete, vitrified clay, and ductile iron.

Next, the research revisited the CSP scale and modified it for better evaluation and reduced subjectivity. Some modifications were minor, while others were major.

CHAPTER FOUR: MODEL IMPLEMENTATION, RESULTS, AND VALIDATION

4.1 Overview

Implementing the validation process on actual case studies will check its applicability, reliability, and validity. The deformation image processing procedure, with actual values found in some reports, is tested and compared in 4.2. Validation equations are used to decide the approach that gives the closest results. Next, settled deposits and surface damage image processing algorithms are implemented on their corresponding images in 4.3 and 4.4, respectively.

The MAUT model is tested using actual case studies from Canada and Qatar in 4.5. The aggregated calculated indexes are exposed to three types of rounding: to the nearest number, up, and down. Validation equations are also used to test the optimum rounding type compared to the index values in the reports.

4.2 Deformation Algorithm Implementation

Four images were tested on the suggested deformation algorithm. Two approaches were developed previously, which will be validated and compared. The mean absolute error (MAE) (equation 4.1) was calculated for the two approaches, ASTM F1216 and the roundness factor. Additionally, the difference percentages between the values from the two approaches were calculated (equation 4.2). Thus, the average of the percentage difference is calculated accordingly:

$$Mean\ Absolute\ Error\ = \left(\frac{\Sigma\ (|\text{Algorithm Value} - \text{Report Value}|)}{Number\ of\ Images}\right)\ [4.1]$$

$$Difference\ Percentage = \left(\frac{(|Algorithm\ 1\ Value - Algorithm\ 2\ Value|)}{\frac{Algorithm\ 1\ Value + Algorithm\ 2\ Value}{2}} * 100 \right) \quad [4.2]$$

Based on Figure 4.1, percentages fluctuate from the actual values, although there were no drastic differences. Table 4.1 lists the results obtained for each case study. The MAEs using the ASTM F1216 formula and the roundness factor were 4.27% and 4.83%, respectively. The average difference percentage between the two approaches was 16.67%. The highest and lowest difference percentages were 40.06% and 0.59%, respectively.

Based on the research, the roundness factor algorithm provided almost similar results compared to the report's results and the ASTM formula. However, the roundness factor could provide different results when the object is closer to a circle, as was found in case study 4.

Table 4.1 Deformation Image Processing Results and Comparisons

#	Report %	Deformation % (Equation 3.4)	Deformation % (Equations 3.6 & 3.7)	Difference %
1	7	14.5	12.5	14.81
2	12	18.54	18.65	0.59
3	16	15.80	17.68	11.23
4	2.5	5.33	8	40.06

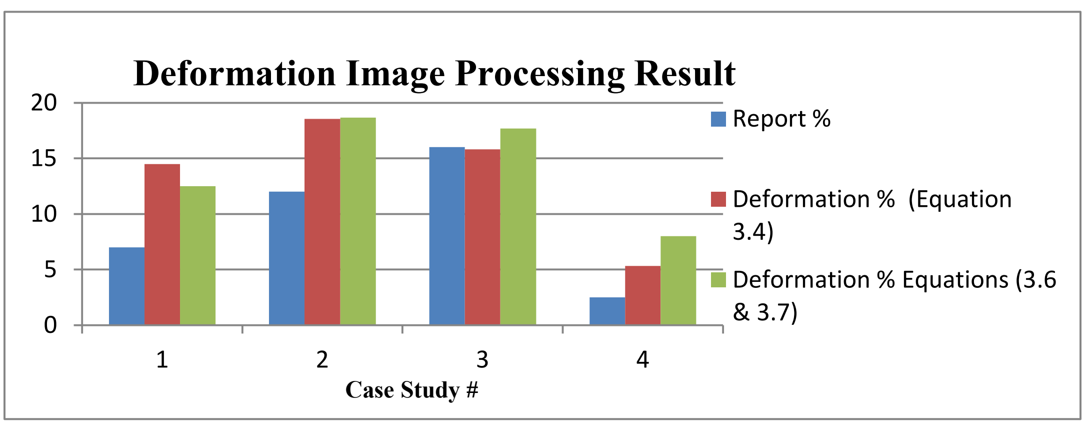

Figure 4.1 Deformation Image Processing Result

4.3 Settled Deposits Algorithm Implementation

The algorithm developed for the settled deposits defect was tested on four different images. The algorithm was able to calculate the settled deposits that presented in the images. The results are summarized in Table 4.2. The highest blockage rate among the images tested was 19.53% and the lowest blockage rate was 6.09%.

Table 4.2 Settled Deposits Image Processing Case Study

#	Settled Deposits Area (Pixels)	Pipe Area (Pixels)	Blockage Rate per Image %
1	2,022	16,417	12.32
2	1,982	16,415	12.07
3	3,153	16,147	19.53
4	983	16,147	6.09

4.4 Surface Damage Algorithm Implementation

The algorithm developed for the surface damage defect was tested on two different images. The algorithm calculated the wall loss maximum distance percentage and the wall loss area. Table 4.3 summarizes the results. Based on the table, the maximum and minimum wall loss area percentages were 8.96% and 7.51%, respectively. The highest percentage for the wall loss maximum distance percentage was 17.43%.

Table 4.3 Surface Damage Image Processing Results

#	Before Subtraction		After Subtraction		Wall Loss Area %	Wall Loss Maximum Distance %
	Major Axis Length (Pixels)	Area (Pixels)	Major Axis Length (Pixels)	Area (Pixels)		
1	180.74	25,274	171.86	23,195	8.96	5.17
2	203.72	24,934	173.48	23,193	7.51	17.43

4.5 Condition Assessment Model Implementation

This section validates the MAUT model developed in this research. The validation is based on testing the MAUT model generated for each defect on actual case studies. The research did not obtain any complete case studies from the suppliers. Therefore, it relied on CCTV reports. The reports collected were from Qatar and Canada. The research analyzed 27 reports from Canada and 670 reports from Qatar. All reports were exposed to a screening step, which disregards reports that do not satisfy certain criteria. The criterion for selecting the report, for the validation part, was that it shall contain only defects that were considered in the research: deformation, settled deposits, infiltration, and surface damage. Based on the screening step, only 17 reports satisfied the criteria: 12 from Qatar and 5 from Canada.

4.5.1 Validation Procedure

To achieve the validation part of the MAUT model, several steps are considered:

A) Use the reports screened to generate indexes for the four defects. The reports contained distinct scales. Qatar's reports considered a scale of 0 to 4, where 4 was considered excellent and 0 critical. Qatar's evaluation was based on the Euro code (EN13508). It provided one scale that described the segment inspected. Canada's reports considered a 1 to 5 scale, where 1 was excellent and 5 was critical. Canada's report evaluation was based on the pipeline assessment certification program PACP code. It provided an aggregated index for the structural defects and another for the operational defects.

B) CCTV reports obtained did not quantify the surface damage defect. Nevertheless, they provided linguistic information and pictures of the defect at different locations. To quantify the defect, the original CSP severities of the surface damage defect were adopted. In the mentioned protocol, the surface damage severities were explained in Table 2.10. In the reports, the linguistic information was given as increased roughness, spalling, missing aggregate, aggregate projecting, reinforcement visible, reinforcement projecting, and reinforcement missing or corroded. Once one of these subdefects is observed, its corresponding depth value from Table 4.4 is considered. If a range is given, the average value is considered. For example, 10 to 15 mm will be taken as 12.5 mm. Therefore, the linguistic information was translated as in Table 4.4. Additionally, to get the width of the wall loss, each picture's number of frames was assumed.

Table 4.4 Surface Damage Subdefect Considered Depths

Surface Damage Subdefect	Considered Depth (mm)
Increased roughness	0
Spalling	2.5
Missing aggregate	7.5
Aggregate projecting	12.5
Reinforcement visible	12.5
Reinforcement projecting	12.5
Reinforcement missing/corroded	15

C) In all of the protocols studied, linguistic infiltration defect information was provided. Therefore, a certain measure had to be assumed to commence validating the model. The common infiltration defects observed in the reports were compared to the infiltration severities in the electro scan. The common infiltration subdefects from lowest severities to highest and according to CSP protocol are seeping, dripping, running, and gushing. In the infiltration MAUT model, there are three grades: 0, 5, and 10. The 0 grade indicates seeping; 5, dripping and running; and 10, gushing.

D) Calculate the indexes using utility functions.

E) Use the relative importance weights to aggregate the indexes. For Qatar's case studies, the computed index shall describe the aggregation of the structural and operational defects.

However, for Canada's reports, two aggregated indexes are computed: structural and operational.

F) Change the aggregated index to the scale used in the CCTV reports.

G) Change the reports' scales and the computed aggregated indexes to a 1 to 5 scale.

H) Because the aggregated computed index will contain decimals, three rounding types are tested and validated using the MAE. The actual values are assumed to be the grades from the reports. The rounding types tested are rounding to the nearest number, rounding up, and rounding down.

I) Compare the results and select the optimum rounding type.

J) The optimum selected rounding type's results are compared with the results found using the CSP methodology.

As a note, the computed aggregated indexes were classified based on the "protocol's name." This means that the deformation and settled deposits severities of the same protocol were used in the utility function's development. For example, WRc computed index means that the index was aggregated from the use of the WRc deformation utility function (equation 3.28), WRc settled deposits utility function (equation 3.31), infiltration utility function (equation 3.34), and any of the surface damage utility functions.

The aforementioned procedure was applied on all case studies obtained. Table 4.5 presents information adapted from the pipeline 1.12 report. As per the computations, the indexes for CSP, WRc, and New Zealand were 3.54, 3.81, and 3.72, respectively.

Table 4.5 Case Study 1, Pipeline 1.12

Inspection Length	9.9 m				
Material	Clay				
Size	150 mm				
Location (m)	**Defect**	**Detail**	**Unit**	**Amount**	**Unit**
0	Settled Deposits	0	%	0	m^2
0.7	Settled Deposits	3	%	0.00028	m^2
2.5	Settled Deposits	5	%	0.00047	m^2
3.3	Settled Deposits	5	%	0.00047	m^2
4	Settled Deposits	2	%	0.00019	m^2
5.3	Settled Deposits	7	%	0.00066	m^2
8.1	Settled Deposits	5	%	0.00047	m^2
9.5	Settled Deposits	10	%	0.00095	m^2
9.9	Settled Deposits	10	%	0.00095	m^2
Total Volume of Deposits	0.0049	m^3			
Debris Area/m	0.000494949	m^2/m			
Blockage Percentage	5.210817444	%			
Protocol	**MAUT Index (0–10)**				
Index CSP	1.15				
Protocol	**MAUT Index (0–10)**				
Index WRc	0.486				
Index New Zealand	0.71				
Protocol	**Grade (0–4)**				
Report Grade	3				
CSP Class	3.54				
WRc Grade	3.81				
New Zealand Grade	3.72				

The same procedure is applied to obtain the indexes of the operational and structural defects for pipeline 2.1, from case study 2. Table 4.6 presents the information of the respective pipeline with the computational results. The index calculated for the structural defects for the CSP, WRc, and New Zealand was 1. However, the indexes calculated for the operational defects for the CSP, WRc, and New Zealand were 1.81, 1.33, and 1.62, respectively.

Table 4.6 Case Study 2, Pipeline 2.1

Inspection Length	25.1 m				
Material	RC				
Size	300 mm				
Location (m)	**Defect**	**Detail**	**Unit**	**Amount**	**Unit**
0	Settled Deposits	0	%	0	m^2
5	Infiltration	4	l/m	0.00531	per pipeline length
9	Settled Deposits	10	%	0.00707	m^2
16.7	Settled Deposits	10	%	0.00707	m^2
25.1	Settled Deposits	15	%	0.0106	m^2
Total Volume of Deposits	0.1604	m^3			
Debris Area/m	0.006390438	m^2/m			
Blockage Percentage	9.045206294	%			
Protocol	**MAUT Index (0–10)**				
Operational CSP	2.03				
Operational WRc	0.8251				
Operational New Zealand	1.54				
Structural CSP	0				
Structural WRc	0				
Structural New Zealand	0				
Protocol	**Grade (1–5)**				
Report Grade (Operational)	3				
Report Grade (Structural)	1				
Operational CSP	1.812				
Operational WRc	1.33				
Operational New Zealand	1.616				
Structural CSP	1				
Structural WRc	1				
Structural New Zealand	1				

4.5.2 Case Study 1: Qatar

Twelve CCTV reports were used to test the utility functions. Many of the reports contained settled deposits defects. Few reports contained the infiltration and surface damage defects. However, deformation defects were not found. Table 4.7 summarizes the results for Qatar's case study. Based on the table, many of the case studies' indexes calculated ranged from 3 to 4. Comparing the third, fourth, and fifth columns shows that the CSP indexes produced lower values than the others did. Therefore, it suggested worse pipeline conditions than the other protocols.

Table 4.7 Case Study 1 Results

Case Study #	Actual Grade (0–4)	CSP (0–4)	WRc (0–4)	New Zealand (0–4)
1.1	2	3.03	3.44	3.036
1.2	4	3.67	3.73	3.71
1.3	4	3.61	3.84	3.77
1.4	3	3.38	3.4	3.39
1.5	3	3.77	3.79	3.77
1.6	3	3.80	3.93	3.89
1.7	3	3.83	3.95	3.91
1.8	3	3.61	3.84	3.77
1.9	2	1.66	2.064	1.67
1.10	3	3.82	3.94	3.9
1.11	4	3.85	3.95	3.92
1.12	3	3.54	3.81	3.72

4.5.2.1 Scale Rounding Types

When changing the MAUT scale to the 1 to 5 grade, the resulting index contained decimals. The MAE values before rounding for CSP, WRc and New Zealand were 0.58, 0.64 and 1.46, respectively. Therefore, the validation model is divided into three parts, to round the index to a whole number. The first part is based on rounding the predicted index to the nearest number (e.g., 1.6 is rounded to 2 and 1.2 is rounded to 1). The second validation is based on rounding up the index. The third validation is based on rounding down the index. Mathematical validation was adopted to achieve the validation parts. The MAE is calculated as per equation 4.3. If the value of the MAE is close to 0, the model is considered reliable (Dikmen et al. 2005).

$$MAE = \frac{\sum_{i=1}^{n}|Ci - Ei|}{n} \quad [4.3]$$

4.5.2.1.1 Rounding to Nearest Number

The MAUT 1 to 5 decimal grades are rounded to the nearest number. Table 4.8 provides a summary of the cases and their actual and predicted indexes. Because many of the computed indexes (see 4.5.2) were not drastically different, many of the case studies rounded to the nearest number produced similar values.

Table 4.8 Case Study 1, Rounding to Nearest Number

Case #	Actual Index Scale 1 to 5	CSP 1 to 5	WRc 1 to 5	New Zealand 1 to 5
1.1	3	2	2	2
1.2	1	2	1	1
1.3	1	1	1	1
1.4	2	2	2	2
1.5	2	1	1	1
1.6	2	1	1	1
1.7	2	1	1	1
1.8	2	1	1	1
1.9	3	3	3	3
1.10	2	1	1	1
1.11	1	1	1	1
1.12	2	1	1	1

4.5.2.1.2 Rounding Up

The indexes computed in 4.5.2 were rounded up and the results are listed in Table 4.9. The table provides a summary of the case numbers and their actual and predicted indexes. Similarly, because the computed indexes in 4.5.2 were not drastically different, many of the rounded values were equivalent.

Table 4.9 Case Study 1, Rounding Up

Case #	Actual Index Scale 1 to 5	CSP 1 to 5	WRc 1 to 5	New Zealand 1 to 5
1.1	3	2	2	2
1.2	1	2	2	2
1.3	1	2	2	2
1.4	2	2	2	2
1.5	2	2	2	2
1.6	2	2	2	2
1.7	2	2	2	2
1.8	2	2	2	2
1.9	3	3	3	4
1.10	2	2	2	2
1.11	1	2	2	2
1.12	2	2	2	2

4.5.2.1.3 Rounding Down

The indexes computed in 4.5.2 were rounded down, and the results are listed in Table 4.10. Similarly, because the computed indexes in section 4.5.2 were not drastically different, many of the rounded values were equivalent.

Table 4.10 Case Study 1, Rounding Down

Case #	Actual Index Scale 1 to 5	CSP 1 to 5	WRc 1 to 5	New Zealand 1 to 5
1.1	3	1	1	1
1.2	1	1	1	1
1.3	1	1	1	1
1.4	2	1	1	1
1.5	2	1	1	1
1.6	2	1	1	1
1.7	2	1	1	1
1.8	2	1	1	1
1.9	3	2	2	3

Table 4.10 Case Study 1, Rounding Down (continued)

1.10	2	1	1	1
1.11	1	1	1	1
1.12	2	1	1	1

4.5.2.2 Results and Discussion

Before testing the rounding types, the MAE values were computed for CSP, WRc and New Zealand and the values were 0.58, 0.64 and 1.46, respectively. After investigating the three types of rounding, they were compared using the MAE. Figure 4.2 is the bar chart of the MAE values for the three rounding types. When rounding the computed grade to the nearest number, the MAEs for CSP, WRc, and New Zealand were 0.67, 0.58, and 0.58, respectively. However, when rounding down the computed index, the MAEs for CSP, WRc, and New Zealand were 0.83, 0.83, and 0.75, respectively. Finally, when rounding up the computed index, the MAEs for CSP, WRc, and New Zealand were 0.33, 0.33, and 0.42, respectively. Comparing the MAE values, rounding up produced the least MAE values; hence, it is more reliable than the other types.

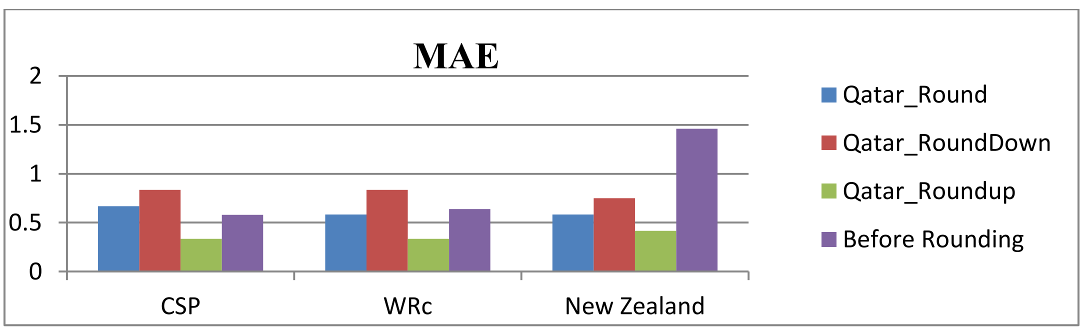

Figure 4.2 Case Study 1, MAE

4.5.3 Case Study 2: Canada

Another five case studies were used to test the MAUT model. The reports contained some of the four defects: settled deposits, surface damage, and infiltration. The reports did not provide one grade for the pipeline; instead, they provided a grade for the structural defects and a grade for the operational defects. Therefore, the utility functions were divided into two separate groups accordingly. Table 4.11 summarizes the results for case study 2. The structural indexes and the operational indexes were computed separately for each protocol's name. The structural defect indexes for the three protocols were equivalent, as the surface damage defect was the only defect observed in the reports.

Table 4.11 Case Study 2 Results

Case Study #	Operational (1–5)				Structural (1–5)			
	Actual Grade	CSP	WRc	New Zealand	Actual Grade	CSP	WRc	New Zealand
2.1	3	1.812	1.33	1.616	1	1	1	1
2.2	2	1.252	1.09	1.14	2	1.26	1.26	1.26
2.3	3	2.012	1.63	1.62	2	1.54	1.54	1.54
2.4	3	1.91	1.5	1.83	3	2.49	2.49	2.49
2.5	3	1.69	1.12	1.56	1	1	1	1

4.5.3.1 Scale Rounding Types

The five case studies were analyzed and the predicted structural and operational grades were calculated. Similar to the previous case study, the best rounding type is studied and the best type is selected based on the MAE calculations.

4.5.3.1.1 Rounding to the Nearest Number

After rounding the computed indexes to the nearest number, they were listed in Table 4.12. The table considers the computation of each defect type for each protocol's name. The rounded computed indexes for the operational defects were observed to be different, unlike the rounded structural indexes.

Table 4.12 Case Study 2, Rounding to the Nearest Number

Case #	Actual Value 1 to 5		CSP 1 to 5		WRc 1 to 5		New Zealand 1 to 5	
	Structural	Operational	Structural	Operational	Structural	Operational	Structural	Operational
2.1	1	3	1	2	1	1	1	2
2.2	2	2	1	1	1	1	1	1
2.3	2	3	2	2	2	2	2	2
2.4	3	3	2	2	2	2	2	2
2.5	1	3	1	2	1	1	1	2

4.5.3.1.2 Rounding Down

After rounding the computed indexes down, they were listed in Table 4.13. The table considers the computation of each defect type for each protocol's name. Similarly, the rounded computed indexes for the operational defects were observed to be different, unlike the rounded structural indexes.

Table 4.13 Case Study 2, Rounding Down

Case #	Actual Value 1 to 5		CSP 1 to 5		WRc 1 to 5		New Zealand 1 to 5	
	Structural	Operational	Structural	Operational	Structural	Operational	Structural	Operational
2.1	1	3	1	1	1	1	1	1
2.2	2	2	1	1	1	1	1	1
2.3	2	3	1	2	1	1	1	2
2.4	3	3	2	1	2	1	2	1
2.5	1	3	1	1	1	1	1	1

4.5.3.1.3 Rounding Up

After rounding the computed indexes up, they were listed in Table 4.14. The table considers the computation of each defect type for each protocol's name. Similarly, the rounded computed indexes for the operational defects were observed to be different, unlike the rounded structural indexes.

Table 4.14 Case Study 2, Rounding Up

Case #	Actual Value 1 to 5		CSP 1 to 5		WRc 1 to 5		New Zealand 1 to 5	
	Structural	Operational	Structural	Operational	Structural	Operational	Structural	Operational
2.1	1	3	1	2	1	2	1	2
2.2	2	2	2	2	2	2	2	2
2.3	2	3	2	3	2	2	2	3
2.4	3	3	3	2	3	2	3	2
2.5	1	3	1	2	1	2	1	2

4.5.3.2 Results and Discussion

Before testing the rounding types on the six categories, the original computed index's MAE values were calculated. The MAE values for the CSP, WRc and New Zealand for structural group was 0.342 in each case. Nevertheless, the MAE values for the CSP, WRc and New Zealand for the operational group were 1.06, 1.47 and 1.25, respectively. Then, the MAE was also used to compare the rounding types of the computed aggregated indexes. To better understand the MAE values, Table 4.15 presents the MAE computations. Figure 4.3 will be used to visualize the results. From the table and the figure, the values for rounding to the nearest number, rounding down, and rounding up the MAE values for the structural defect indexes were 0.4, 0.6, and 0, respectively. Hence, rounding up produced the lowest value. In addition, the values for rounding to the nearest number, rounding down, and rounding up for the CSP operational indexes were 1, 1.6, and 0.6, respectively. Similarly, the values for rounding to the nearest number, rounding down, and rounding up for the WRc operational indexes were 1.4, 1.8, and 0.8. The values for rounding to the nearest number, rounding down, and rounding up for the New Zealand operational indexes were 1, 1.6, and 0.6, respectively. As a result, rounding up the aggregated index is more reliable than the other rounding types.

Table 4.15 MAE Values for Case Study 2

Detail	Before Rounding	Rounding to the Nearest Number	Rounding Down	Rounding Up
CSP Structural	0.342	0.4	0.6	0
CSP Operational	1.06	1	1.6	0.6
WRc Structural	0.342	0.4	0.6	0
WRc Operational	1.47	1.4	1.8	0.8
New Zealand Structural	0.342	0.4	0.6	0
New Zealand Operational	1.25	1	1.6	0.6

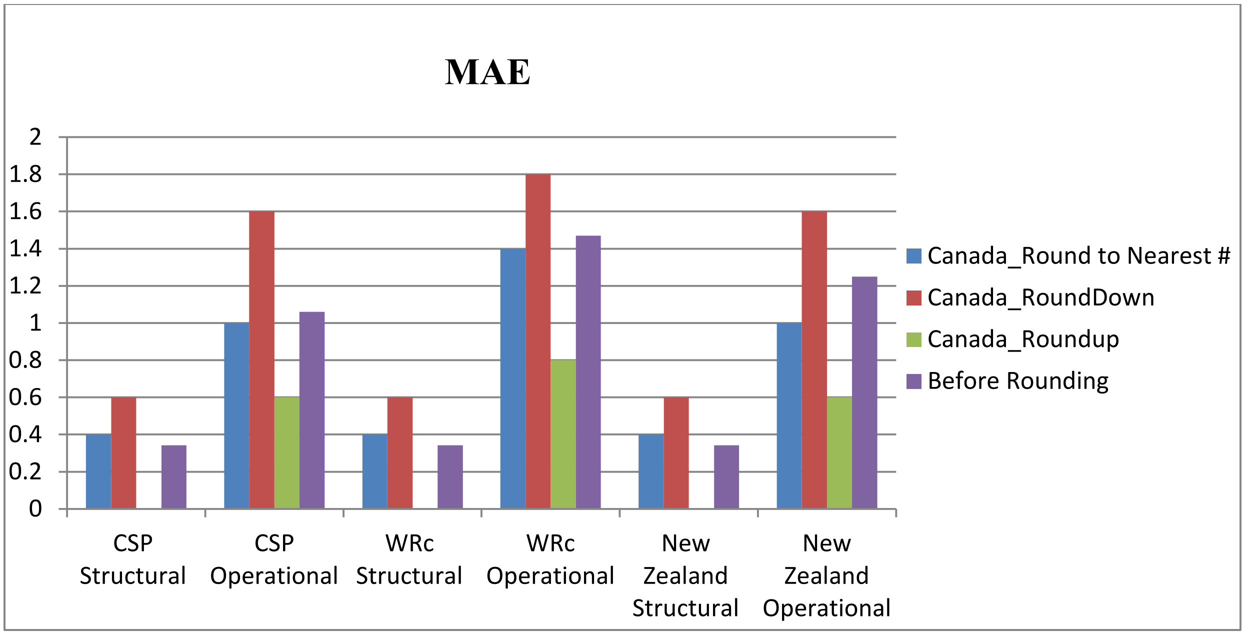

Figure 4.3 MAE Values for Case Study 2

4.5.4 CSP Grading Method vs. CSP MAUT Grading Method

Based on the two previous case studies, rounding up the aggregated index provided the closest results to the actual grades from the reports. The CSP grading methodology developed by Daher (2015) was used for the same Qatar case studies. The grades from 1 to 5 were calculated and compared with the results already investigated in the CSP MAUT rounding up approach. Table 4.16 demonstrates the values of the two approaches. Daher's (2015) methodology provided an MAE of 0.25; however, the MAUT methodology provided an MAE of 0.33. The average difference percentage between the two approaches was calculated as 3.33%. In spite of the lower MAE value for the CSP methodology, a minimal difference was observed between the two methods.

Table 4.16 Case Study 1: CSP Daher Method vs. CSP MAUT Method

Case #	CSP by Daher Method Grade 1–5	CSP MAUT Grade 1–5
1.1	3	2
1.2	2	2
1.3	2	2
1.4	2	2
1.5	2	2
1.6	2	2
1.7	2	2
1.8	2	2
1.9	3	3
1.10	2	2
1.11	2	2
1.12	2	2

4.6 Summary

First, the chapter implemented the image processing algorithms to quantify the three defects. Later, the deformation algorithm was validated using the MAE. The MAE value for the ASTM F1216 was found to be 4.27%, while the MAE for the roundness factor was found to be 4.83%. Additionally, the difference in percentages was calculated between the ASTM and roundness factor concepts. The maximum value was found to be 40.06%, whereas the minimum was found to be 0.59%. The calculated average difference percentage was 16.67%.

CCTV report results were used in the validation of the MAUT model. Twelve reports were brought from Qatar and another five reports from Canada. The MAUT grades using the three protocols were calculated using three rounding types: rounding to the nearest number, rounding up, and rounding down. The resulting values were validated with the actual values using the MAE. As a result, rounding up provided the closest results to the actual grades.

Later, the rounding up results were further compared with the CSP code methodology results. The MAE of the CSP methodology was calculated as 0.25, whereas the MAE using the MAUT approach was 0.33. In addition, the average difference percentage was found to be 3.33%. Although the CSP methodology provides a slightly lower MAE value, a minimal difference between the two approaches was seen.

CHAPTER FIVE: AUTOMATED TOOL

5.1 Introduction

The research assessed four defects of sewer pipelines: deformation, settled deposits, infiltration, and surface damage. These defects are detected using technologies such as the laser profiler, sonar, and electro scan. Some technologies produce images, while others produce numerical values, which are used as inputs for the automated tool. Each defect had its own quantification algorithm. Many codes and mathematical equations were used for this purpose. Another objective of the research was to form an approach to grade the pipeline based on the four defects. Hence, the MAUT approach was utilized. After developing the automated tool for each of the four defects and generating all utility functions, they were combined in one practical interface. Graphical user interface design environment (GUIDE) was implemented to incorporate all codes and equations.

5.2 Automated Sewer Inspection Analysis (ASIA)

Automated sewer inspection analysis (ASIA) consists of three major parts. The first component acts as the help tool. It provides the user with the necessary information to export the data to the interface and to run the program. It also gives an overview about the defects and their inputs, outputs, and method of calculation. The second component includes several image processing codes and equations that process and analyze the four defects. The third component contains the model for the grading scheme. Deformation and settled deposits possessed three different utility functions from three different sewer protocols; infiltration had only one utility function; and the surface damage defect included a number of utility functions. The tool is equipped with all utility functions generated for all of the defects.

5.3 ASIA Snapshots

Figure 5.1 is the cover window of the interface.

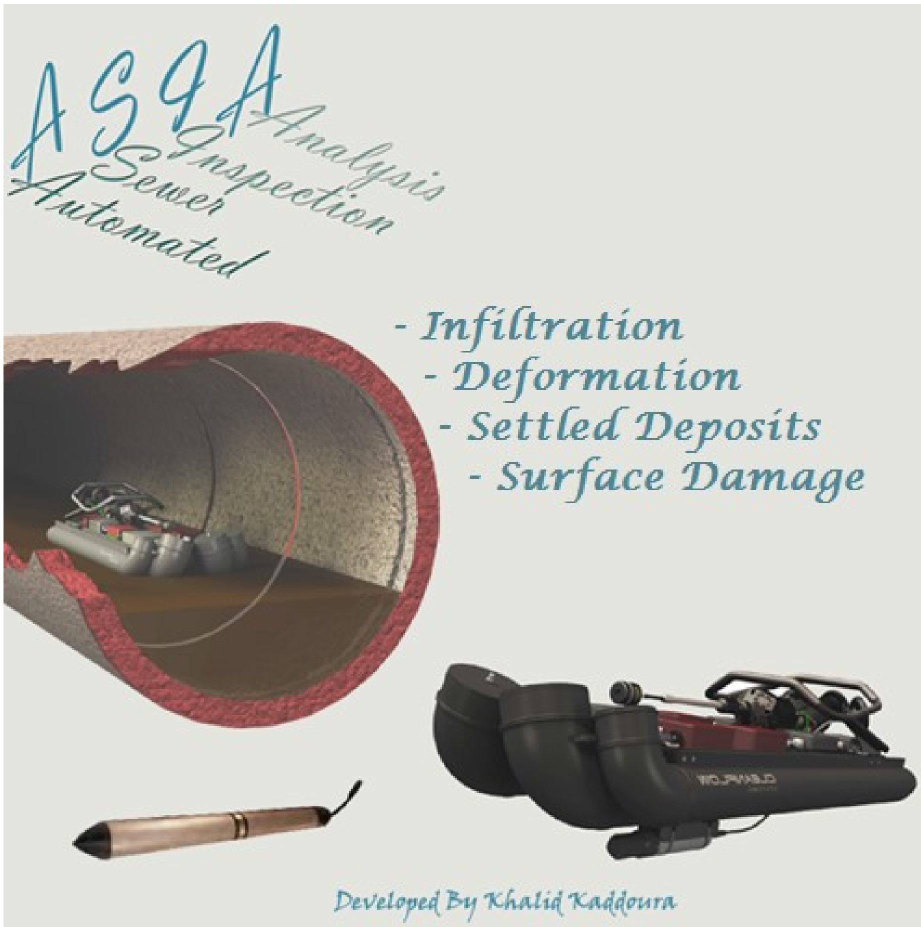

Figure 5.1 ASIA Cover Window

Figure 5.2 contains two buttons. Clicking "Calculations" provides the user with the defect quantification options.

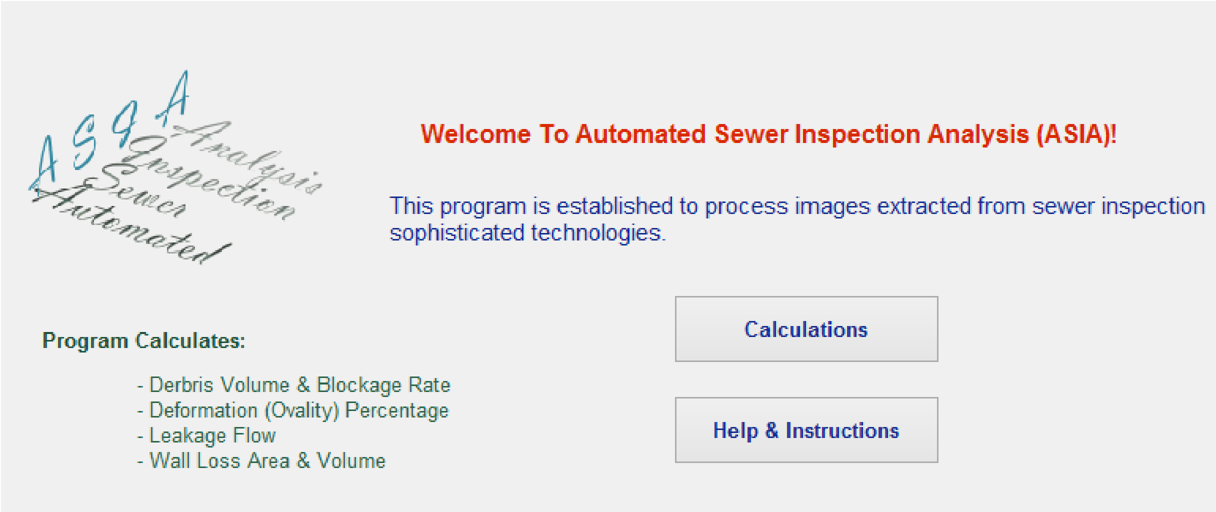

Figure 5.2 Home Window Page

Figure 5.3 is a help tool. It instructs the user about the program in general. Additionally, it includes an overview about the defects and technologies used for sewer inspection.

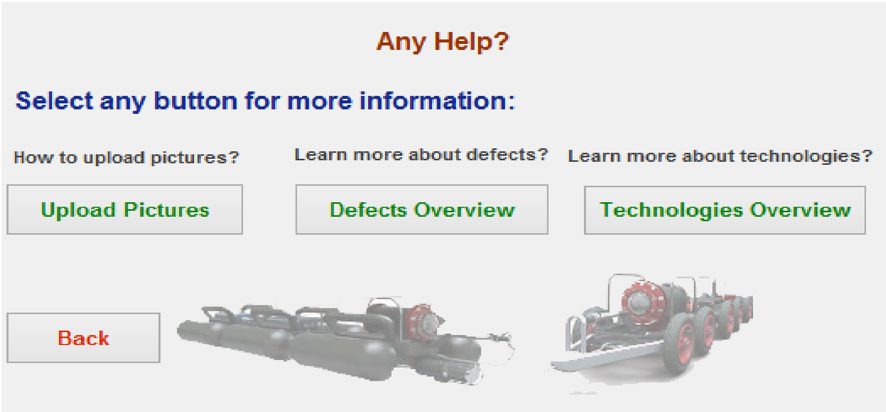

Figure 5.3 Help Window Page

Figure 5.4 is a snapshot of multiple choices that enable the user to start any of the quantification techniques.

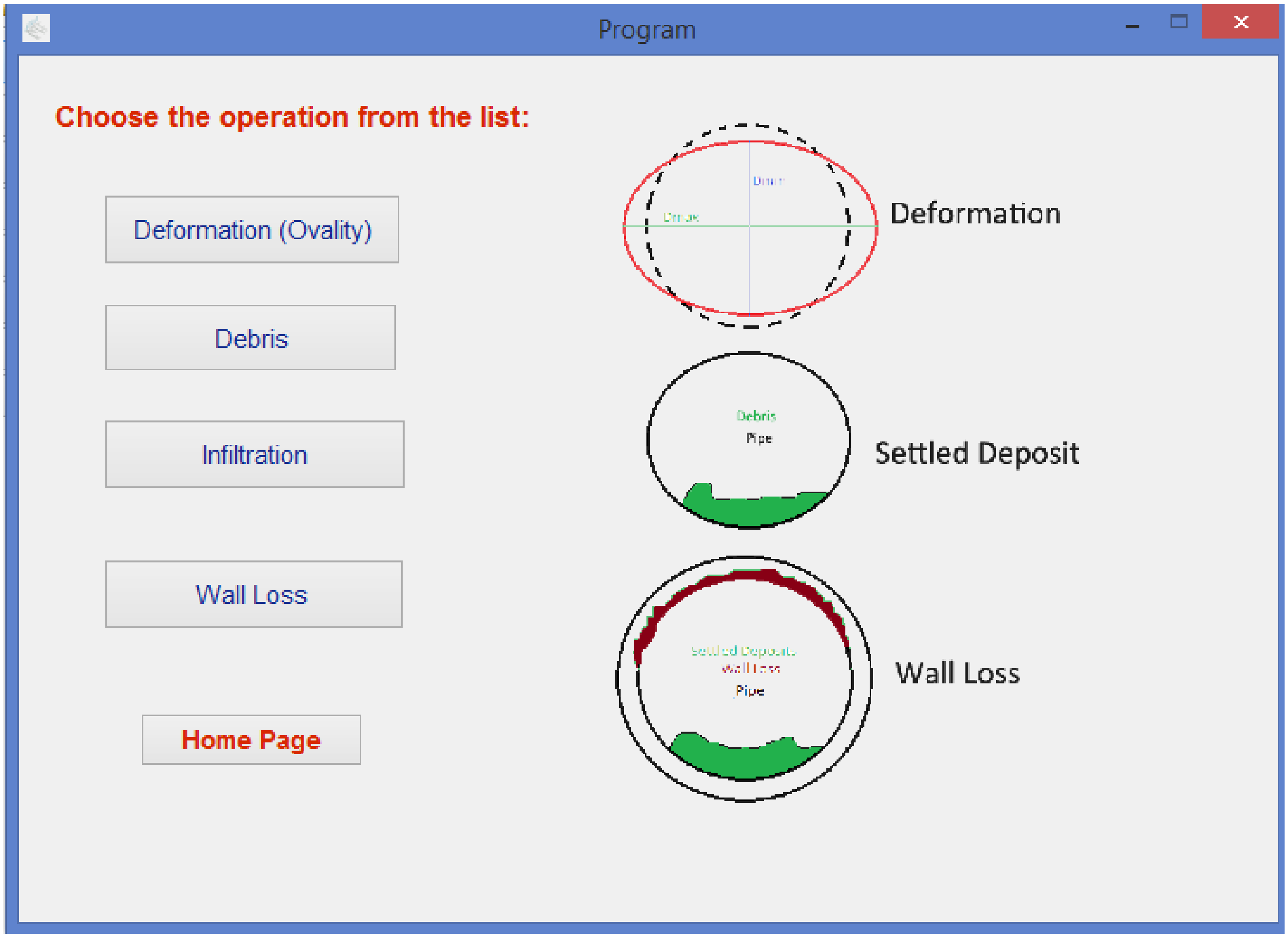

Figure 5.4 Calculations Window Page

When selecting the "Deformation (Ovality)" button, the operations in Figures 3.12 to 3.17 are automatically generated for each image to produce the percentages using the ASTM formula and the roundness factor. Selecting the "Debris" button will generate the operations done in Figures 3.22 to 3.33 for each imported image. The "Infiltration" button automatically translates the imported current values, using equation 3.17, to flow rates. Finally, selecting the "Wall Loss" button will generate the operations done in Figures 3.37 to 3.44 for each image to supply the user with the aforementioned parameters.

Figure 5.5 is a window that enables the user to insert the pipeline information, which can be saved for future purposes.

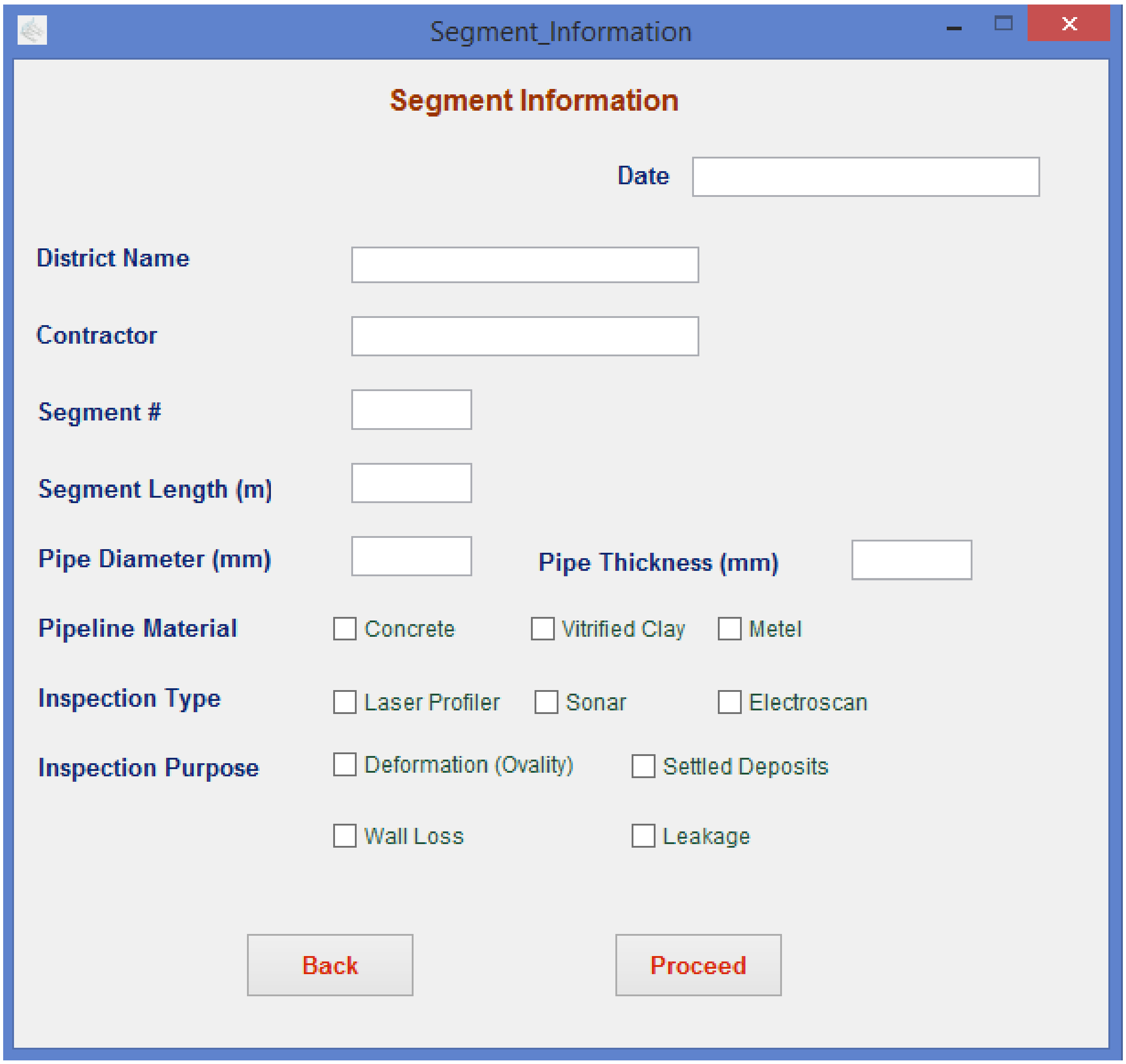

Figure 5.5 Pipeline Information

Figure 5.6 is a window that gives the user options for overviews of multiple sewer inspection technologies. Figure 5.7 is a window that offers information about the defects and the calculation methods.

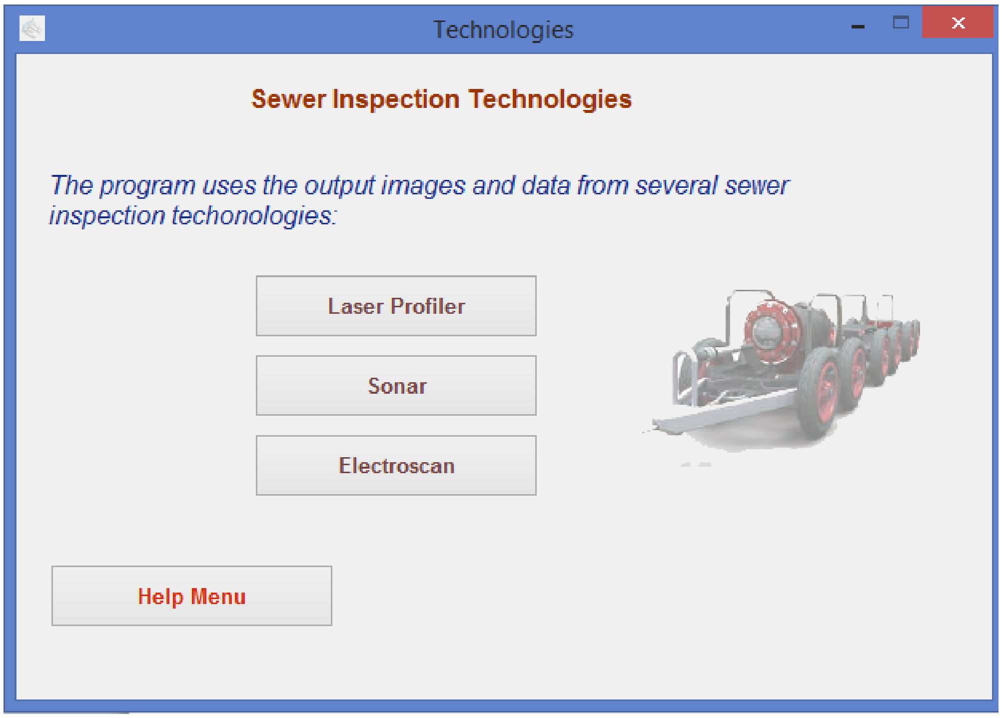

Figure 5.6 Sewer Inspection Technologies Window Page

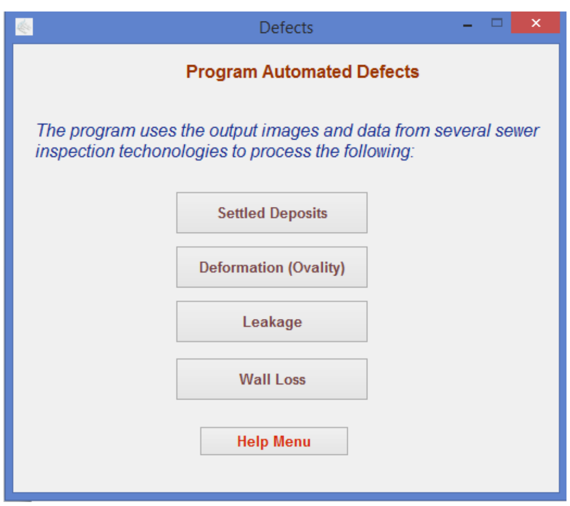

Figure 5.7 Defects Options Window Page

Figure 5.8 is a window that is concerned with the index calculation. The user can select the material of the sewer pipeline as well as the sewer protocol. The calculation method is based on the utility functions. The three protocols were used in the development of deformation and settled deposits utility functions. Therefore, the buttons refer to their names. For example, the "WRc" button under "Concrete" will calculate the grade based on the WRc utility deformation equation, WRc utility settled deposits equation, electro scan utility infiltration equation, and concrete utility equation based on the pipeline size.

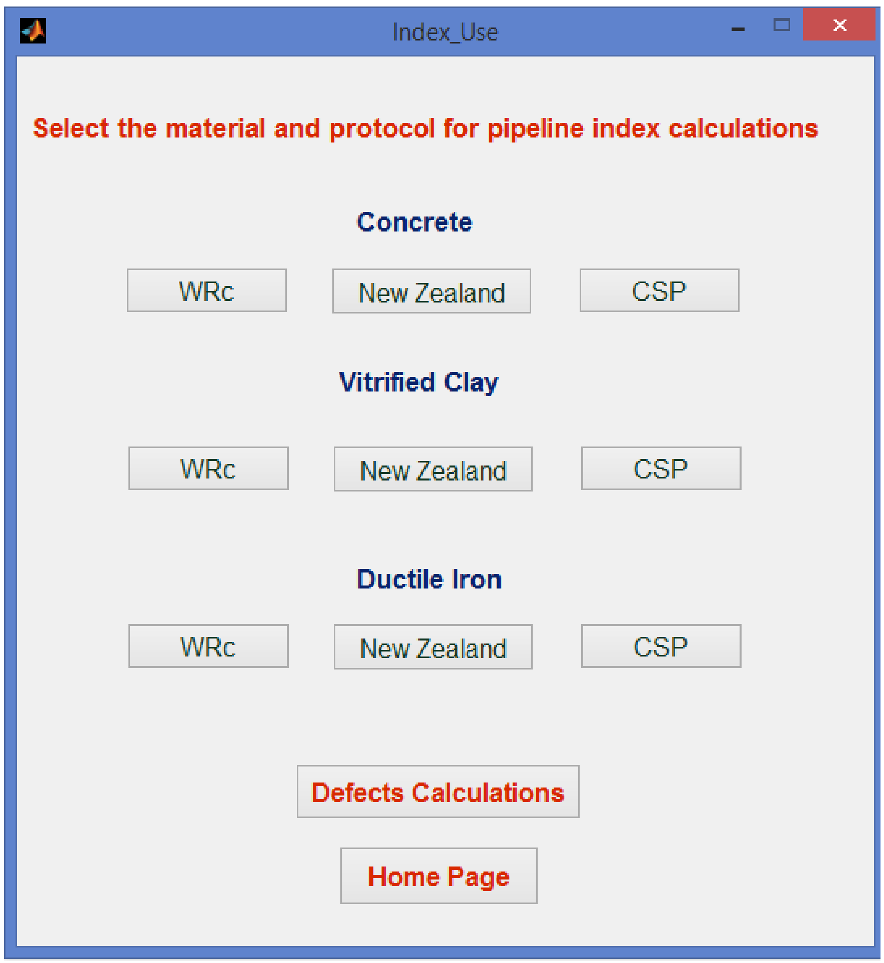

Figure 5.8 Grade Calculation Window Page

5.4 Summary

A practical tool was delivered to incorporate the automated tools and MAUT model. This chapter provided snapshots pertinent to the ASIA tool. The tool consists of three essential deliverables. The first part is a help tool, which provides the user with the inspection technologies considered, the defects quantification algorithms, and the directions to import the data. The second part is concerned with analyzing the imported data and is designed to quantify the deformation, settled deposits, infiltration, and surface damage sewer defects. The third part of the tool assesses the pipeline of concern. It consists of the utility functions developed for each defect. After considering the information generated by the automated quantification tool, the condition assessment model will supply the user with an aggregated index.

CHAPTER SIX: CONCLUSIONS AND RECOMMENDATIONS

6.1 Research Summary

This research used the outputs provided by sewer inspection technologies, such as the laser profiler, sonar, and electro scan. One of the main objectives was to quantify four defects: deformation, settled deposits, infiltration, and surface damage. Image processing techniques and mathematical equations were used to quantify deformation, settled deposits, and surface damage defects. Each defect had its own methodology. The image processing techniques used from the MATLAB image processing toolbox were image segmentation, contrast adjustment, structuring elements, dilation, and erosion. However, infiltration defects were quantified by implementing an automated electro scan method that transferred changes in current to infiltration flow.

The other objective was to use a new model that explains the condition of the pipeline, in other words, to provide an aggregated grade for the inspected sewer pipeline. Therefore, the MAUT method was used to generate functions for the four defects. WRc, CSP, and New Zealand sewer protocols were used to extract the severities of deformation and settled deposits defects. Three utility functions, based on severities, were generated for each defect. The infiltration utility function was developed using the electro scan severity information. Three sewer pipeline materials were considered in forming the utility functions for the surface damage defect: reinforced concrete, vitrified clay, and ductile iron. The structural behavior of each material was investigated before forming the utility functions. Each standard pipeline size for each material had one utility function.

Later, the research modified some of the CSP scale to account for the numerical evaluations of surface damage and infiltration. Next, the research used relative importance weights from previous research to aggregate the defect indexes and produce a grade for sewer pipelines. Furthermore, the research developed a user interface tool, via GUIDE, that combined all the research. The tool contained the algorithms that quantified the studied defects. In addition, all utility functions designed were embedded in the tool to produce an aggregated grade for the sewer pipeline under inspection.

Finally, the automated tool was used to implement and validate the developed image processing algorithms and to test the MAUT model on actual case studies. Because the aggregated index contained decimals, the model used three rounding types: rounding to the nearest number, rounding up, and rounding down. The research selected the type that produced the lowest MAE values. The optimum rounding type was then used to compare the CSP methodology in grading sewer pipelines with the MAUT methodology.

6.2 Research Conclusions

The research used image processing techniques and the MAUT model to analyze and assess sewer pipelines based on four defects. Several points can be drawn from the research:

- Several image segmentation techniques were used to detect the 2-D laser light. The techniques utilized were Sobel, Canny, Roberts, LoG, Prewitt, and intensity thresholding. However, the research proved that intensity thresholding of 0.4 produced the best isolated 2-D laser light.
- Two approaches were used to quantify deformation from the 2-D laser light: ASTM F1216 and the roundness factor. The MAE of the first approach was 4.27%, while the MAE of the second approach was 4.83%. Almost similar MAE percentages were observed. The maximum difference percentage was 40.06%, whereas the minimum was 0.59%. The average difference percentage was calculated as 16.67%. Hence, the research proved the reliability of using the roundness factor to quantify the deformation defect.

- To segment the settled deposits area from the inside pipeline area in the image, intensity thresholding segmentation was used with a threshold of 0.5.
- The automated tool was able to calculate the segment's total blockage rate in the sewer pipeline segment and the volume of the settled deposits in a pipeline.
- To remove the noise occurring from the image's gridlines, Weiner's noise removal technique was used with a neighborhood of $m = 5$ and $n = 5$.
- The automated tool was able to calculate the maximum wall distance percentage compared to the inside diameter of the pipeline and the wall loss area percentage compared to the inside pipeline area. In addition, the volume of the wall loss material can be calculated.
- To scale the percentage of deformation into an index using the MAUT approach, severities from three protocols were investigated. The WRc utility deformation curve was a polynomial of degree 2 and $R^2 = 1$. The CSP utility deformation curve was of degree 3 and $R^2 = 0.9995$. The New Zealand utility deformation produced a straight-line function. Based on the R^2 calculated, the regression type perfectly fits the data considered.
- To scale the percentage of the segment's total blockage rate using the MAUT approach, severities from three protocols were used. The WRc utility curve was a polynomial of degree 3 with $R^2 = 0.9993$. The CSP utility curve was a polynomial of degree 3 with $R^2 = 1$. However, the New Zealand utility curve was a polynomial of degree 2 and $R^2 = 1$. Based on the R^2 calculated, the regression type perfectly fits the data considered.
- The research generated a utility function that was able to grade the infiltration defect based on the infiltration's flow. Electro scan's severities were used for this matter. The utility curve generated was a polynomial of degree 2 and $R^2 = 1$. Based on the R^2 calculated, the regression type perfectly fits the data considered.

- The research developed a detailed approach to evaluate the surface damage defect using the MAUT approach for three sewer pipeline materials: reinforced concrete, vitrified clay, and ductile iron. The approach was able to calculate the maximum wall loss occurring per image as well as the area of the wall loss in the same image. The algorithm was equipped with a methodology to calculate the volume of the wall loss along a segment.
- The research modified the CSP scale to change some linguistic evaluations to numeric ones in terms of infiltration and surface damage defects. These modifications reduced the subjectivity when evaluating the aforementioned defects.
- The research investigated the best rounding type that changes the aggregated index, containing decimals, to a whole number. The validation was implemented on 17 case studies from Qatar and Canada. Rounding up produced the best results after comparing the results using the MAE values.
- The rounded-up aggregated index using the MAUT approach was compared with the CSP methodology. The comparison was done on 12 case studies from Qatar. The MAE value for the CSP methodology was 0.25; however, the MAE value for the MAUT methodology was 0.33. The average difference percentage between the two approaches was 3.33%. Hence, a minimal difference was observed between the two approaches.
- The final grade shall provide asset managers with a representation of the pipeline's condition for improved budget allocation and rehabilitation prioritization.

6.3 Research Contributions

The developed research provided contributions including, but not limited to, the following:

- Proposed a new method to quantify deformation defects using the roundness factor via an image processing tool
- Provided algorithms to automate settled deposits quantification and surface damage defects
- Developed a new approach that evaluates the surface damage defects numerically, thereby omitting subjectivity
- Utilized the MAUT method in calculating an index for each defect and aggregated the indexes to grade the inspected pipeline
- Developed an ASIA user interface that was able to run the image processing tools, quantify defects, and grade the inspected sewer pipeline

6.4 Research Limitations

The research has some limitations that can be enhanced in future work:

- To have an extensive evaluation of surface damage defects, comprehensive structural behavior that applies to all bedding conditions must be studied. It will require the calculation of the actual design strength of vitrified clay and ductile iron.
- The aggregated index 1 to 5 was based on only four defects: deformation, settled deposits, infiltration, and surface damage.
- The deformation image processing technique was validated using only four 2-D laser images.
- The image segmentation technique utilized in the deformation and settled deposits algorithms is based on manual insertion of the threshold and may depend on the images provided.

- Settled deposits and surface damage defect image processing algorithms were implemented on four and two images, respectively.
- Validation of the MAUT model was done by using CCTV reports with assumptions for infiltration and surface damage defects.
- The defects' quantification algorithms were able to quantify the studied defects separately. In fact, more than one defect may exist per section.
- A third polynomial utility function may not represent the actual predication of the index due to change in concavity.
- The relative importance weights that decomposed the calculation of the aggregated index were adopted from other research, which was based on Canada and Qatar practitioners' responses and more than four defects.
- The aggregated index, which is highly dependent on the relative importance weights, may provide lower overall grade though one defect may be in critical condition.
- The infiltration grades from the electro scan were randomly considered 0, 5, and 10 when the utility function was generated.

6.5 Recommendations

This research designed an automated tool to quantify four different defects. In addition, it built a condition assessment model to grade the condition of sewer pipelines. Later, the research work was combined in a user interface tool called ASIA. In fact, the research provides some recommendations for future work that can produce comprehensive automation and assessment models. The recommendations, in fact, are divided into two sections: enhancements and extensions.

6.5.1 Research Enhancements

- More operational and structural defects can be added to the condition assessment model. Integrating many of the sewer defects would provide a comprehensive assessment of the section in concern. After including these defects, the computed aggregated grade will represent the current condition of the pipeline. Hence, it would help establish better rehabilitation and maintenance plans and budgets.
- Additional sewer inspection technologies can be incorporated to account for the pipelines' surrounding environments, which are expected to provide a better evaluation of sewer pipelines. As an example is the PPR technology, which is able to provide information about the embedment as well as the rebar alignment.
- The condition assessment model can incorporate multiple components of sewer systems such as manholes, connections, pumps, and other accessories. The comprehensive grade can be aggregated after finding relative importance weights of the components and their respective defects. Therefore, the provided grade can present the condition of the entire system rather than that of one component.
- The automated tool can be expanded not only to quantify the defects but also to classify them. Classification of defects facilitates recognizing the defects once the images are imported. This can be done using recognition and classification processing techniques.
- The automated tool can be enhanced by applying automatic image segmentation techniques rather than a change-driven technique (intensity thresholding). After incorporating an automatic segmentation technique, any image from any resource can be processed.

6.5.2 Research Extensions

- Provide a rehabilitation plan for each defect by integrating the developed condition assessment model with a rehabilitation methodology.

- Incorporate environmental factors into the model developed to provide decision makers with a comprehensive pipeline evaluation.
- Use the condition index resulting from a risk assessment model to predict the future deterioration of the sewers.
- Study comprehensively and extensively the structural behavior of different sewer pipeline materials to enhance the evaluation of surface damage defects. The study shall include finding the actual design thicknesses and, if possible, disregarding the safety factor. As a result, the failure point can be exactly determined rather than being conservative.
- Consider using similar automation methodology for other infrastructure facilities such as water pipelines.
- Develop the automated tool to provide a 3-D graphical representation of the sewer pipeline tested after feeding the tool with images.

REFERENCES

Abdel-Qader, I., Abudayyeh, O., & Kelly, M. E. (2003). "Analysis of edge-detection techniques for crack identification in bridges." *Journal of Computing in Civil Engineering*, 17(4), 255-263.

Abraham, D. M., Wirahadikusumah, R., Short, T. J., & Shahbahrami, S. (1998). "Optimization modeling for sewer network management." *Journal of construction engineering and management,*124(5), 402-410.

American Concrete Pipe Association (ACPA). (1980). *Concrete Pipe Design Manual,* USA.

Association of Metropolitan Sewerage Agencies (AMSA). (2003). *Wet Weather Survey-Final Report.* Washington.

Ananda, J., & Herath, G. (2005). "Evaluating public risk preferences in forest land-use choices using multi-attribute utility theory." *Ecological Economics*, 55(3), 408-419.

Andrews, M. E., & Eng, P. (1998, September). "Large diameter sewer condition assessment using combined sonar and CCTV equipment." In *APWA International Public Works Congress, NRCC/CPWA Seminar series "Innovations in Urban Infrastructure", Las Vegas, Nevada*.

Ariaratnam, S. T., El-Assaly, A., & Yang, Y. (2001). "Assessment of infrastructure inspection needs using logistic models." *Journal of infrastructure systems*, 7(4), 160-165.

American Society of Civil Engineers (ASCE). (2004). "Report Card for America's Infrastructure 2003 Progress report." <http://www.asce.org/reportcard/> (Jan. 15, 2015).

American Society for Testing and Materials (ASTM). (2011). *Standard specifications for Reinforced Concrete Culverts, Storm Drain and Sewer Pipe.*< www.astm.org/Standards/C76M.htm> (Jan. 16,2015).

Baur, R., & Herz, R. (2002). "Selective inspection planning with ageing forecast for sewer types." *Water Science & Technology*, 46(6-7), 389-396.

Besl, P. J., Delp, E. J., & Jain, R. (1985). "Automatic visual solder joint inspection." *Robotics and Automation, IEEE Journal of*, 1(1), 42-56.

Birks, A., & Green, R. (1991). *Nondestructive testing handbook,* American Society for Nondestructive Testing, Ohio.

Chae, M. J., & Abraham, D. M. (2000). "Automated Condition Assessment of Sanitary Sewer Pipelines." *Computing in Civil and Building Engineering,* 1196-1203.

Chae, M. J., & Abraham, D. M. (2001). “Neuro-fuzzy approaches for sanitary sewer pipeline condition assessment.” *Journal of Computing in Civil engineering*, 15(1), 4-14.

Chan, C., Fulton, R., Feng, D. D., & Meikle, S. (2010, October). “Median non-local means filtering for low SNR image denoising: Application to PET with anatomical knowledge.” *Nuclear Science Symposium Conference Record (NSS/MIC),* 3613-3618.

Cheng, H. D., & Miyojim, M. (1998). “Novel system for automatic pavement distress detection.” *Journal of computing in civil engineering*, 12(3), 145-152.

Chughtai, F. (2007). *Integrated Condition Assessment Models for Sustainable Sewer Pipelines Masters Thesis*, Montreal.

Chughtai, F., & Zayed, T. (2008). “Infrastructure condition prediction models for sustainable sewer pipelines.” *Journal of Performance of Constructed Facilities,* 22(5), 333-341.

Daher, S. (2015). *Defect-based Condition Assessment Model and Protocol of Sewer Pipelines. Master's Thesis*, Montreal.

deMonsabert, S., & Thornton, P. (1997). “A benders decomposition model for sewer rehabilitation planning for infiltration and inflow planning.” *Water environment research*, 162-167.

Denys, B., Elisio, V., & Pascal, L. (2004). “Decision Making in Sewer Maintenance Strategies: Simulaton as a Practical Tool.” *1st International Forum on Engineering Decision Making (IFED).*

DeSilva, D., Marlow, D., Beale, D., & Marney, D. (2011). “Sewer blockage management: Australian perspective.” *Journal of Pipeline Systems Engineering and Practice*, 2(4), 139-145.

Dettmer, A., Hall, D., Hegab, H., & Swanbom, M. (2005). “Refining laser profiling methods used for pipeline assessment.” *North American Society for Trenchless Technology (NASTT) NO-DIG, Orlando, FL*, 1-9.

Dikmen, I., Birgonul, M., & Kiziltas, S. (2005). “Prediction of Organizational Effectiveness in Construction Companies.” *Journal of Construction Engineering and Management*, 131(2), 252-261.

Duran, O., Althoefer, K., & Seneviratne, L. D. (2002). “Automated sewer pipe inspection through image processing.” *Robotics and Automation Proceedings,ICRA'02, IEEE International Conference,* 2551-2556.

Duran, O., Althoefer, K., & Seneviratne, L. D. (2007). “Automated pipe defect detection and categorization using camera/laser-based profiler and artificial neural network.” *Automation Science and Engineering, IEEE Transactions on*, 4(1), 118-126.

Eiswirth, M., Heske, C., Burn, L. S., & DeSilva, D. (2001, October). New methods for water pipeline assessment. *Proceedings of the 2nd World Water Congress of the International Water Association*.

Electoscan. (2013). "Comparing CCTV and Electro Scan In Locating Infiltration".

Electroscan. (2014). "Inspection Summary." Geneve.

US Army Corps of Engineers. (2013). "GUIDANCE FOR CCTV AND SONAR INSPECTION PIPES PENETRATING LEVEES."

Environmental Protection Agency (EPA). (2000). *Wastewater Technology Fact Sheet. Pipe Construction and Materials,* United States.

Feeney, C. S., Thayer, S., Bonomo, M., & Martel, K. (2009). *White Paper on Condition Assessment of Wastewater Collection Systems,* Environmental Protection Agency, United States.

Félio, G. (2012). "Canada's Infrastructure Report Card." < http://www.canadainfrastructure.ca/en/index.html> (Jan. 25, 2015)

Fenner, R. A., Sweeting, L., & Marriott, M. J. (2000). "A new approach for directing proactive sewer maintenance." *Proceedings of the ICE-Water and Maritime Engineering*, 67-77.

Fujita, Y., Mitani, Y., & Hamamoto, Y. (2006). "A method for crack detection on a concrete structure." In *Pattern Recognition, ICPR 2006, 18th International Conference,* 901-904.

Gutierrez, F. (2005). *ULTRASONIC SENSING METHODS FOR SEWER PIPE INSPECTION. Doctor of Philosophy Thesis*, London.

Guo, W., Soilbelman, L., & Jr., J. G. (2009). "Automated defect detection for sewer pipeline inspection and condition assessment." *Automation in Construction*, 18(5), 587-596.

Halfawy, M. R., & Hengmeechai, J. (2014). "Efficient Algorithm for Crack Detection in Sewer Images from Closed-Circuit Television Inspections." *Infrastruct. Syst.,* 20(2).

Harris, R. J., & Tasello, J. (2004). "Sewer Leak Detection-Electro-Scan Adds a New Dimension Case Study: City Of Redding, California." *ASCE Pipelines*.

Harris, R. J., & Dobson, C. (2006). "Sewer pipe infiltration assessment: Comparison of Electro-Scan, joint pressure testing, and CCTV inspection." *Proceedings of the 2006 Pipeline Division Specialty Conference-Pipelines*.

Hartley, R., & Zisserman, A. (2003). *Multiple view geometry in computer vision*, Cambridge university press.

Harvey, R. R., & McBean, E. A. (2014). “Predicting the structural condition of individual sanitary sewer pipes with random forest.” *Canadian Journal of Civil Engineering,*, 294-303.

Hobrecht. (1902). “Vitrified clay.” <http://www.unitracc.com/know-how/fachbuecher/rehabilitation-and-maintenance-of-drains-and-sewers/structure-and-limiting-conditions-of-sewer-systems-historical-outline/piping-materials-and-the-design-of-pipe-connections/vitrified-clay-en> (Dec. 15, 2014).

Humes. (2009). “Concrete Pipes Reference Manual.*”*<http://www.humes.com.au/fileadmin/templates/HUMES/doc/Brochures/Humes_ConcretePipeManual.pdf> (Dec. 18, 2014).

Islam, M. M., Ali, A., & Purtell, J. (2009). “Enhanced Condition Assessment Methodologies of Buried Infrastructure.” *Pipelines 2009: Infrastructure's Hidden Assets*,1417-1426.

Joannis, C., Commaille, J., & Dupasquier, F. (2002). Assessing infiltration flow-rates into sewers . *Global Solutions for Urban Drainage*.

Joannis, C., Commaille, J. F., & Dupasquier, B. (2002). “Assessing infiltration flow-rates into sewers.” *9th International Conference on Urban Drainage*, 8-13.

Kirstein, S., Müller, K., Walecki-Mingers, M., & Deserno, T. M. (2012). “Robust adaptive flow line detection in sewer pipes.” *Automation in Construction*, *21*, 24-31.

Koo, D.-H., & Ariaratnam, S. T. (2006). “Innovative method for assessment of underground sewer pipe condition.” *Automation in Construction*, 479 – 488.

Kulandaivel, G. (2004). *Sewer Pipeline Condition Prediction Using Neural Network Models. Masters Thesis*, USA.

Kuntze, H.-B., & Haffner, H. (1998). “Experiences with the Development of a Robot for Smart Multisensoric Pipe Inspection.” *Proceedings of the IEEE International Conference on Robotics and Automation.*

Law, M. F., & Deasy, P. B. (1998). “Use of hydrophilic polymers with microcrystalline cellulose to improve extrusion–spheronization.” *European Journal of Pharmaceutics and Biopharmaceutics*, 57-65.

Law, T., Itoh, H., & Seki, H. (1996). “Image filtering, edge detection, and edge tracing using fuzzy reasoning.” *Pattern Analysis and Machine Intelligence, IEEE Transactions,*18(5), 481-491.

Littlewood, K., & Butler, D. (2003). “Movement mechanisms of gross solids in intermittent flow.” *Water Science & Technology*, 47(4), 45-50.

Hastak, M., & Skibniewski, M. J. (1993). “Automation potential of pipe laying operations.” *Automation in construction*, 2(1), 65-79.

Makar, J. M. (1999). “Diagnostic techniques for sewer systems.” *Journal of Infrastructure Systems*, 5(2), 69-78.

American Pipe Manual. *American Ductile Iron Manual*, <www.american-usa.com> (Mar. 01, 2015).

Maode, Y., Shaobo, B., Kun, X., & Yuyao, H. (2007). “Pavement crack detection and analysis for high-grade highway.” *Electronic Measurement and Instruments, ICEMI'07, 8th International Conference,* 4-548.

Marchewka, A. (2010). “Crack detection on asphalt surface image using local minimum analysis.” *Image Processing and Communications Challenges 2,* 353-359.

Martel, K., Tuccillo, M. E., Rowe, R., Feeney, C. S., Hogan, S., DeBlois, G., et al. (2010). *Innovative Internal Camera Inspection and Data Management for for Effective Condition Assessment of Collection Systems,* United States Environmental Protection Agency.

Mashford, J., Marlow, D., & Burn, S. (2009). “An approach to pipe image interpretation based condition assessment for automatic pipe inspection.” *Advances in Civil Engineering*.

Mashford, J., Marlow, D., Tran, D., & May, R. (2010a). “Prediction of sewer condition grade using support vector machines.” *Journal of Computing in Civil Engineering*, 25(4), 283-290.

Mashford, J., Davis, P., & Rahilly, M. (2007). “Pixel-based colour image segmentation using support vector machine for automatic pipe inspection“. *AI 2007: Advances in Artificial Intelligence,* 739-743.

Mashford, J., Rahilly, M., Davis, P., & Burn, S. (2010b). “A morphological approach to pipe image interpretation based on segmentation by support vector machine.” *Automation in Construction*, 19(7), 875-883.

Rinker Materials. (2009). *STORM SEWER PIPELINE LASER PROFILING.*

Mattsson, J., Hedström, A., Viklander, M., & Blecken, G. T. (2014). “Fat, Oil, and Grease Accumulation in Sewer Systems: Comprehensive Survey of Experiences of Scandinavian Municipalities.” *Journal of environmental engineering*, 140(3).

Montironi, R., Mazzucchelli, R., Santinelli, A., Scarpelli, M., Beltran, A. L., & Bostwick, D. G. (2005). “Incidentally detected prostate cancer in cystoprostatectomies: pathological and morphometric comparison with clinically detected cancer in totally embedded specimens.” *Human pathology*, 36(6), 646-654.

Morrison, R. S., & Thomson, J. C. (2003). Innovative Inspection Methodologies for Wastewater Systems. *Pipelines 2003: New Pipeline Technologies, Security and Safety.*

Moselhi, O., & Shehab-Eldeen, T. (1999a). "An Al-based system for detection and classification of defects in sewers." *INFRA 99*, 42–54.

Moselhi, O., & Shehab-Eldeen, T. (1999b). "Automated detection of surface defects in water and sewer pipes." *Autom. Construct*, 581-588.

Moselhi, O., & Shehab-Eldeen, T. (2000). "Classification of defects in sewer pipes using neural networks." *J. Infrastruct. Syst*, 6(3), 97-104.

Motahari, A., & Abolmaali, A. (2010). "Structural Deformation Characteristics of Installed HDPE Circular Pipelines." *J. Transp. Eng.*, 136(4), 298-303.

Moy, T., Wilmut, C. G., & Harris, R. J. (2012). "USEPA Sewer Electro Scan Field Demonstration Revisited." *Proceedings of the Water Environment Federation*, (16), 1100-1131.

Najafi, M., & Kulandaivel, G. (2005). "Pipeline condition prediction using neural network models." *Pipelines 2005: Optimizing Pipeline Design, Operations, and Maintenance in Today's Economy,* 767-781.

Nelson, R., Rowe, R., & Varghese, V. (2010). Process for Evaluating Sanitary Sewer Pipe and Manhole Condition Assessment Data. *Pipelines 2010: Climbing New Peaks to Infrastructure Reliability: Renew, Rehab, and Reinvest*, 743-752.

NPTEL. "Sewer Material." *NPTEL IIT Kharagpur Web Courses*, <nptel.ac.in/courses/105105048/M3L3.pdf> (May 29, 2015).

New Zealand Water and Waste Water Association (NZWWWA). (2006). *New Zealand Pipe Inspection Manual,* Third Edition.

O'Keefe, A. (2013). "Comprehensive Sewer Condition Assessment Using CCTV and Electro Scan: International Cases." In *Pipelines 2013: Pipelines and Trenchless Construction and Renewals—A Global Perspective*, 113-123.

O'Neill, B. (1997). *Elementary Differential Geometry,* San Diego.

Redzone. (2008). *Multi-Frequency Sonar: Fine Tuning Your Pipe Inspection System,* http://www.redzone.com/ViewDocs.asp?sectionID=35605&ID=117&CatID=1> (Dec. 12, 2014).

Reyna, S. M., Vanegas, J. A., & Khan, A. H. (1994). "Construction technologies for sewer rehabilitation." *Journal of Construction Engineering and management*, 120(3), 467-487.

Ruwanpura, J., Ariaratnam, S., & El-Assaly, A. (2004). "Prediction models for sewer infrastructure utilizing rule-based simulation." *Civ. Eng. Environ. Syst.*, 21(3), 169–185.

Savage, L. (1954). *The Foundations of Statistics,* New York.

Schäfer, R. (2001). "Rules for using multi-attribute utility theory for estimating a user's interests." *Ninth Workshop Adaptivität und Benutzermodellierung in Interaktiven Softwaresystemen*, 8-10.

SewerVUE. (2014). "SewerVUE". <www.sewervue.com> (Nov. 11, 2014).

Shehab-Eldeen, T., & Moselhi, O. (2005). "Automated detection and classification of infiltration in sewer pipes." *J. Infrastruct. Syst*, 11(3), 165-171.

Siddiqui, S., & Mirza, S. (1996). *The state of municipal infrastructure in Canada,* McGill Univ., Montreal.

Sinha, S. K., & Fieguth, P. W. (2006). "Automated detection of cracks in buried concrete pipe images." *Automation in Construction*, 15(1), 58-72.

Solomon, C., & Breckon, T. (2011). *Fundamentals of Digital Image Processing,* Wiley-Blackwell.

Sonyok, D. R., Zhang, B., & Zhang, J. (2008). "Applications of Non-Destructive Evaluation (NDE) in Pipeline Inspection." In *Pipelines 2008: Pipeline Asset Management: Maximizing Performance of our Pipeline Infrastructure* 1-10.

Sousa, V., Matos, J. P., & Matias, N. (2014). "Evaluation of artificial intelligence tool performance and uncertainity for predicting sewer structural condition." *Automation in Construction*, 44, 84-91.

Stein, I., & Partner, G. (2005). "European Study of the Performance of Various Pipe Systems." *Germany: European Expert Panel Report.*

Sterling, R., Anspach, J., Allouche, E., Simicevic, J., Rogers, C., Weston, K., et al. (2009). "Utility Characterization Technologies." *Report prepared for the Transportation Research Board Strategic Highway Research Program 2,* Washington, D.C.

Tang, H. L., Xie, Y. F., & Chen, Y. C. (2012). "Use of Bio-Amp, a commercial bio-additive for the treatment of grease trap wastewater containing fat, oil, and grease." *Bioresource technology*, 124, 52-58.

Thayer, S., & Hallmark, M. (2009). "New construction verification by measurement of ovality and deflection with 3-D LADAR." *Pipelines 2009: Infrastructure's Hidden Assets*, 1156-1161.

Thomson, J., Hayward, P., Hazelden, G., Morisson, R., Sangster, T., Williams, D., et al. (2004). "An Examination of Innovative Methods used in the Inspection of Wastewater Systems." *VA and IWA Publishing:*.

Thornhill, R., & Wildbore, P. (2005). "Sewer Defects: Origins and Distination." *U-Tech Underground Construction Paper*.

Thorsen, A., & O.S.Kjesbu. (2001). "A rapid method for estimation of oocyte size and potential fecudity in Atlantic cod using computer-aided particle analysis system." *Sea Research*, 295-308.

Tuccillo, M., Jolley, J., Martel, K., & Boyd, G. (2010). *Report on Condition Assessment of Wastewater Collection Systems ,* United States Environmental Protection Agency.

Vinay Kumar, M. N. (2008). "IMAGE PROCESSING IN FREQUENCY DOMAIN USING MATLAB®: A STUDY FOR BEGINNERS." <https://hal.inria.fr/inria-00321613> (June 15, 2014).

Wade, M. G. (2002). "Assessing the Sanitary Sewer Infrastructure." *Pipelines,* 1-16.

Water Research Centre (WRc). (2004). *Sewerage Rehabilitation Manual,* Fourth Edition *,* UK.

Xu, K., Luxmoore, A. R., & Davies, T. (1998). "Sewer pipe deformation assessment by image analysis of video surveys." *Pattern Recognition*, 31(2), 169-180.

Yan, J. M., & Vairavamoorthy, K. (2003). "Fuzzy approach for pipe condition assessment." *Pipeline Engineering and Construction International Conference 2003*.

Yang, M. D., & Su, T. C. (2009). "Segmenting ideal morphologies of sewer pipe defects on CCTV images for automated diagnosis." *Expert Systems with Applications*, 36(2), 3562-3573.

APPENDIX A

Case Study 1 Results

Pipeline 1.1

Inspection Length	65.39	m			
Material	Clay				
Size	150	mm			
Location (m)	**Defect**	**Detail**	**Unit**	**Amount**	**Unit**
0	Settled Deposits	0	%	0	m^2
0.8	Settled Deposits	5	%	0.00047493	m^2
3.8	Settled Deposits	6	%	0.00056991	m^2
43.1	Settled Deposits	30	%	0.00284955	m^2
Total Volume of Deposits	0.0689	m3			
Debris Area /m	0.001598608	m			
Blockage Percentage	16.83010884	%			
Protocol	**MAUT Grade(0-10)**				
Index CSP	2.417718917				
Index WRc	1.406462215				
Index New Zealand	2.409350222				
Protocol	**Grade (0-4)**				
Report Grade	2				
CSP Class	3.032912433				
WRc Grade	3.437415114				
New Zealand Grade	3.036259911				

Pipeline 1.2

Inspection Length	75.05	m			
Material	Clay				
Size	200	mm			
Location (m)	**Defect**	**Detail**	**Unit**	**Amount**	**Unit**
0	Settled Deposits	0	%	0	m2
27	Surface Damage	7.5	mm	0.000504032	per meter
38.7	Settled Deposits	1	%	0.000182322	m2
68.2	Settled Deposits	1	%	0.000182322	m2
74.1	Settled Deposits	3	%	0.000546967	m2
74.4	Settled Deposits	5	%	0.000911611	m2
74.1	Settled Deposits	0	%	0	m2
Total Volume of Deposits	0.0111	m3			
Debris Area /m	0.000149194	m			
Blockage Percentage	0.818296046	%			
Protocol	**MAUT Grade(0-10)**				
Index CSP	0.83				
Index WRc	0.66				
Index New Zealand	0.722				
Protocol	**Grade (0-4)**				
Report Grade	4				
CSP Class	3.67				
WRc Grade	3.7338				
New Zealand Grade	3.71				

Pipeline 1.3

Inspection Length	70.44	m			
Material	Clay				
Size	300	mm			
Location (m)	**Defect**	**Detail**	**Unit**	**Amount**	**Unit**
0	Settled Deposits	0	%	0	m2
4	Settled Deposits	5	%	0.00227	m2
13.3	Settled Deposits	5	%	0.00227	m2
38.3	Settled Deposits	3	%	0.00136	m2
40.8	Settled Deposits	8	%	0.00363	m2
45.5	Settled Deposits	5	%	0.00227	m2
48.9	Settled Deposits	3	%	0.00136	m2
56	Settled Deposits	3	%	0.00136	m2
57.4	Settled Deposits	5	%	0.00227	m2
58	Settled Deposits	5	%	0.00227	m2
58.3	Settled Deposits	0	%	0	m2
Total Volume of Deposits	0.1111	m3			
Debris Area /m	0.00190566	m2/m			
Blockage Percentage	4.204054194	%			
Protocol	**MAUT Grade(0-10)**				
Index CSP	0.963				
Index WRc	0.391297				
Index New Zealand	0.568453				
Protocol	**Grade (0-4)**				
Actual Grade	4				
CSP Class	3.61				
WRc Grade	3.84				
New Zealand Grade	3.77				

Pipeline 1.4

Inspection Length	22.1	m			
Material	Clay				
Size	150	mm			
Location (m)	**Defect**	**Detail**	**Unit**	**Amount**	**Unit**
0	Settled Deposits	0	%	0	m^2
0.5	Settled Deposits	5	%	0.00227	m^2
3	Surface Damage	2.5	mm	0.0026	per meter
5.8	Settled Deposits	5	%	0.00227	m^2
9.9	Settled Deposits	3	%	0.00136	m^2
14.5	Settled Deposits	8	%	0.00363	m^2
21.6	Settled Deposits	5	%	0.00227	m^2
22.1	Settled Deposits	3	%	0.00136	m^2
Total Volume of Deposits	0.0033	m3			
Debris Area /m	0.000149321	m2/m			
Blockage Percentage	0.135746606	%			
Protocol	**MAUT Grade(0-10)**				
Index CSP	1.54				
Index WRc	1.48				
Index New Zealand	1.522				
Protocol	**Grade (0-4)**				
Actual Grade	3				
CSP Class	3.38				
WRc Grade	3.4				
New Zealand Grade	3.39				

Pipeline 1.5

Inspection Length	65.2	m			
Material	Clay				
Size	150	mm			
Location (m)	**Defect**	Detail	**Unit**	**Amount**	**Unit**
0	Settled Deposits	0	%	0	m^2
1.9	Settled Deposits	1	%	9.5E-05	m^2
7.5	Surface Damage	2.5	mm	0.00096	per meter
9.8	Settled Deposits	1	%	9.5E-05	m^2
38.3	Settled Deposits	1	%	9.5E-05	m^2
65.2	Settled Deposits	0	%	0	m^2
Total Volume of Deposits	0.0048	m3			
Debris Area /m	7.36196E-05	m2/m			
Blockage Percentage	0.066926938	%			
Protocol	**MAUT Grade(0-10)**				
Index CSP	0.572				
Index WRc	0.5264				
Index New Zealand	0.563				
Protocol	**Grade (0-4)**				
Actual Grade	3				
CSP Class	3.77				
WRc Grade	3.79				
New Zealand Grade	3.77				

Pipeline 1.6

Inspection Length	29.8	m			
Material	Clay				
Size	250	mm			
Location (m)	**Defect**	**Detail**	**Unit**	**Amount**	**Unit**
0	Settled Deposits	1	%	0.0003	m^2
3.2	Settled Deposits	3	%	0.00091	m^2
3.6	Settled Deposits	2	%	0.0006	m^2
5.2	Settled Deposits	2	%	0.0006	m2
9	Settled Deposits	1	%	0.0003	m^2
9.4	Settled Deposits	3	%	0.00091	m^2
12.7	Settled Deposits	2	%	0.0006	m^2
15.8	Settled Deposits	2	%	0.0006	m^2
18.3	Settled Deposits	3	%	0.00091	m^2
19.9	Settled Deposits	1	%	0.0003	m^2
21.6	Settled Deposits	2	%	0.0006	m^2
24.3	Settled Deposits	1	%	0.0003	m^2
27.5	Settled Deposits	2	%	0.0006	m^2
28.7	Settled Deposits	3	%	0.00091	m^2
28.9	Settled Deposits	2	%	0.0006	m^2
29.5	Settled Deposits	5	%	0.00151	m^2
29.8	Settled Deposits	0	%	0	m^2
Total Volume of Deposits	0.0178	m^3			
Debris Area /m	0.000597315	m2/m			
Blockage Percentage	1.976678668	%			
Protocol	**MAUT Grade(0-10)**				
Index CSP	0.4899				
Index WRc	0.1713				
Index New Zealand	0.2645				
Protocol	**Grade (0-4)**				
Report Grade	3				
CSP Class	3.804				
WRc Grade	3.9315				
New Zealand Grade	3.8942				

Pipeline 1.7

Inspection Length	37.4	m			
Material	Clay				
Size	200	mm			
Location (m)	**Defect**	Detail	**Unit**	**Amount**	**Unit**
0	Settled Deposits	0	%	0	m^2
1.6	Settled Deposits	2	%	0.00036	m^2
2.7	Settled Deposits	3	%	0.00055	m^2
3.7	Settled Deposits	3	%	0.00055	m^2
6.1	Settled Deposits	2	%	0.00036	m^2
6.5	Settled Deposits	3	%	0.00055	m2
7.4	Settled Deposits	5	%	0.00091	m^2
8.6	Settled Deposits	2	%	0.00036	m^2
10.5	Settled Deposits	1	%	0.00018	m^2
13.9	Settled Deposits	1	%	0.00018	m^2
15.5	Settled Deposits	1	%	0.00018	m^2
21.8	Settled Deposits	2	%	0.00036	m^2
25.5	Settled Deposits	2	%	0.00036	m^2
30.3	Settled Deposits	1	%	0.00018	m^2
32.8	Settled Deposits	1	%	0.00018	m^2
34.9	Settled Deposits	1	%	0.00018	m^2
35.2	Settled Deposits	2	%	0.00036	m^2
37.4	Settled Deposits	0	%	0	m^2
Total Volume of Deposits	0.0112	m3			
Debris Area /m	0.000299465	m2/m			
Blockage Percentage	1.64250549	%			
Protocol	**MAUT Grade(0-10)**				
Index CSP	0.4119				
Index WRc	0.1372				
Index New Zealand	0.2194				
Protocol	**Grade (0-4)**				
Report Grade	3				
CSP Class	3.83				
WRc Grade	3.95				

New Zealand Grade	3.91

Pipeline 1.8

Inspection Length	17.4	m			
Material	Clay				
Size	200	mm			
Location (m)	**Defect**	Detail	**Unit**	**Amount**	**Unit**
0	Settled Deposits	0	%	0	m^2
0.1	Settled Deposits	2	%	0.00036	m^2
0.8	Settled Deposits	3	%	0.00055	m^2
1.3	Settled Deposits	2	%	0.00036	m^2
3.1	Settled Deposits	2	%	0.00036	m^2
3.6	Settled Deposits	2	%	0.00036	m^2
4.8	Settled Deposits	2	%	0.00036	m^2
5.9	Settled Deposits	2	%	0.00036	m^2
7.1	Settled Deposits	3	%	0.00055	m^2
7.5	Settled Deposits	3	%	0.00055	m^2
8.9	Settled Deposits	10	%	0.00182	m^2
9.6	Settled Deposits	10	%	0.00182	m^2
12.2	Settled Deposits	5	%	0.00091	m^2
16.2	Settled Deposits	2	%	0.00036	m^2
17.1	Settled Deposits	5	%	0.00091	m^2
17.4	Settled Deposits	30	%	0.00547	m^2
Total Volume of Deposits	0.0136	m^3			
Debris Area /m	0.000781609	m^2/m			
Blockage Percentage	4.286966298	%			
Protocol	**MAUT Grade(0-10)**				
Index CSP	0.98				
Index WRc	0.4				
Index New Zealand	0.58				
Protocol	**Grade (0-4)**				
Report Grade	3				
CSP Class	3.61				

WRc Grade	3.84
New Zealand Grade	3.77

Pipeline 1.9

Inspection Length	7.7	m			
Material	Clay				
Size	150	mm			
Location (m)	**Defect**	**Detail**	**Unit**	**Amount**	**Unit**
0	Settled Deposits	0	%	0	m^2
0.3	Settled Deposits	2	%	0.00036	m^2
1.5	Settled Deposits	3	%	0.00055	m^2
1.7	Settled Deposits	2	%	0.00036	m^2
2.3	Settled Deposits	2	%	0.00036	m^2
3.1	Surface Damage	7.5	mm	0.00487	per meter
3.7	Settled Deposits	2	%	0.00036	m^2
4.9	Settled Deposits	2	%	0.00036	m^2
7.4	Settled Deposits	2	%	0.00036	m^2
7.7	Settled Deposits	3	%	0.00055	m^2
Total Volume of Deposits	0.0121	m^3			
Debris Area /m	0.001571429	m^2/m			
Blockage Percentage	16.54396559	%			
Protocol	**MAUT Index (0-10)**				
Index CSP	5.85				
Index WRc	4.84				
Index New Zealand	5.82				
Protocol	**Grade (0-4)**				
Report Grade	2				
CSP Class	1.66				
WRc Grade	2.064				
New Zealand Grade	1.67				

Pipeline 1.10

Inspection Length	33.1	m			
Material	Clay				
Size	300	mm			
Location (m)	**Defect**	**Detail**	**Unit**	**Amount**	**Unit**
0	Settled Deposits	3	%	0.00136	m^2
6	Settled Deposits	1	%	0.00045	m^2
9	Settled Deposits	1	%	0.00045	m^2
12.8	Settled Deposits	2	%	0.00091	m^2
16.8	Settled Deposits	2	%	0.00091	m^2
18.9	Settled Deposits	2	%	0.00091	m^2
20.8	Settled Deposits	2	%	0.00091	m^2
24.7	Settled Deposits	2	%	0.00091	m^2
28.6	Settled Deposits	2	%	0.00091	m^2
30.4	Settled Deposits	2	%	0.00091	m^2
31.3	Settled Deposits	3	%	0.00136	m^2
33.1	Settled Deposits	0	%	0	m^2
Total Volume of Deposits	0.0276	m3			
Debris Area /m	0.000833837	m2/m			
Blockage Percentage	1.839517357	%			
Protocol	**MAUT Grade(0-10)**				
Index CSP	0.46				
Index WRc	0.16				
Index New Zealand	0.25				
Protocol	**Grade (0-4)**				
Report Grade	3				
CSP Class	3.82				
WRc Grade	3.94				
New Zealand Grade	3.9				

Pipeline 1.11

Inspection Length	63.7	m			
Material	Clay				
Size	200	mm			
Location (m)	**Defect**	**Detail**	**Unit**	**Amount**	**Unit**
0	Settled Deposits	0	%	0	m^2
49.2	Settled Deposits	3	%	0.00055	m^2
50.3	Settled Deposits	3	%	0.00055	m^2
50.9	Settled Deposits	3	%	0.00055	m^2
51.4	Settled Deposits	2	%	0.00036	m^2
53.1	Settled Deposits	1	%	0.00018	m^2
55.2	Settled Deposits	2	%	0.00036	m^2
57.3	Settled Deposits	1	%	0.00018	m^2
63.7	Settled Deposits	0	%	0	m^2
Total Volume of Deposits	0.0168	m^3			
Debris Area /m	0.000263736	m^2/m			
Blockage Percentage	1.446539371	%			
Protocol	**MAUT Index (0-10)**				
Index CSP	0.365				
Index WRc	0.117				
Index New Zealand	0.193				
Protocol	**Grade (0-4)**				
Report Grade	4				
CSP Class	3.85				
WRc Grade	3.95				
New Zealand Grade	3.92				

APPENDIX B

Case Study 2 Results

Pipeline 2.2

Inspection Length	57.1	m			
Material	RC				
Size	300	mm			
Location (m)	**Defect**	**Detail**	**Unit**	**Amount**	**Unit**
0	Settled Deposits	0	%	0	m^2
10	Surface Damage	7.5	mm	0.00158	per pipeline length
25.6	Settled Deposits	5	%	0.00353	m^2
27.91	Settled Deposits	5	%	0.00353	m^2
57.1	Settled Deposits	0	%	0	m^2
Total Volume of Deposits	0.1049	m^3			
Debris Area /m	0.001837128	m^2/m			
Blockage Percentage	2.600322499	%			
Protocol	**MAUT Index(0-10)**				
Operational CSP	0.63				
Operational WRc	0.234				
Operational New Zealand	0.39				
Structural CSP	0.65				
Structural WRc	0.65				
Structural New Zealand	0.65				
Protocol	**Grade (1-5)**				
Report Grade (Operational)	2				
Report Grade (Structural)	2				
Operational CSP	1.252				
Operational WRc	1.09				
Operational New Zealand	1.14				
Structural CSP	1.26				
Structural WRc	1.26				
Structural New Zealand	1.26				

Pipeline 2.3

Inspection Length	22.8	m			
Material	RC				
Size	300	mm			
Location (m)	**Defect**	**Detail**	**Unit**	**Amount**	**Unit**
0	Settled Deposits	0	%	0	m^2
2.1	Surface Damage	7.5	mm	0.00329	per pipeline length
6.1	Settled Deposits	20	%	0.01413	m^2
9.5	Settled Deposits	20	%	0.01413	m^2
25.1	Settled Deposits	20	%	0.01413	m^2
Total Volume of Deposits	0.3116	m^3			
Debris Area /m	0.013666667	m^2/m			
Blockage Percentage	19.34418495	%			

Protocol	**MAUT Index(0-10)**
Operational CSP	2.53
Operational WRc	1.566
Operational New Zealand	2.8
Structural CSP	1.35
Structural WRc	1.35
Structural New Zealand	1.35

Protocol	**Grade (1-5)**
Report Grade (Operational)	2
Report Grade (Structural)	2
Operational CSP	2.012
Operational WRc	1.63
Operational New Zealand	1.62
Structural CSP	1.54
Structural WRc	1.54
Structural New Zealand	1.54

Pipeline 2.4

Inspection Length	63.5	m			
Material	RC				
Size	300	mm			
Location (m)	**Defect**	**Detail**	**Unit**	**Amount**	**Unit**
0	Settled Deposits	0	%	0	m^2
1.4	Settled Deposits	25	%	0.01766	m^2
14	Settled Deposits	10	%	0.00707	m^2
20	Surface Damage	12.5	mm	0.00906	Per pipeline length
53	Settled Deposits	20	%	0.01413	m^2
63.5	Settled Deposits	0	%	0	m^2
Total Volume of Deposits	0.6556	m^3			
Debris Area /m	0.010324409	m^2/m			
Blockage Percentage	14.61345994	%			
Protocol	**MAUT index (0-10)**				
Operational CSP	2.28				
Operational WRc	1.25				
Operational New Zealand	2.07				
Structural CSP	3.72				
Structural WRc	3.72				
Structural New Zealand	3.72				
Protocol	**Grade (1-5)**				
Report Grade (Operational)	3				
Report Grade (Structural)	3				
Operational CSP	1.91				
Operational WRc	1.5				
Operational New Zealand	1.83				
Structural CSP	2.49				
Structural WRc	2.49				
Structural New Zealand	2.49				

Pipeline 2.5

Inspection Length	95	m			
Material	RC				
Size	300	mm			
Location (m)	**Defect**	**Detail**	**Unit**	**Amount**	**Unit**
0	Settled Deposits	0	%	0	m^2
2.3	Settled Deposits	5	%	0.00353	m^2
7	Settled Deposits	5	%	0.00353	m^2
7.1	Settled Deposits	0	%	0	m^2
51.2	Infiltration	15	l/m		
61	Settled Deposits	5	%	0.00353	m^2
61.6	Settled Deposits	5	%	0.00353	m^2
81.6	Settled Deposits	5	%	0.00353	m^2
95	Settled Deposits	0	%	0	m^2
Total Volume of Deposits	0.2125	m3			
Debris Area /m	0.002236842	m2/m			
Blockage Percentage	3.166089321	%			

Protocol	**MAUT Index (0-10)**
Operational CSP	2.28
Operational WRc	1.25
Operational New Zealand	2.07
Structural CSP	0
Structural WRc	0
Structural New Zealand	0
Protocol	**Grade (1-5)**
Actual Grade (Operational)	3
Actual Grade (Structural)	1
Operational CSP	1.69
Operational WRc	1.12
Operational New Zealand	1.56
Structural CSP	1
Structural WRc	1
Structural New Zealand	1